104
38

BIREFRINGENT SINGLE-ARM FIBER OPTIC ENTHALPIMETER FOR CATALYTIC REACTION MONITORING

by

Eric William Richmond

Dissertation submitted to the Faculty of the
Virginia Polytechnical Institute and State University
in partial fullfillment of the requirements for the degree of

DOCTOR OF PHILOSOPHY

in

Analytical Chemistry

APPROVED:

R. E. Dessy, Chairman

G. L. Long

J. G. Mason

H. M. McNair

J. D. Wightman

January,1990

Blacksburg, Virginia

BIREFRINGENT SINGLE ARM FIBEROPTIC ENTALPIMETER FOR CATALYTIC REACTION MONITORING

by

Eric Richmond

Committee Chairman: Raymond E. Dessy
Analytical Chemistry

(ABSTRACT)

Changes in heat content are almost universally associated with chemical reactions. Thermometry as an analytical tool has been extensively researched and developed. Finding solutions to problems involving thermal isolation, specificity, sensitivity, and cross-sensitivity remain as active areas of interest.

Fiberoptic interferometers, which use phase phenomena associated with propagating light, are extremely sensitive to heat. This research has focused on a special "birefringent" optical fiber. Two channels of information are generated in this single-fiber interferometer which correspond to the heat evolved from a catalytic reaction isolated on the fiber surface.

Because of the unique transduction mechanism associated with the "birefringent" optical fiber, this device is sensitive to heat and remarkably insensitive to pressure.

Details of the characterization and development of the birefringent optical fiber into a useful analytical probe are presented.

Acknowledgements

There are many people whose contribution to this research was invaluable. I would like to express my gratitude for the support, guidance, and kindness shown to me by Dr. Raymond Dessy, Lee Dessy, and the members of my committee.

Mark Wingered, Jim Peterson, Lee Kang, and other members of my research group were involved in numerous illuminating discussions - thanks.

The support personnel associated with the chemistry department are consummate professionals and skilled craftsman. Many of these I consider friends.

Several wonderful people helped take care of my family during my absences. Special thanks to Owen and Olivia Strickler, Hazel Burner and family.

Finally, I would like to dedicate this work to my mother and father (I wish he could have been here). They taught me much which helped to sustain and guide me.

My wife and two children somehow managed to put up with me through everything, this work is especially for them ...

Sharon, Lauren, and Ben

Table of Contents

List of Figures

I. Introduction

Research in chemical sensor development based on optical fibers is a relatively young discipline. In the late seventies and early eighties much of the theoretical groundwork and technical difficulties were being understood and overcome. Considerable effort is now being focused on solutions to problems inherent in the two basic fiber optic sensor configurations: intensity and phase modulated systems. Initially, this field of study belonged to optical and electrical engineering disciplines, but work has eventually overlapped into other areas. Materials science, chemistry, and integrated optics are playing an increasing role in finding solutions to problems and broadening the field of applications for fiber optic based sensors. In this research, the intention was to investigate the development of a simple, inexpensive and generic analytical probe for the chemist based on fiber optics.

Presently, fiber optic sensors applicable to chemistry are designed basically as light pipes. Light is brought to a process which is to be monitored, is affected and returned to the detection electronics by the same fiber or a return fiber. This type of optical fiber sensor is known as an "extrinsic" fiber optic sensor. These sensors do not take advantage of the fact that an optical fiber is itself a mechanical and chemical system in equilibrium with the light propagating in the fiber. Very slight perturbations

to the fiber or its environment can have measurable effects on light transmission down the fiber. Optical fiber sensors whose transduction mechanism is based on disturbances to this equilibrium are known as "intrinsic" fiber optic sensors.

Many optical and electronic designs have been proposed to attain and use as a sensing element, the theoretical sensitivity of optical fibers to perturbations such as temperature and pressure. These sensitivities approach a millionth of a degree C and micro-pascals of pressure (1,2). The transduction mechanism, which produces these responses, is the effect of heat and pressure on the refractive index profile and physical dimensions of the optical fiber. Figure 1 shows a typical optical fiber, its geometry and refractive index profile. These two parameters establish the fibers ability to guide light from source to detector and also defines the temporal characteristics of the propagating light. An optical fiber will efficiently guide light when the refractive index of the core glass is higher than that of the cladding glass. Intensity modulated systems, such as microbending plates (3), cause the propagating light to be lost either by change in the optical fiber's refractive index profile and/or fiber geometry. Phase modulated instruments are designed to develop and extract temporal information from these same changes.

They are classified as interferometers, and are among the most sensitive methods for measuring physical perturba-

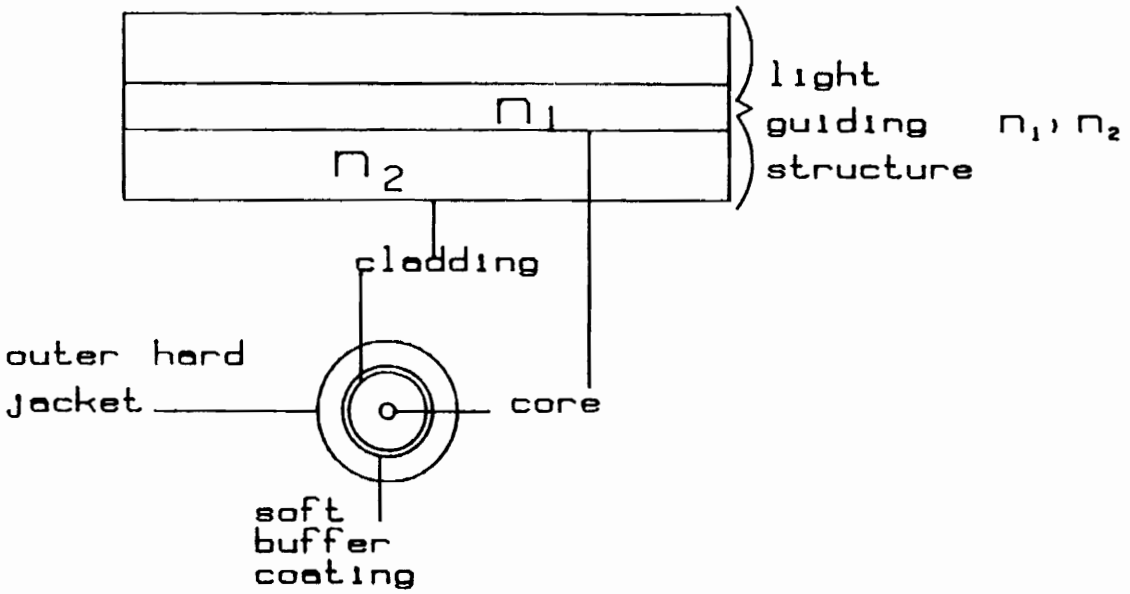

Figure 1. Fiber geometry and refractive index profile

tions.

The generic sensor in this work is based on induced phase differences between different modes of light in the same fiber caused by the effect of heat on the refractive index profile of the fiber. A specific application involves the reactions between surrounding gases and platinum, palladium noble metal catalysts which have been isolated on the fiber. This particular combination of chemistry and optical fiber responds to hydrogen gas concentrations above and below the lower explosive limit (4% by volume in air).

Light energy being transmitted in an optical fiber is not an ignition source and makes an ideal configuration for detecting volatile processes. Other advantages include remote sensing capabilities, where the sensor is physically located long distances from the launching and analyzing instrumentation. Fiber optic based sensor systems are also immune to electromagnetic interference which can plague electrical based sensors (60 cycle power line frequency, and higher frequency radio energy). The combination of these advantages, plus good sensitivity, makes research on fiber optic based sensors a promising endeavor.

II. History

The historical perspective for this research must include the two main areas of investigation, interferometry and noble-metal catalyst systems. While there has been extensive research performed in each separate area, the combination has received little attention.

A. Interferometry

Optical schemes for developing and detecting phase related information can be quite complex, requiring not only exotic optical components, but also elaborate computer and electronic peripherals (4). The most widely used instruments for phase detection are the interferometers. There are basically four types used in fiber optic based sensor research, they are the Mach-Zehnder, Sagnac, Michelson, and Fabry-Perot interferometers. An excellent review of the essential layouts and operating principles can be found in reference 4. The principles behind the Mach-Zehnder configuration are basic to the understanding of interferometric systems. The following discussion of this system will lay the foundation for examining a particular type of interferometry known as " single-arm" interferometry.

Figure 2 depicts a basic configuration for an all fiber Mach-Zehnder interferometer. Light, from a laser, is launched into a 3 db coupler, where the light energy is split and guided into the sensing and reference arms. In

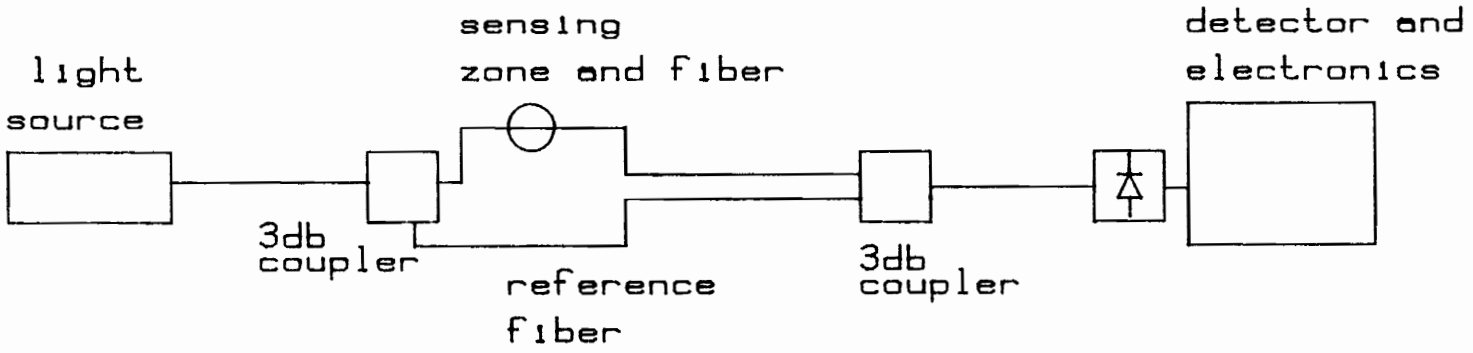

Figure 2. Fiber optic Mach-Zehnder interferemoter

theory, the sensing and reference arm and their environments are identical. However, the reference arm is not exposed to the perturbation which is affecting the sensing arm of the interferometer. A change in the refractive index profile and length of the sensing fiber causes a change in the phase of the light being transmitted. When light from the sensing and reference fiber are combined via another 3 db coupler, the change in phase between the two arms modulates the intensity at the output. This is caused by constructive and destructive interferences of the two light beams recombining in and out of phase at the output coupler. Several methods have been proposed to develop a signal from this output and are discussed in the following paragraphs.

In the early eighties, two investigators demonstrated the feasibility of optical fiber interferometry in monitoring chemical processes. Burgess et al. (5) studied the use of an all-fiber modified Mach-Zehnder in conjuncton with enyzyme chemistry isolated on the sensing arm of the interferometer. Heat from the enthalpy of the reaction produced a phase shift between the two arms. In this particular detection scheme, a fringe pattern was developed by overlapping the output beams in the far field onto a linear photodiode array. Light and dark alternating stripes are developed on the detection surface by the same constructive and destructive interferences discussed above. A computer and transform methods were used to develop the signal from

the diode array into phase information and finally into substrate concentration.

Butler et al.(6) investigated the use of a very thick palladium coating (10 microns) on the sensing arm of a Mach-Zehnder configuration to detect the presence of hydrogen gas. Hydrogen diffuses into the palladium crystal lattice, enlarging the lattice dimensions, affecting the fiber length. A phase difference is developed. After the light beams were combined at the output, the modulated intensity was measured by a single photodiode. Butler has recently published work which has examined and theoretically modelled the transduction mechanism. This new work showed a detection range from 20 parts per billion to 2% in 1 atmosphere of nitrogen (7).

This research had as one of its primary goals the development of a sensor which responded to temperature, not lattice distortion in a thick coating.

Mach-Zehnder interferometers used in research today are generally more complex than the instruments I have described. Figure 3 shows an example of a method for extracting phase information known as optical frequency shifting. This and other configurations (8) have been developed to eliminate problems associated with interferometry. Unfortunately, the trade-off that exists between alleviating problems and the cost and experimental difficulties associated with the complex apparatus required to achieve this goal, is often not balanced for success.

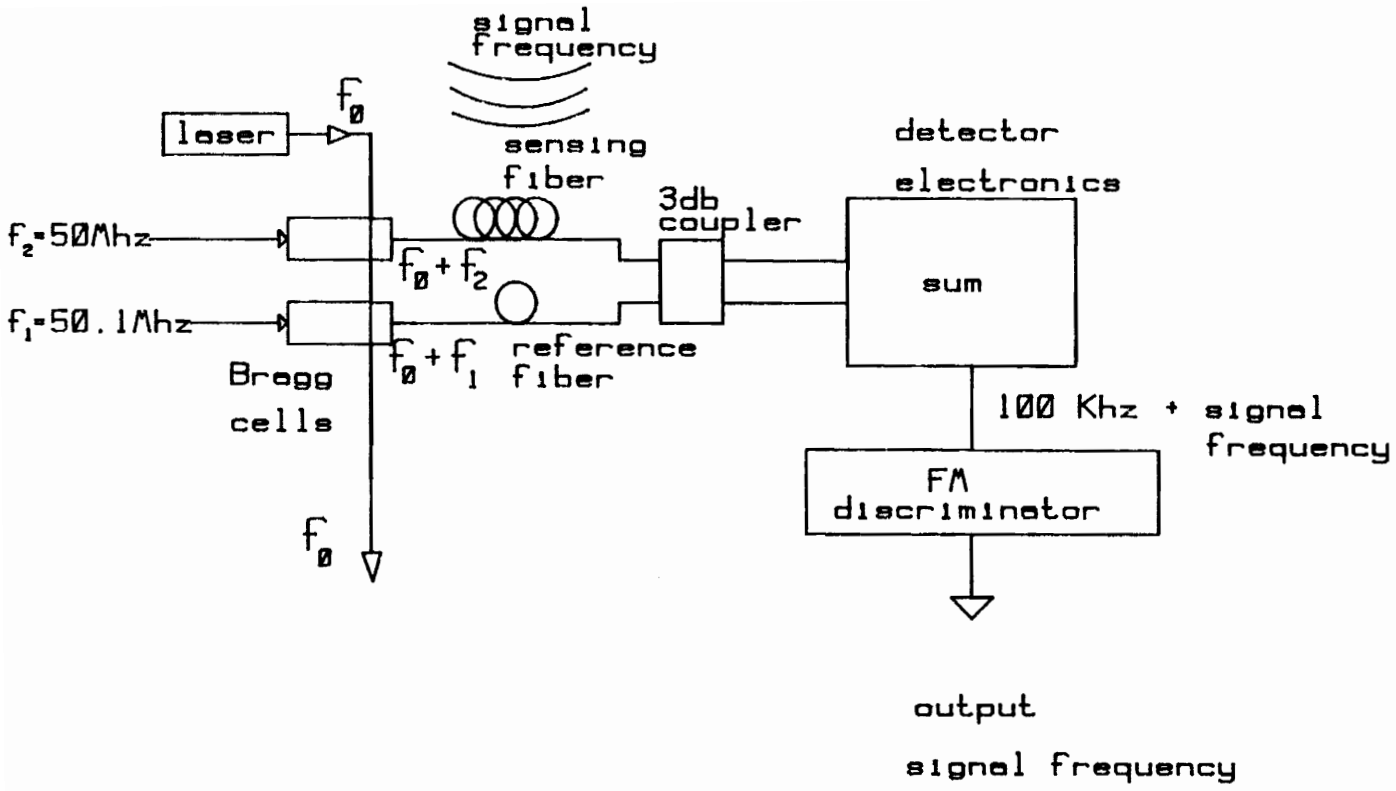

Figure 3. Frequency shifting for interferometric measurements

Interferometry does offer good sensitivity, but this sensitivity is also an Achilles heel. Both fibers, the sensing and the reference fiber are "intrinisic" sensing elements. Even though the reference fiber is isolated from the event which is to be monitored, its own environment (unless it is meticulously controlled) is causing subtle but noise producing effects at the output of the interferometer. Both fibers are responsive along their entire length and can introduce substantial amounts of noise in the signal being developed. Optical glasses have refractive indices which are temperature dependent (9). Length variations due to temperature are caused by differences in thermal expansion coefficients. Pressure changes can have an effect on the fiber geometry as well as causing density variations affecting the refractive indices. When two perturbations (temperature and pressure) cause the same type of signal to be developed in a sensor, it is known as cross-sensitivity and must be minimized. Other problems include; initial length variations, improper source to-fiber-to-detector coupling, and thermal anomalies associated with electronic and optical components. A more detailed discussion of these and other difficulties will be given in appropriate sections.

In the early eighties Eickhoff et al. investigated the use of specialty fibers known as bow-tie and elliptical core fibers (10). These fibers are made with a refractive index profile along the x and y radial directions of the

fiber that are not equal, these are known as a "birefringent" optical fibers (fig.4). When polarized light is launched at the correct angle into this type of fiber, light being transmitted can be resolved into two orthogonal components. These two energy modes potentially make up two arms of an interferometer, but are carried by a single fiber. Anisotropies in the thermal and mechanical properties associated with the refractive index profile along the fiber cause the light energy in each orthogonal mode to propagate at different rates. Perturbations to this type of fiber cause the phase in each energy mode to respond differently, and an interference signal is developed proportional to the disturbance. Several detection schemes have been developed to extract information from this configuration, ranging from the use of a single photo-detector to four photo-detectors (11). Theories behind the chemical and optical interactions associated with signal production in these "birefringent" fibers are a central part of the instrument developed in this research and will be addressed in greater detail.

B. Noble-metal Catalysis

Perhaps no other metal/gas system has been studied in more detail than the palladium/hydrogen combination (12). Initially, observations of the permeability of palladium to hydrogen were made by Deville and Troost in 1863. This and subsequent works, including the present research into "cold fusion" by Fleischman, Pons, and other researchers (13),

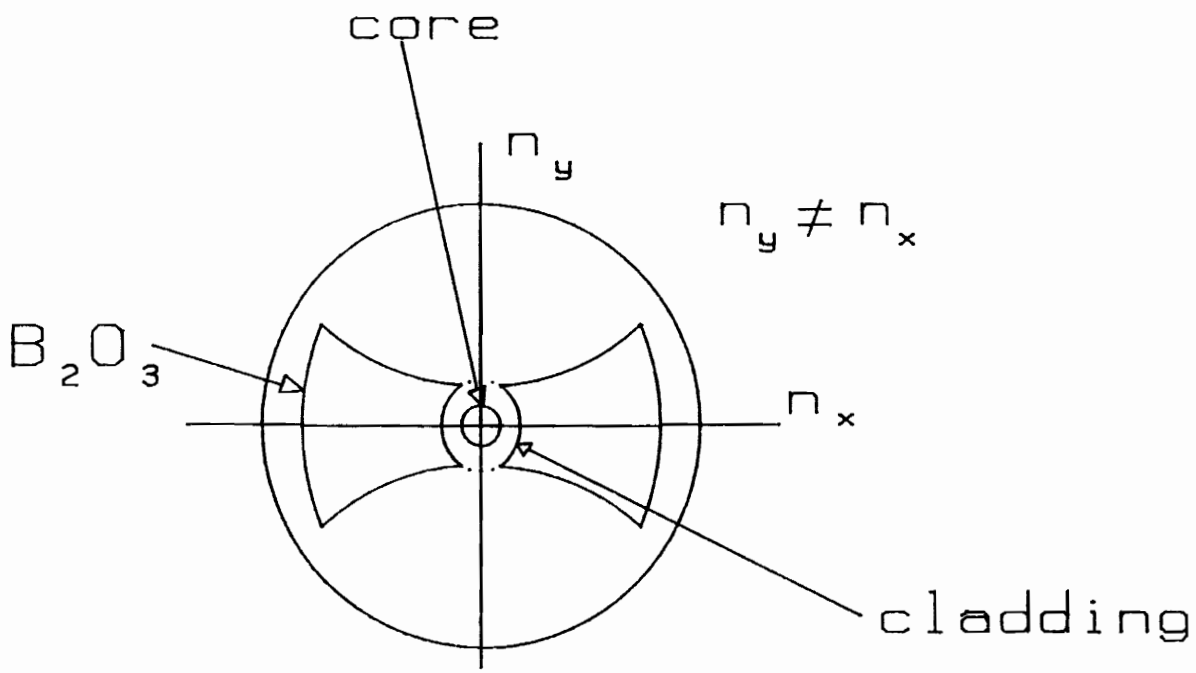

Figure 4. Bowtie fiber—refractive index profile

focuses interests into the mechanisms involved with this chemistry.

Early investigations were performed to better understand the pressure-composition-temperature curves associated with the introduction of hydrogen into a chamber containing palladium (14). Figure 5 depicts a typical result at a temperature of 30 degrees C. These experiments showed a consistent sharp initial increase in equilibrium hydrogen pressure and very little hydrogen/palladium loading. After achieving H/Pd ratios around 0.03, a plateau is established, which remains level until H/Pd ratios reached approximately 0.63. Hydrogen pressure then rose abruptly with a slight increase in gas to metal loading.

Interpretation of this shape has lead to labeling of the particular regions. Pure alpha hydride formation occurs during the early sharp rise. Along the plateau a transition is believed to be taking place from pure alpha hydride to beta hydride formation. Finally, the last sharp increase is indicative of pure beta hydride formation.

It would appear that at low pressure hydrogen does not permeate the metal lattice structure appreciably. When a certain pressure is attained (18-19 mm. Hg.) the lattice structure is forced to accommodate more H atoms. Measurements of the lattice spacing shows small but linear increases while the alpha hydride is forming. During the alpha to beta hydride transition an increase from 3.89 A to 4.03 A is measured (15). An overall increase as high as

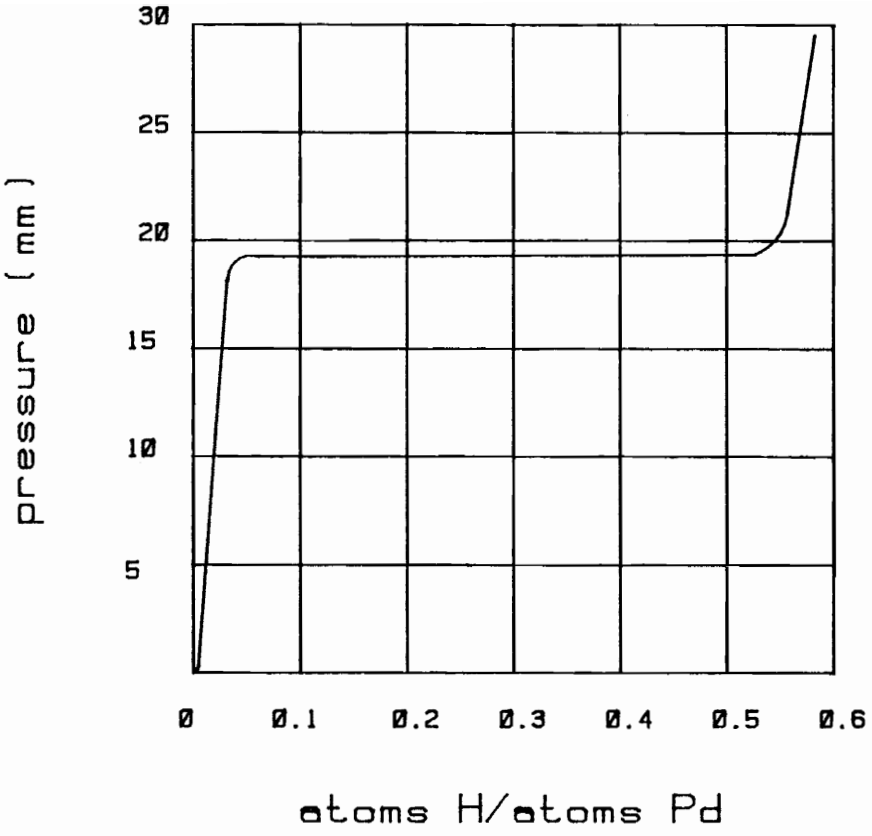

Figure 5. Typical isotherm at 30°C for hydrogen in bulk palladium

10% has been observed in the lattice spacings during beta hydride formation (16).

Free-standing palladium has a dimensional response to hydrogen content in the alpha phase which is related by

(1) $d = [(\text{delta } a)/a] = 0.026(x)$

where "a" is the lattice constant and x is the hydrogen content in the palladium. In the alpha phase the partial pressure of hydrogen follows Sievert's law and is related to x by

(2) $p^{1/2} = K(x)$

where K is the Sievert coefficient (7). Equations (1) and (2) describe the relationship between the partial pressure of hydrogen and the response of a sensor dependent on palladium lattice dimensions.

Diffusion is another parameter of interest which affects the way palladium responds when exposed to hydrogen. Studies by Jewett and Makrides gave mean values for the diffusion coefficient in the alpha and beta phases of (17):

$D(\text{alpha}) = 1.6*10^{-7}(cm^2/sec)$

$D(\text{beta}) = 1.5*10^{-6}(cm^2/sec)$

A constant diffusion coefficient would be required for the linear relationship between hydrogen pressure and the palladium loading seen at low pressures of hydrogen.

Effects of cleaning the palladium surface, for determining its effect on the permeation rates, was also investigated. Surfaces were alternately oxidized by heating in

air and then reduced by exposure to hydrogen. An alternate procedure, where a thin layer of palladium black was electrolytically deposited on a palladium membrane and then exposed to oxidation/reduction gave the best reproducibility. Simple degreasing and rinsing with distilled water gave permeation rates which were 5 orders of magnitude lower than the rates obtained with oxidation/reduction cleaning techniques. These results indicate that the dissociation of molecular hydrogen on palladium is inhibited by contaminants, especially at room temperatures (17).

Heats of absorption of hydrogen on palladium were investigated in the thirties and again in the late fifties (18,19). Results were in general agreement. In this research the heat of reaction for:

$4Pd + H_2 \rightarrow 2Pd_2H$

will be taken to be -9605 cal./mole. Other heats of reaction which will be of interest are the following :

$2Pd_2H + 1/2O_2 \rightarrow H_2O + 4Pd$ -9600 cal./mole

$H_2 + 1/2O_2 \rightarrow H_2O$ -57,800 cal./mole

These exothermic reactions will be examined as possible sources for a transduction mechanism related to the sensor developed in this research. Recent investigations have focused much attention on the results obtained by Fleischman and Pons (20). In their experiments, extreme electrolytic loading of palladium with deuterium was apparently achieved. Large amounts of anomalous heat production were reported. Claims were made that attributed the heat gener-

ation to "fusion" at room temperature. At present many investigators have been unable to confirm their results. But the implications of such a possibility are of enormous importance and will continue to fuel interest in H/Pd chemistries. This work would have been incomplete without an attempt to compare the sensor response to hydrogen and deuterium.

III. Instrument Design

A schematic of the basic instrument configuration is shown in figure 6. This instrument is designed in three major sections. Only light is coupled between separate areas. This gives freedom from unwanted perturbations such as mechanical coupling of vibration, and allows for efficient alignment procedures.

Any sensor based on fiber optics must meet several stringent requirements. Interferometers are sensitive to environmental factors (temperature, pressure, and vibration), therefore isolation is important. All of these perturbations can impact the refractive index profile of a fiber. Minimizing all responses except the one of interest is important. However, this should be balanced with an ability to manipulate instrument parameters easily. Discussion of each major section, its purpose, and functional form follows.

To help with vibration, alignment, and support problems, this instrument is mounted on Newport Research Corporation optical air table (4'x10'). All equipment was designed to mount on this table using 1/4-20 bolts mounted in threaded holes centered 1" apart on the table surface.

A. Laser Launching Components

The final instrument configuration is based on kinematic principles (21). There are six degrees of freedom for a rigid object. They are translation along x, y, and z axes

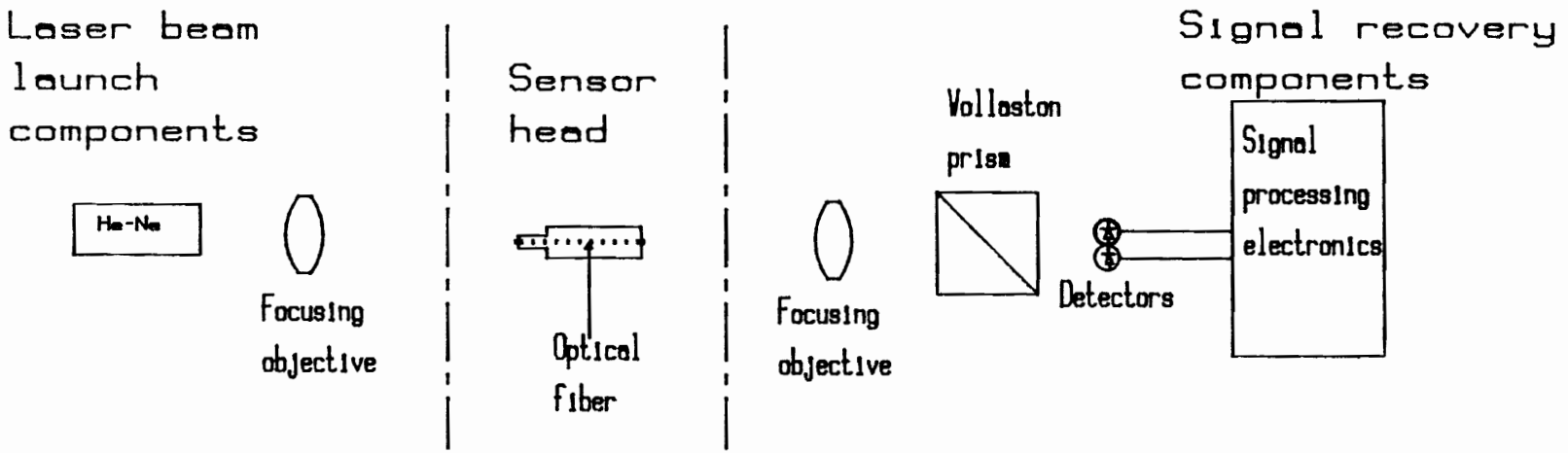

Figure 6. Basic instrument layout

and rotation around these axes. Different motions of an object can be considered linear combinations of these six basic movements. By constraining points on an object to remain in contact with a support surface, it is possible to restrict the degrees of freedom. An example is shown in figure 7. Here the laser tube used in this research (Spectra Physics Model 105-1) is mounted in its support bracket. The ability to rotate this laser was an initial requirement. This would allow the plane of polarized light from the laser to be varied around the z-axis. Because stringent alignment is needed between the laser light and optical fiber input, the v-block and yoke structure restrict movement of the tube in two translational planes, x and y. Also, end-to-end rotation in all three planes has been minimized. Translational motion and rotation, along and around the z-axis, are the only free movements allowed. While movement along the z-axis can be tolerated, it is eventually eliminated by butting the dust snout of the laser tube against the fiber input launching stage.

In order to facilitate initial instrument start-up and experimental reproducibility, a circular protractor is placed around the laser tube. This allows orientation of the desired plane of polarization from the laser. Determination of the vertical laser polarization plane is done by focusing the laser onto a polarizer and measuring intensity at different polarizer rotation angles. Vertical polarization corresponds to 0^{o} and maximum intensity passing

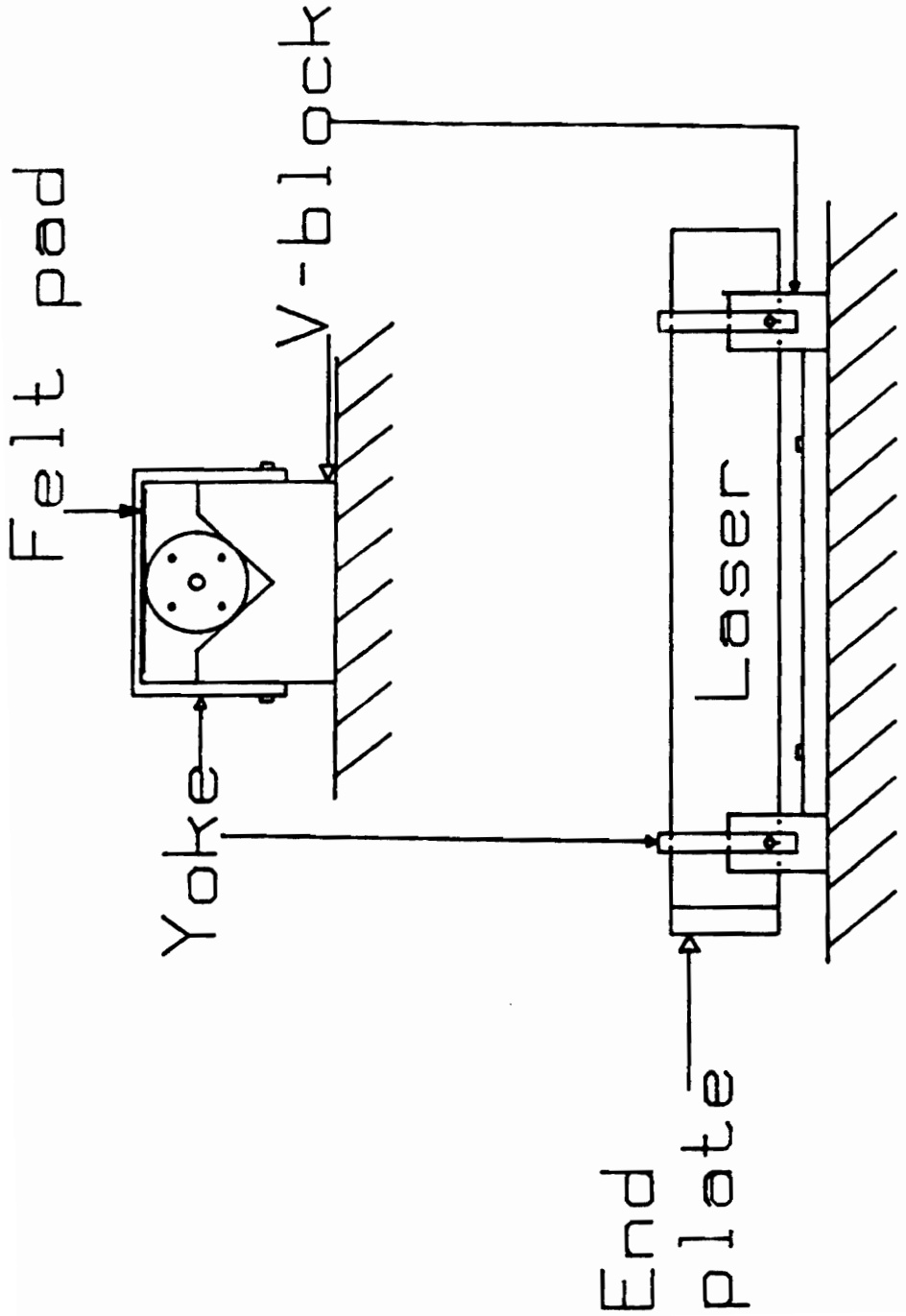

Figure 7. Laser support structure

through the polarizer set at 0^{o}. Marks were placed on the tube, establishing polarization planes associated with the laser (0,90,180,270 degrees).

Proper alignment of the laser and optical fiber is achieved initially by butting the output end of the laser tube to the fiber launching stage. Holes were drilled in both laser and launching stage endplates (figures 7 and 8). When mated with screws these endplates center the laser beam in proper vertical and horizontal planes. At this point the focusing objective and fiber input translation stage, which are attached to the launching stage, are then properly coincident with the beam. After this, the laser support bracket and yokes are bolted in place. Then the launching stage is secured. It has brackets which allow vertical and horizontal adjustment to maintain proper alignment without placing stress on the tube or stage.

Dust particles can cause severe scattering problems and these are alleviated by use of a dust snout. The initial setup is completed by separating laser and launching end plates to allow insertion of the snout. It is a black tube attached to the laser endplate. When the snout is in place, the laser is moved forward to mate with the launching stage, allowing the laser to remain properly aligned, with minimal interference from dust.

Figure 8 depicts the component orientation associated with the launching stage. Modification of this stage (Newport Research Corporation Model FP-2) was done to allow the

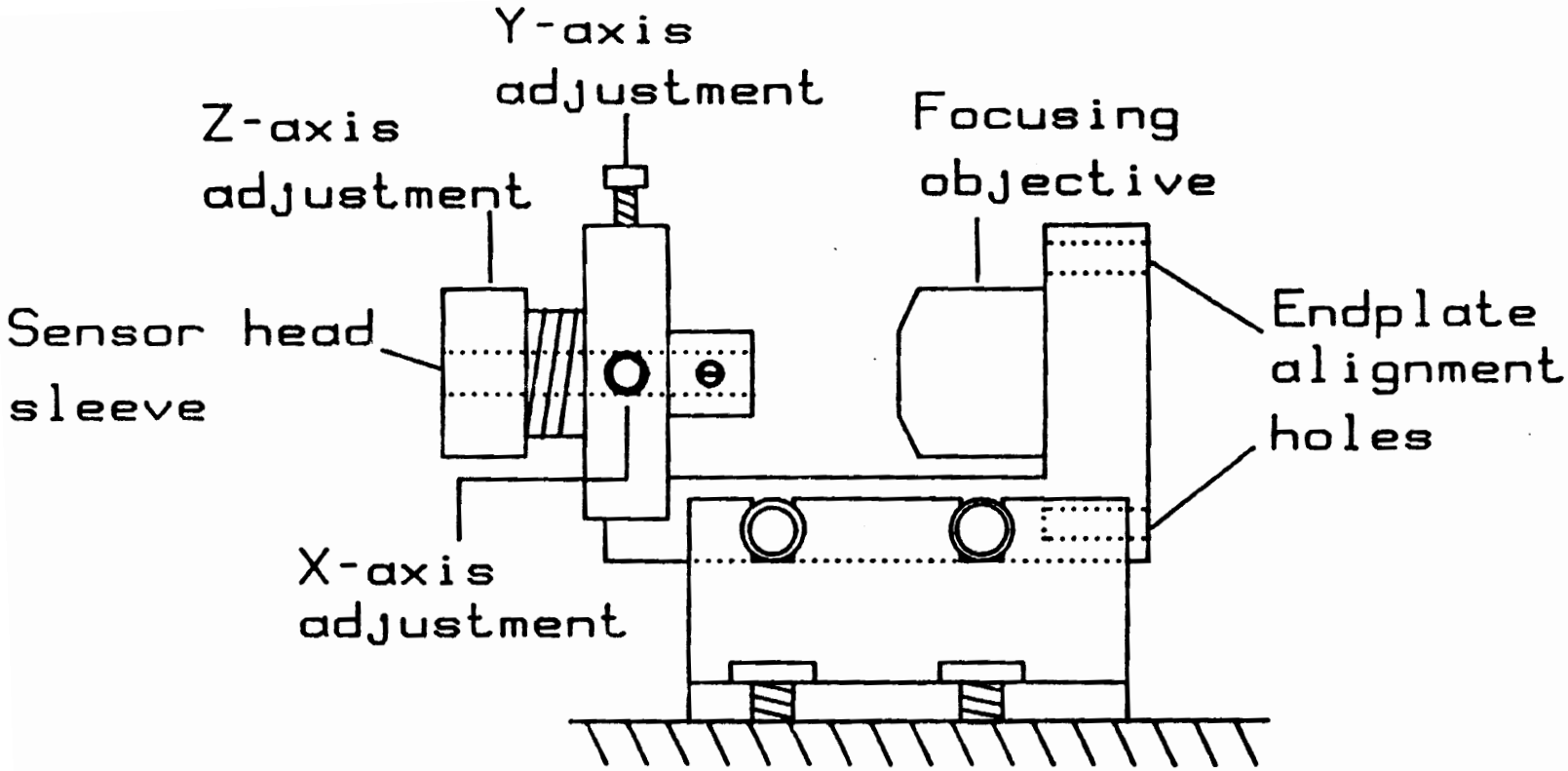

Figure 8. Launching stage
(side view)

alignment discussed in previous paragraphs. Proper focusing of the laser light beam is performed using a microscope objective with a numerical aperature of 0.25. Actual translation of the fiber input end, is performed by an x-y-z manipulator (NRC FP-2). Mounted in the center chuck of this manipulator is the narrow end of the sensor head (figure 9), which houses the sensing fiber . By adjusting either the x-screw and/or y-screw, the fiber input can be manipulated in a vertical plane normal to the fiber axis. Translation along the z-direction is controlled using a collar screw-type adjustment.

There is also a support bracket (figure 10) for the output end of the sensor head. When the sensor head is mounted in both supports, springs associated with the output support bracket allow the input translation stage to move without binding. Figure 11 shows the sensor head mounted in its working position with both supports in place.

B. Sensor Head

Mounted in the aluminum block shown in figure 9 is the sensing optical fiber. A specialty optical "bow-tie" fiber manufactured by Newport Corporation (F-SPV-10) was used in this research. Figure 4 shows the geometry and dimensions of an unjacketed "bow-tie" fiber. Compare this with figure 1 which depicts a "normal" optical fiber. How the fiber plays a role in the overall sensing mechanism is discussed in sections dealing with transduction processes.

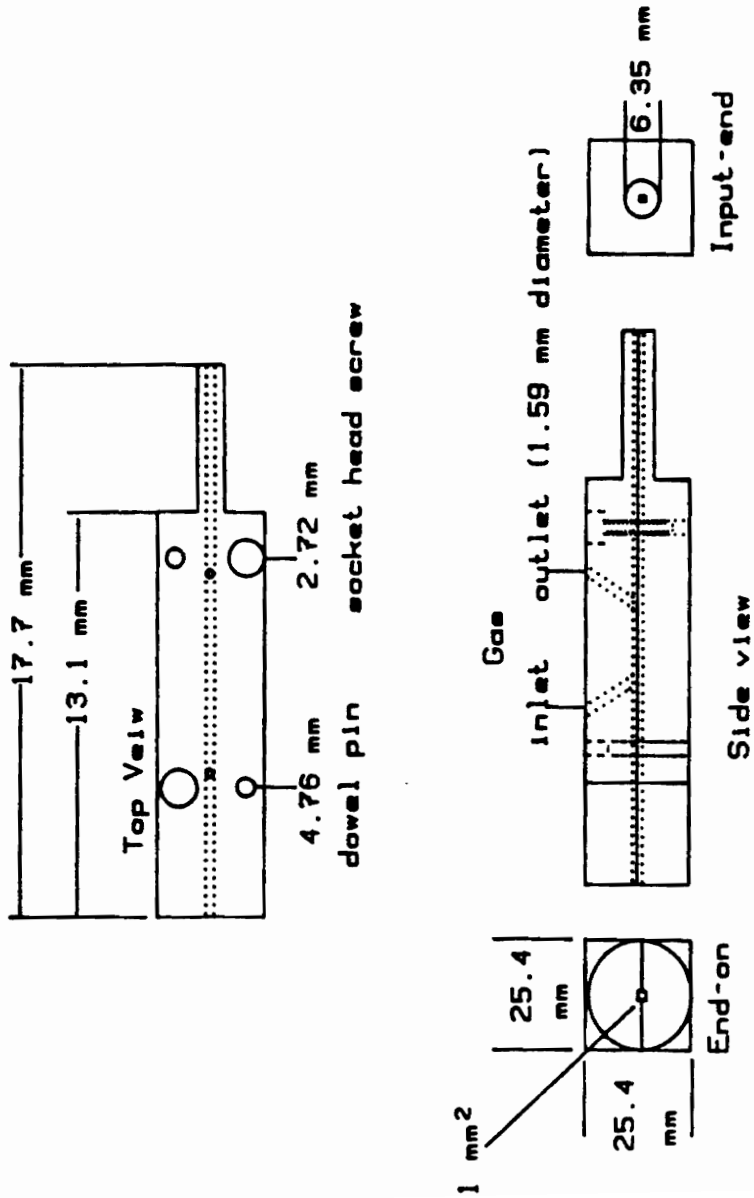

Figure 9. Sensor head

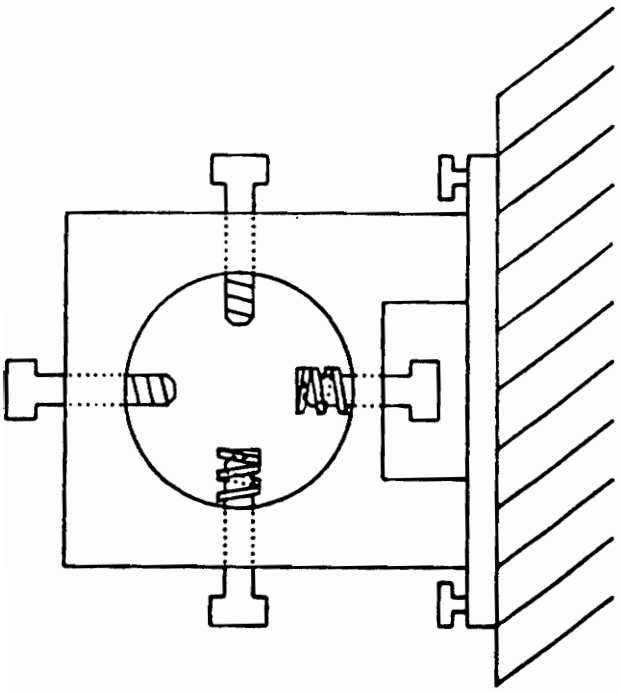

Figure 10. Sensor head output support bracket

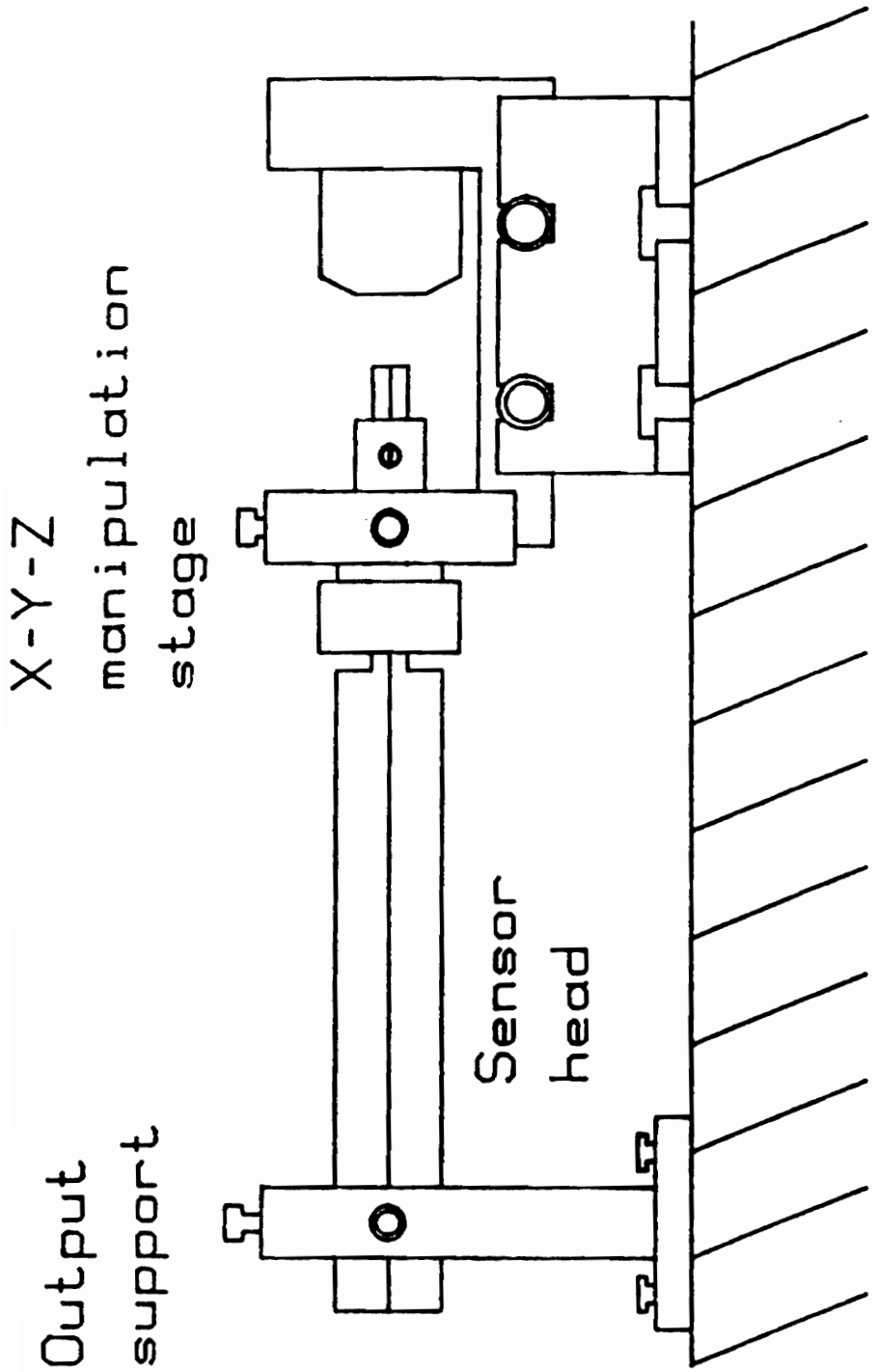

Figure 11. Sensor head mounted

It is important to understand that these fibers are very sensitive to uneven pressures that may be imposed by the manner in which they are mounted. A channel is machined in each half of the sensor head from end to end. Approximately 4 cm on each end of this channel, in both halves, is filled flush with high temperature lubricant. Mounting the sensing fiber in this material allows stability in the output signal but does not cause significant variations from fiber to fiber (see results section). These variations can be caused by bends or pressure points on the fiber from less forgiving mounting materials which may develop stresses upon curing.

Construction of a sensing element begins with measuring a 23 cm length of fiber. Double sided sticky tape is placed on the horizintal edge of a work bench. First, press approximately one inch of the fiber perpendicular to the workbench and onto the tape. By placing single sided tape over the fiber, a secure fiber holder is made. A ruler is then aligned with the end of the secured fiber and placed parallel to the fiber. The ruler is also taped in place on the bench edge. Measuring 7.6 cm from the secured end of the fiber, a razor blade is used to strip away approximately 7.6 cm of the outer plastic jacket toward the unsecured end of the fiber. As the unjacketed fiber is only 125 microns in diameter and made of glass, great care must be taken with this and subsequent preparation procedures.

Once initial stripping has been accomplished, vapor

deposition of palladium can be done. A Denon Model-15 vacuum vapor deposition chamber was fitted with a specially constructed jig (figure 12) to hold the fiber over a tungsten wire basket containing 7.6 cm of 0.25 mm diameter palladium wire (99.9% Aldrich #32,669-0). One half of the fiber is coated, then manual rotation of the fiber by 180^{o} was done to coat the remaining half of the fiber using another tungsten wire basket and palladium. Double coating was performed to develop a thicker film, but yielded unsatisfactory results. A single coating was eventually found to be the optimum coating thickness (60 angstroms, approximately 2 ug).

Platinum deposition was performed in an Edwards sputter coater Model S150B. A 50 mm x 50 mm x 0.025 mm platinum foil (99.9% Aldrich #26,724-4) was used as a target. An apparatus was constructed as a fiber holder (figure 13), which would allow 180 degree rotation, coating both sides of the sensing fiber. Sputtering times were varied. The optimum time (see results) appeared to be approximately 2 minutes per side at 40 ma of electrode current. This gave a coating of approximately 300 angstroms of platinum.

Thicknesses were estimated based upon conversations with the sputtering and vacuum equipment manufacturers. Scanning electron microscopy and weighing techniques are used to measure the thickness of sputtered and deposited films.

In order for the sensing element to guide light effi-

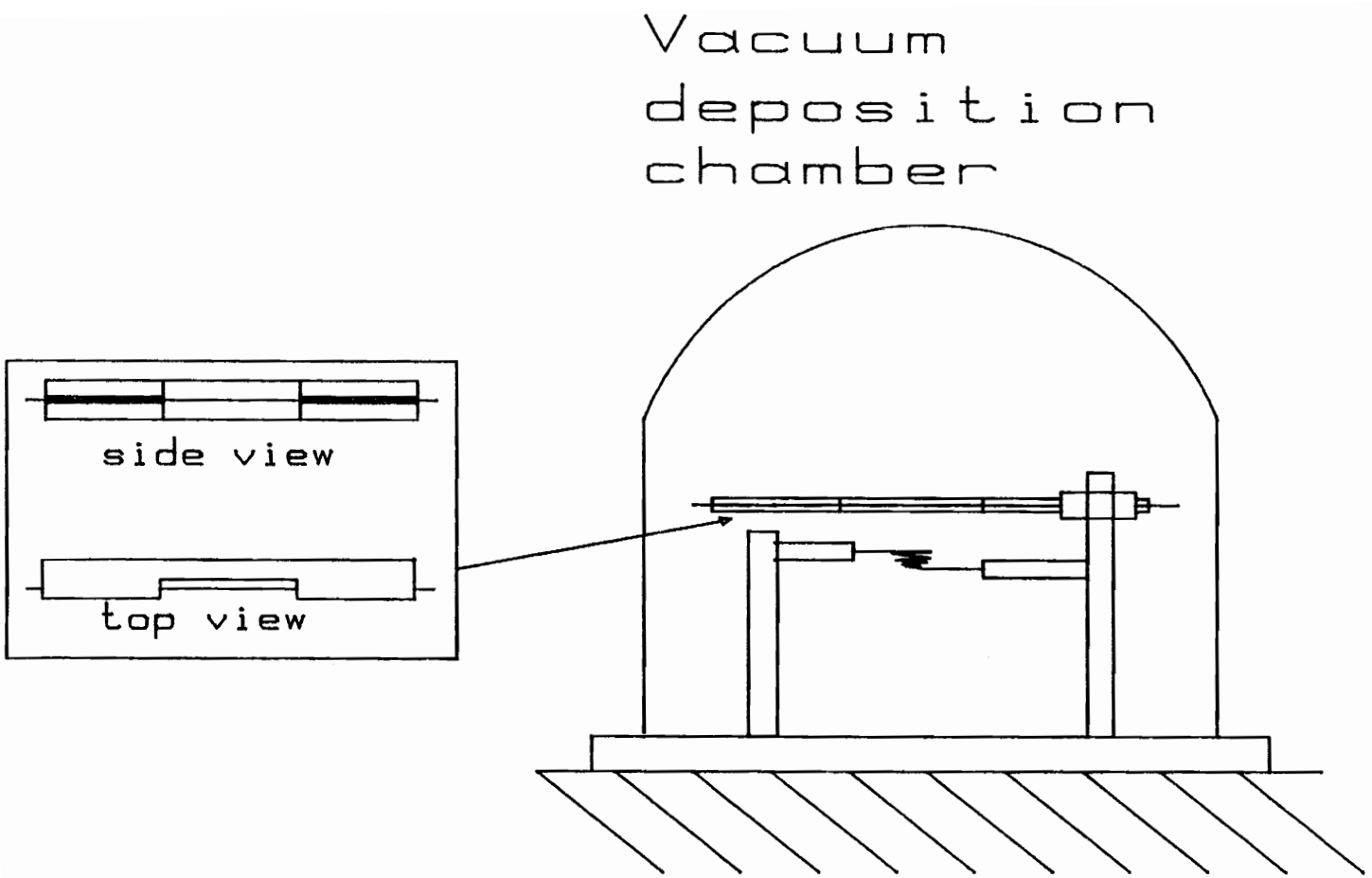

Figure 12. Vacuum depostion chamber and fiber jig

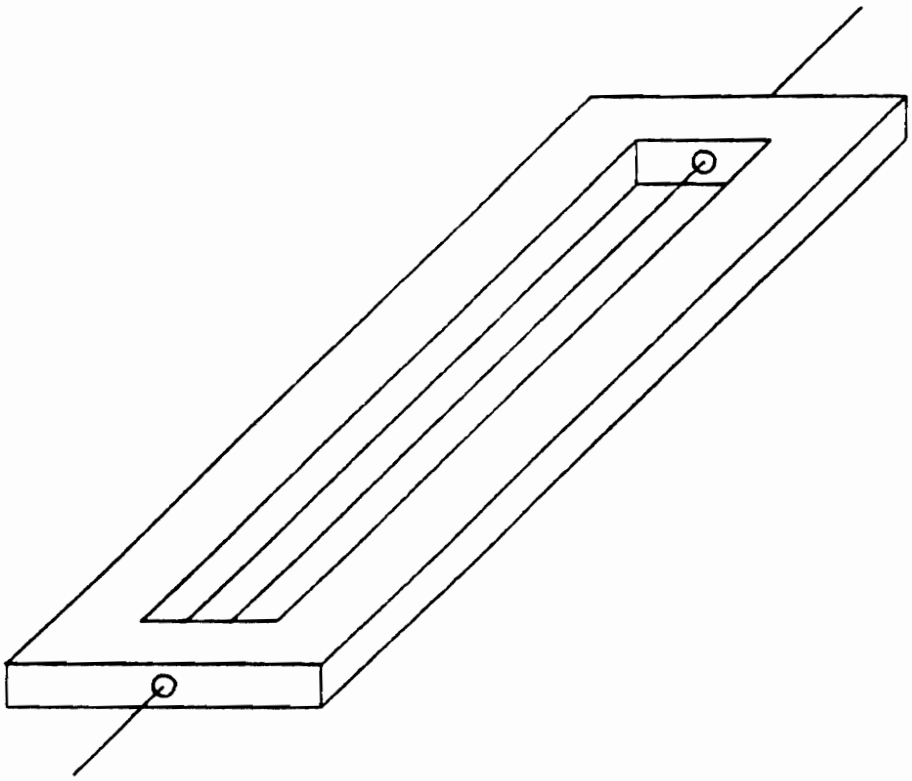

FIGURE 13. Sputtering jig

ciently, it must have both the input and output ends of the fiber cleaved as optically flat and imperfection-free as possible. This allows light to be properly focused on the input and at the output fiber ends without scatter or depolarization effects.

After the catalyst system has been deposited, the fiber is ready to be trimmed to the proper length and cleaved. Once again the fiber is mounted in a secure tape holder as described above. Measuring 2.2 cm from secured end of fiber, strip away 0.6 cm of outer plastic jacket. A diamond tip cleaver (Amp PN 228793-1) is gently drawn across the fiber where the distal end of the stripped fiber and jacketed fiber meet. By maintaining a slight pull on the unsecured end of the fiber a proper cleave is achieved. Rotate and mount the opposite end of fiber, and perform the same stripping and cleaving procedures as before to complete preparation of the sensing element.

The fiber is now ready to mount in the sensing head. This is done by aligning the fiber center with the sensor head channel, being careful not to get lubricant on the input or output ends. By smoothing over the surface with a spatula, the fiber is pushed gently down and a flush surface is prepared. Mating of the opposite half of the sensor head will not cause undue pressure points. Bolting of both halves completes the sensing fiber mounting procedure. When done correctly a small length of fiber should be visible at each end of the sensor head.

Gas is brought to and from sensor head by 1/16 inch Tygon tubing attached to 1/16 inch polypropylene elbow fittings inserted into holes drilled in the sensor head. Gases are mixed in a metal tee after exiting from their respective rotameters. A Matheson Model 602 rotameter is used for hydrogen flow control. Carrier gas flow (nitrogen or air) is controlled by a Matheson Model 603 rotameter . All gases used were prepurified and terminally filtered using dessicants- 5 angstrom molecular sieve, and activated charcoal. A DEC LSI-11 computer was used to control release of hydrogen into the carrier stream via a reed relay and a two port gas solenoid (5V coil). Programs for control were written in Polyforth and are in Appendix A.

C. Signal Recovery Components

A transducer is only good if the information it can provide can be interrogated in a manner which is efficient and reliable. In this instrument a combination of optics and electronics performs this task.

Polarized light exiting from the sensing fiber is a vector quantity and can therefore be resolved into two orthogonal electromagnetic vibrations (see transduction mechanism). In this interferometric instrument, the beam exiting from the fiber is focused by a microscope objective onto a Wollaston prism, which splits the beam into its two components. These two beams are directed at two photodiodes (Silicon Detector Corporation Model Sd-290-12-22-241) mounted side by side. All three components

nents, objective, Wollaston, and detectors are mounted in a black Delrin tube (figure 14). Because it is necessary to rotate the Wollaston around the z-axis (light path axis), a circular positioner (Newport Research Corporation Model RSA-2) was modified to accept the black detector tube. In order to assure correct alignment with the signal beam, the circular postioner was attached to a specially designed platform (figure 15). This platform is allowed to translate in the x and y directions in a plane perpendicular to the light beam path. For a discussion of the Wollaston prism and its unique light guiding properties, see the appropriate sections discussing signal recovery.

Electronic recovery of the detector signals is performed by a circuit (figure 16) whose final output is the difference between signal intensities from each detector divided by the sum of both intensities (see signal recovery section). This signal is digitized by a 12-bit analog-to-digital converter and stored using a DEC LSI-11 running a Polyforth operating system and programed in Polyforth. Program listings and a brief description of their functions are listed in Appendix A. Transfer programs were written to take data from DEC TU-58 storage media to 5-1/4 inch storage media. This allowed use of several different proprietary software packages for data analysis. These included Lotus, Spia, Generic Cadd, and Asystant.

Alignment procedures for the electronic circuit are discussed in reference "22". Optical alignment is dis-

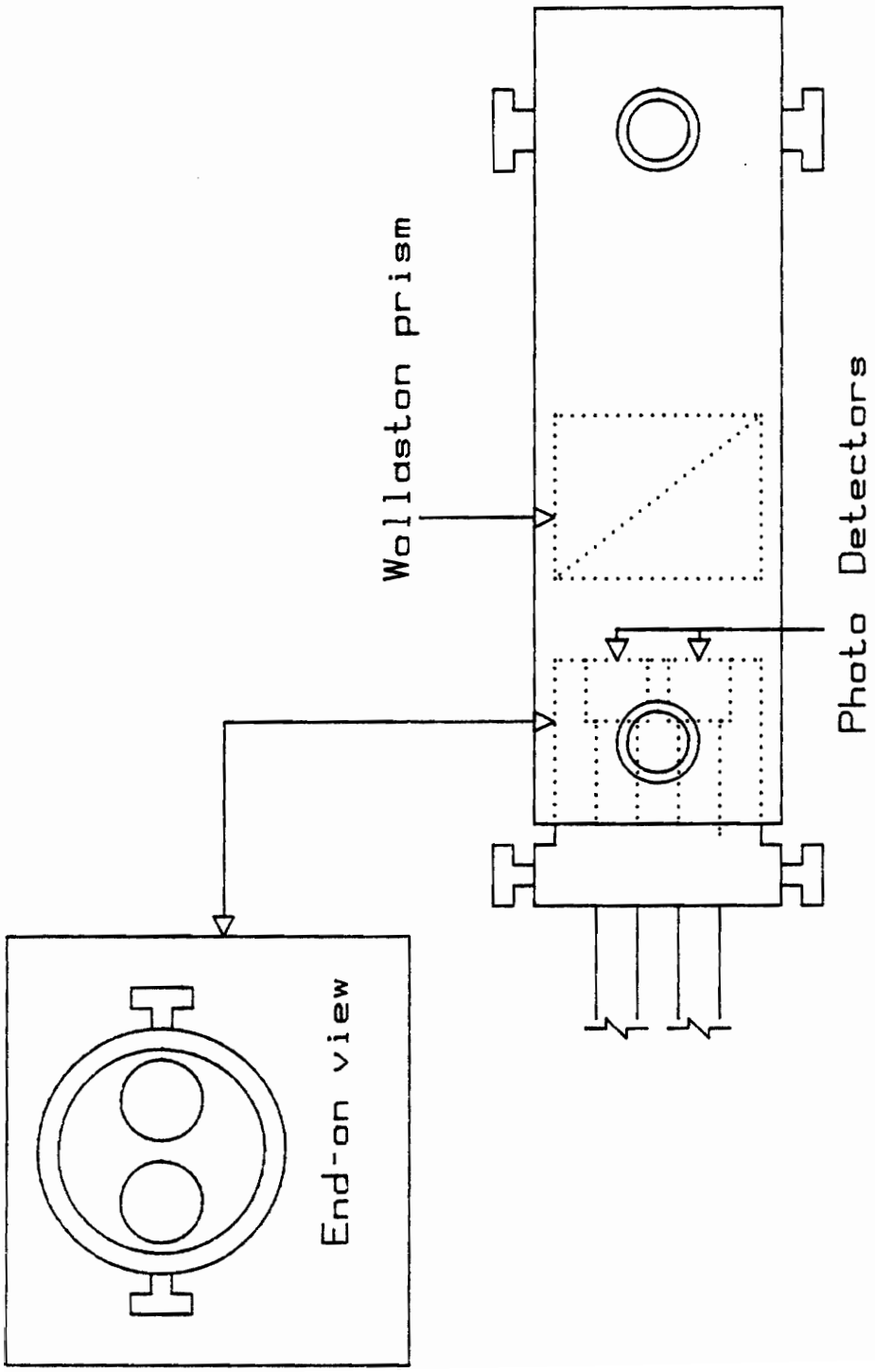

Figure 14. Wollaston and detector tube

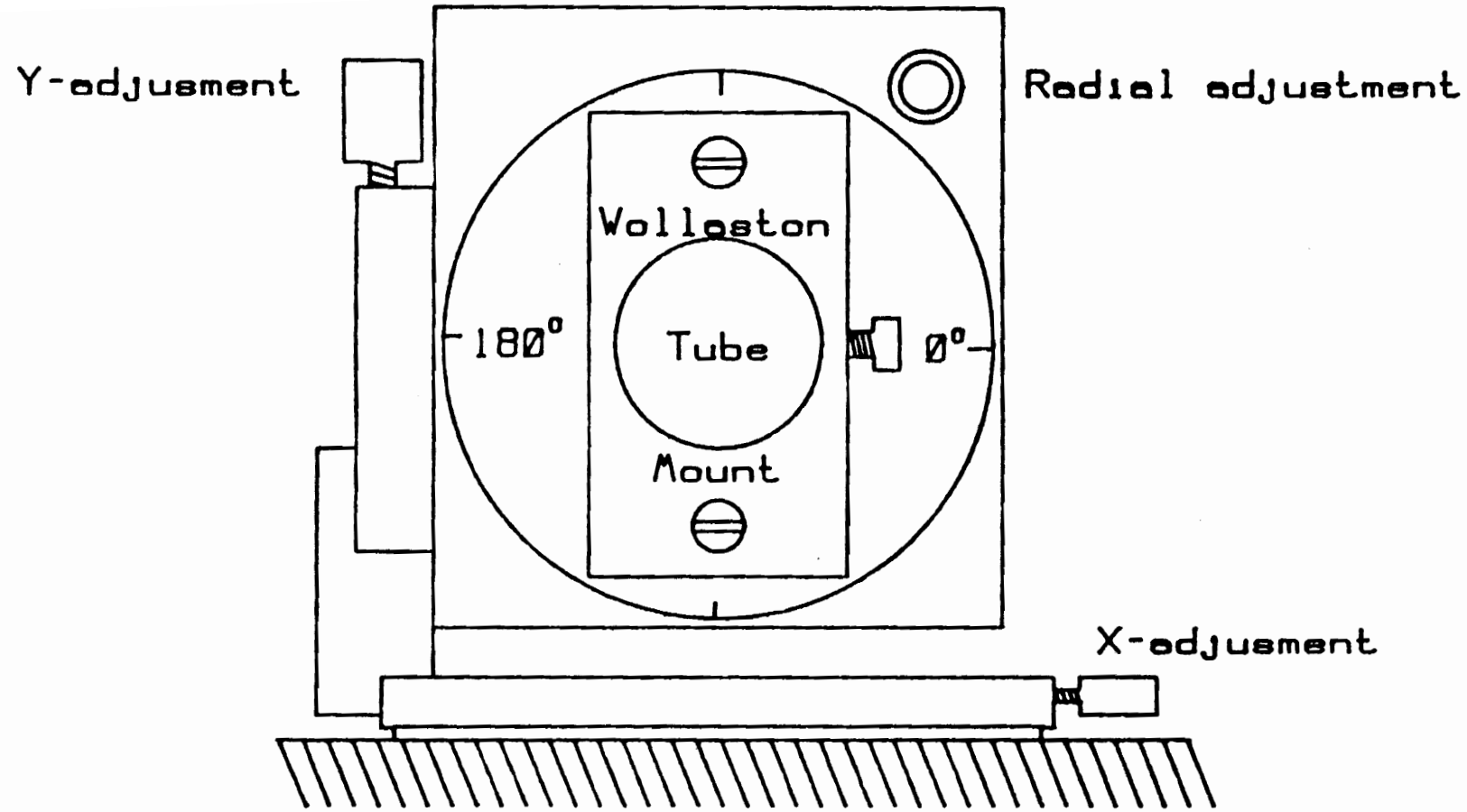

Figure 15. Wollaston positioner (light path is perpindicular to drawing plane)

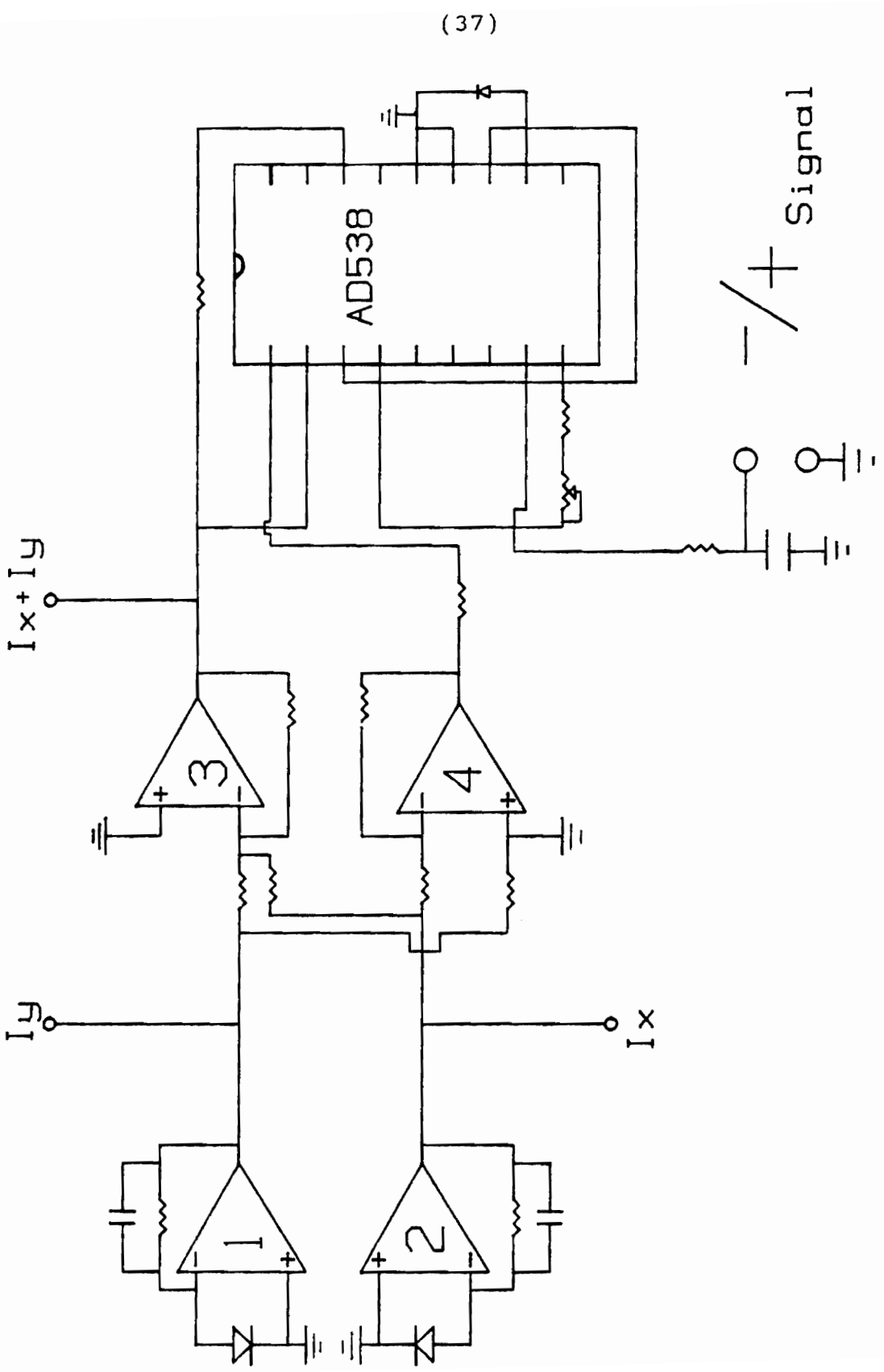

Figure 16. Amplifier schematic

cussed in the optics and experimental sections.

IV. Catalytic Chemistries

The sensor in this research develops a signal in response to heat evolved from catalytic reactions isolated on the surface of the birefringent optical fiber. To characterize the processes which are taking place in the optical fiber, a chemical system was chosen, whose behavior was well established. This allowed the research to focus on developing and understanding the transduction mechanism within the birefringent fiber. Therefore, although the goal of this research was to develop a general purpose thermal sensor, this work will now describe and discuss the chemical test system.

Figure 17 shows the layered structure of the sensing element. Palladium and platinum were chosen because of their ability to activate molecular hydrogen (H_2gas --> 2H). Palladium and platinum films of different thicknesses were examined to determine optimum sensor configuration. The values shown in figure 17 represent the optimum thickness. Use of this hydrogen/noble metal catalyst system , as a probe, provided insight to guide experimentation and theoretical development of the instrument.

Palladium itself has been seen glowing red in the presence of oxygen and hydrogen. It is also well known for its ability to solubilize or "occlude" large quantities of hydrogen gas (23). A sensing element with only palladium deposited on the optical fiber was tested . While this

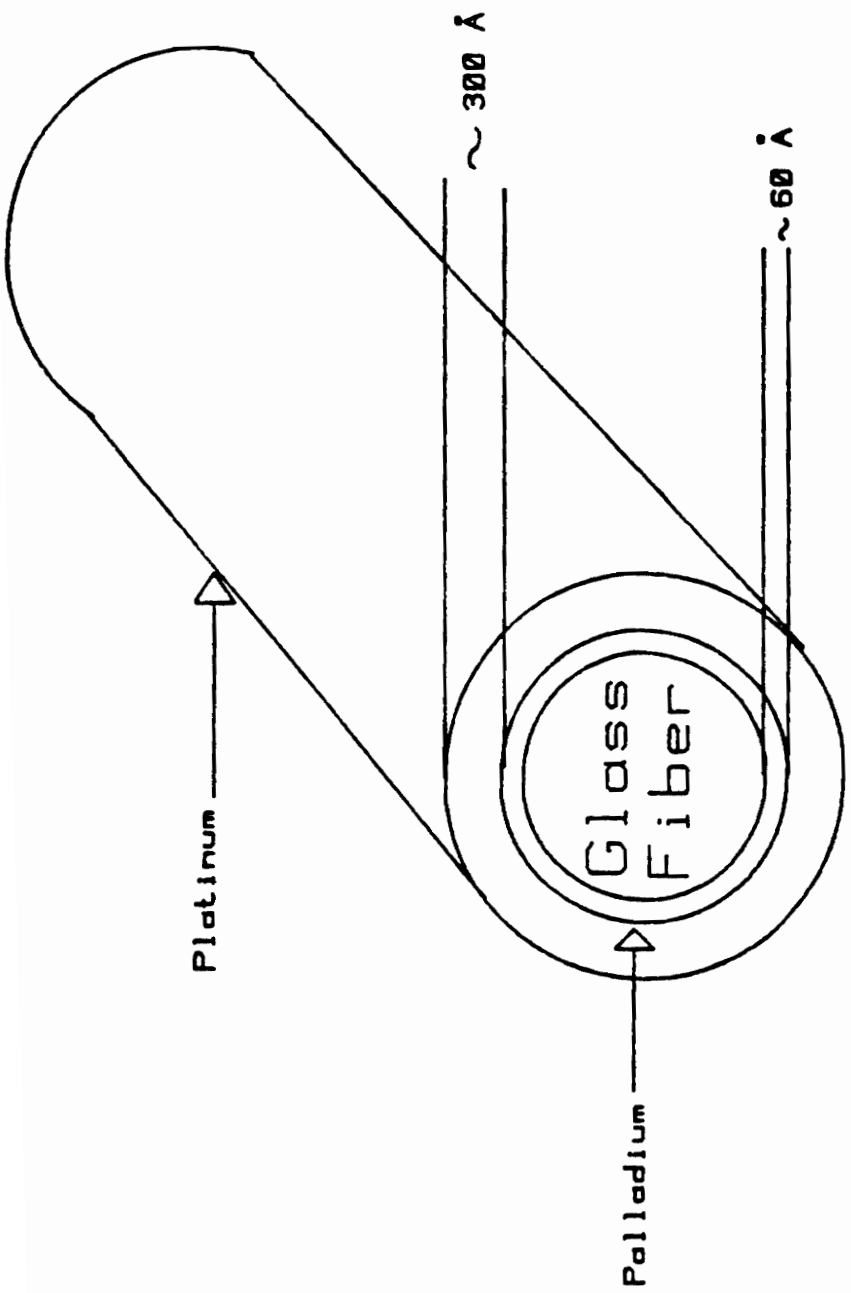

Figure 17. Sensing fiber cross-section

single layer palladium element detected the presence of hydrogen gas initially, its signal deteriorated within twenty-four hours. In contrast, a platinum and palladium element remains effective for several days.

Platinum is used as a sensitizing element in solid state metal oxide semiconductor gas sensing detectors (24). Studies have shown that platinum activates molecular hydrogen to a greater extent than palladium. In this instrument, the platinum layer thickness must be optimized to allow diffusion of atomic hydrogen into the underlying palladium layer. Use of platinum alone on the birefringent fiber displayed an output which was not useful for characterizing the birefringent fiber. Reactions which are associated with the platinum surface are not believed to be the reactions which produce the final sensor output (see below).

Several reactions are taking place on and in the surface of the sensing element (25,26):

1) H_2gas --> $2H_A$ ("A" implies adsorbed state)

2) O_2gas --> $2O_A$

3) O_A+ H_A --> OH_A

4) OH_A + H_A --> H_2Ogas

5) $2H_A$ --> H_2gas

6) $4Pd + H_2$ --> $2Pd_2H$ (ratio H/Pd is normally <1)

Figure 18 shows the evolution of a typical sensor signal and the associated chemical processes taking place at both the surface of the platinum and in the palladium layer.

Reactions 1-5 take place at the surface of the platinum (27). Reaction 6 describes the ability of palladium to preferentially adsorb hydrogen atoms and form a hydride phase. The hydride phase composition varies from low ratios of hydrogen/palladium stoichiometry to larger values . An alpha hydride phase is described as ratios up to about 0.03 hydrogen atoms per palladium atom. Beta phase hydride formation begins around 0.55 hydrogen atoms per palladium atom. In figure 5, the alpha and beta regions are basically at the begining and the end of the isotherm. The plateau represents the transition from the alpha to beta hydride formation. This reaction is reversible and is responsible for the specificity of the sensing element. Overall the entire process is exothermic and produces sufficient heat to allow detection of hydrogen due to the effect of heat on the transmission characteristics of the birefringent optical fiber.

Several reactions are competing for the hydrogen atom. Activation of molecular hydrogen and its dissociation into atomic hydrogen is represented in reaction 1. Reactions

2-4 show the formation of water. Reaction 5 depicts the tendency of an adsorbed hydrogen atom to return to the molecular gaseous state from the metal. This reaction has been shown to be slow even at 150 ^{o}C and is highly exothermic (470 kJ/mole) (25). The initial and final stages of the sensor output are effected by these first five reactions as shown in figure 18.

Palladium hydride is formed in reaction 6. Although the bonding is formally shown as having integral stoichiometry, it is normally fractional. This depends on the loading of the palladium with hydrogen (H/Pd). Values for hydrogen to metal content can reach unity under extreme pressures (28).

Bonding in the palladium hydride is believed to be covalent because of the decrease in magnetization of the metal upon exposure to hydrogen (29). An unpaired d-orbital electron in the palladium is paired off with the unpaired electron in the hydrogen atom decreasing the magnetization of the metal. There is still debate about the possibility that the hydrogen atom may give up its electron at the surface of the metal and enter the lattice as a proton (29).

The left side of figure 18 depicts a pristine catalytic structure. Only air has been allowed to come in contact with the sensing element. Because of this, the surface is covered with oxygen atoms. Oxygen blocks the adsorption of hydrogen into the platinum and subsequently into the palladium lattice. Competition for the active sites on the platinum surface between H_2(gas) and O_2(gas) determines which

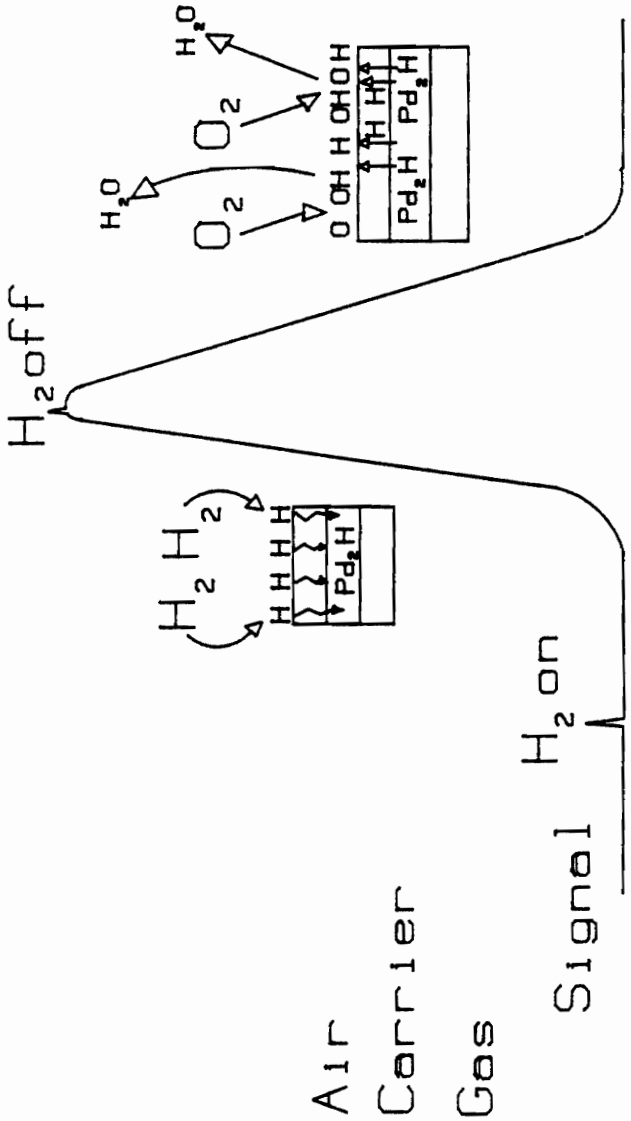

Figure 18. Sensor signal development

of the reaction, 1-6, become dominant.

It is possible that molecular hydrogen (gaseous) and atomic oxygen (adsorbed) could react to form water. But experiments by Harris et al. have shown that this process is unlikely (27).

Studies performed by Petersson et al have shown the probability of a hydrogen atom becoming incorporated into a water molecule is 0.7 on an oxygen covered surface at 373 K (30). They have also shown the formation of water to be temperature dependent (thermally activated). At room temperature the probability of hydrogen atoms forming water with oxygen on a metal surface is slightly less than 0.7. On the oxygen covered surface of platinum the overall reaction taking place with the hydrogen atom is the formation of water.

The formation and evaporation of water has a cooling effect on the sensing fiber. Water formation is limited to the amount of pre-adsorbed oxygen atoms on the surface of the platinum and to the competition between hydrogen and oxygen adsorption.

Experiments have shown the sticking coefficients for molecular hydrogen and molecular oxygen to be 0.62 and 0.38 respectively (31). Sticking coefficients are a measure of the ability of the adspecies (hydrogen or oxygen) to adsorb to a metal surface.

In an air carrier gas stream the platinum surface is covered with oxygen molecules. Hydrogen is introduced and

begins to disassociate forming water with the adsorbed oxygen atoms. As the adsorbed oxygen layer is depleted, hydrogen atoms, because of their higher sticking coefficient, start to cover the platinum surface. Due to the diminishing oxygen coverage, hydrogen atoms diffuse through the platinum layer and into the palladium forming palladium hydride (reaction 6). Eventually, the oxygen coverage is depleted. Hydrogen atom dissociation, diffusion and palladium hydride formation dominate the processes taking place on and in the sensing element. Palladium hydride formation is exothermic (40 kJ/mole) and the sensor signal begins to respond to the evolving heat.

Heat from reaction 6 is believed to be a major contributer to the signal shape and amplitude shown by the optical fiber catalytic sensing element. This conclusion is based on the following experimental observations :

1) A signal is developed from the sensor in air, and in oxygen-free nitrogen carrier gases. Without oxygen, water formation cannot take place.

2) Hydrogen desorption (reaction 5) is exothermic, but very slow.

3) If reactions 1-5, which take place on the surface of the platinum, were responsible for heat evolution, the palladium layer would not be required. Experiments have shown that the palladium layer is essential.

4) The kinetics for reaction 6 must be considerably faster than both those for water formation and desorption.

If not, the other reaction which evolves heat, palladium hydride formation, would not take place. Diffusion of hydrogen into palladium has been shown to be very fast (17). This prevents reactions 2-5 (water formation and hydrogen desorption) from taking place in significant amounts in a hydrogen containing air sample stream.

After hydrogen is removed from the air sampling stream, reactions 2-5 play a large role in the sensor's return to baseline (fig.18). As less hydrogen is available to diffuse into the platinum and palladium from the sample gas stream, oxygen begins to cover the platinum surface. Oxygen in turn reacts with hydrogen atoms diffusing back out of the palladium to the platinum surface forming water. In the flowing gas stream water desorption causes a cooling effect and the sensor's return to baseline.

In an oxygen-free nitrogen carrier gas stream, there should be a slower return to baseline because of the absence of water formation and no cooling effect. Baseline return is eventually established by hydrogen desorption processes. These are exothermic and slow, which contributes to the length of time required to return to baseline (see experimental).

Other factors which may play a role in the kinetics of reactions 1-6 are the effects of catalyst sample morphology, surface contamination and palladium lattice energies.

Surface contamination and changes in structure have been shown to inhibit the dissociation of hydrogen on pal-

ladium (17). In this sensor the platinum layer not only disassociates molecular hydrogen but protects the palladium from contamination by impurities in the gas stream.

Experiments with very thin layers of palladium have shown that the critical temperature value for dissolved hydrogen is less than 300 K (32). In bulk palladium it is 560 K. Critical temperature is the temperature above which a gas can no longer be condensed to a liquid or liquid-like state. In very thin films (less than 500 angstroms thick) there is a different characteristic shape for the adsorption isotherm (figure 19). Adsorption isotherms for hydrogen in palladium represent graphically the function of the ratio of hydrogen to metal content called loading. Loading can be measured in solution, electrolytically (32). In figure 19A (bulk palladium) there is a plateau region, in figure 19B (60 angstrom palladium film) this plateau is absent. A plateau is indicative of hydrogen to hydrogen interactions in the palladium lattice which show a gas to liquid-like transition. This region indicates a transition from alpha-Pd_2H to beta-Pd_2H formation. The beta-hydride has the highest loading ratio.

The shape of the thin film isotherm is interesting. Signals produced by the optical fiber catalytic sensor should have similar shapes (see experimental). Signals from the sensor are caused by the heat of reaction associated with the formation of palladium hydride. Both the sensor output and the thin film absorption isotherm are repre-

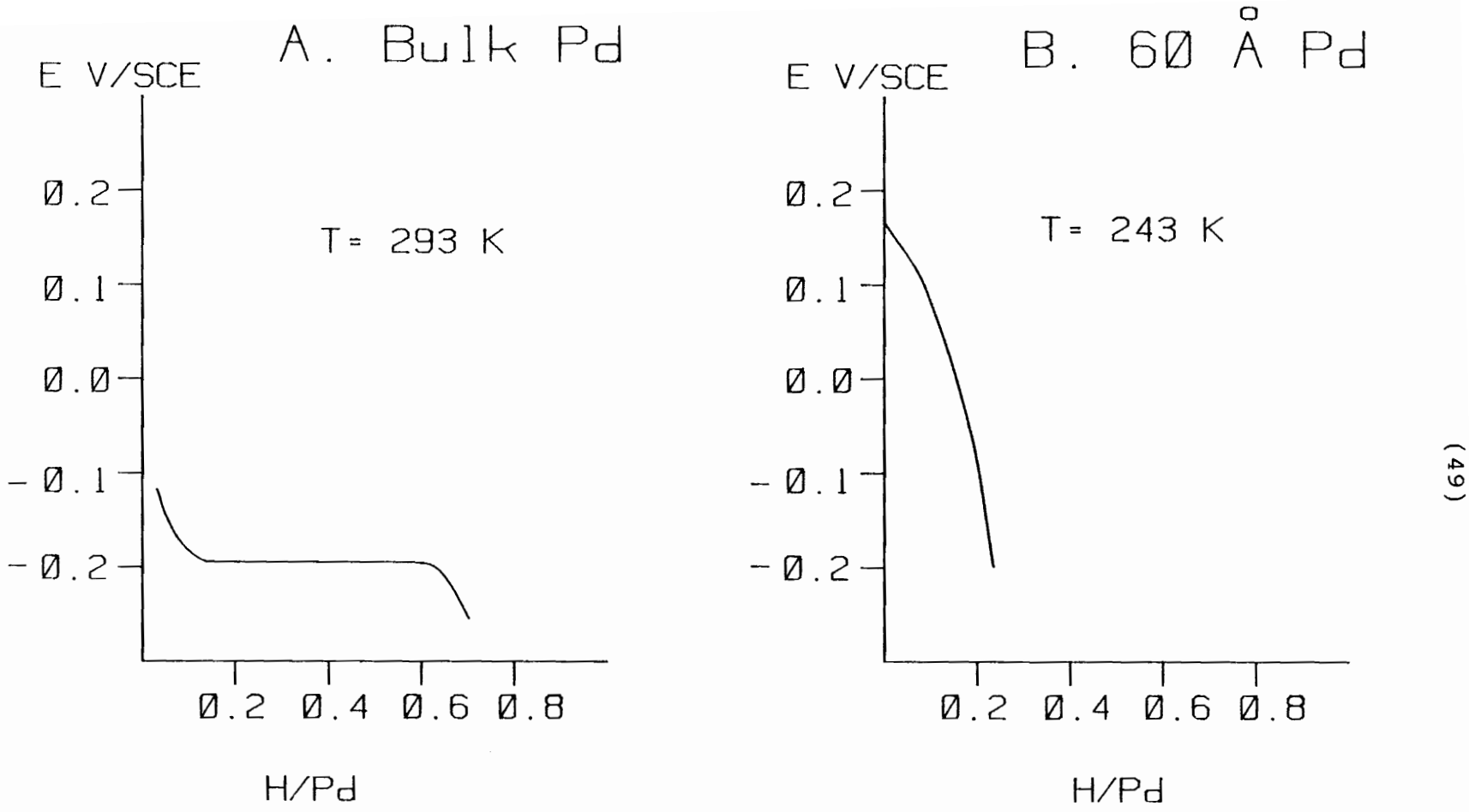

Figure 19. Isotherms (ref. 32)

(49)

sentative of the extent of hydrogen to palladium loading.

Figure 20 shows the lattice cell diagram for palladium. Hydrogen occupies the interstitial sites of the face centered cubic structure. It has been demonstrated that the H-H interactions associated with the plateau region are related to elastic deformation of the host lattice (32). This would help explain the evolution of the isotherm shape for a thin palladium layer towards that of a bulk film upon repeated cycling of air and hydrogen. Initially, the thin film lattice is resilient. When hydrogen enters the lattice, interactions between hydrogen atoms in the lattice are minimal. As the lattice becomes filled with hydrogen (some hydrogen is irreversibly bound), it can no longer prevent H-H interactions from taking place and a plateau evolves.

Plastic deformation may take place in the lattice which would prevent the H-H interactions. This is particularly the case with very thin films (less than 100 angstroms). Because of the loss of bulk support, the lattice structure of very thin films are subjected to clamping stresses (32). These are stresses associated with physical dislocations in the palladium lattice. They are caused by the morphology of the substrate on which the very thin film of palladium is deposited. These dislocations effect the lattice dimensions and may prevent H-H interactions.

If total disruption of the crystal lattice structure takes place, it is doubtful that any of the catalytic chem-

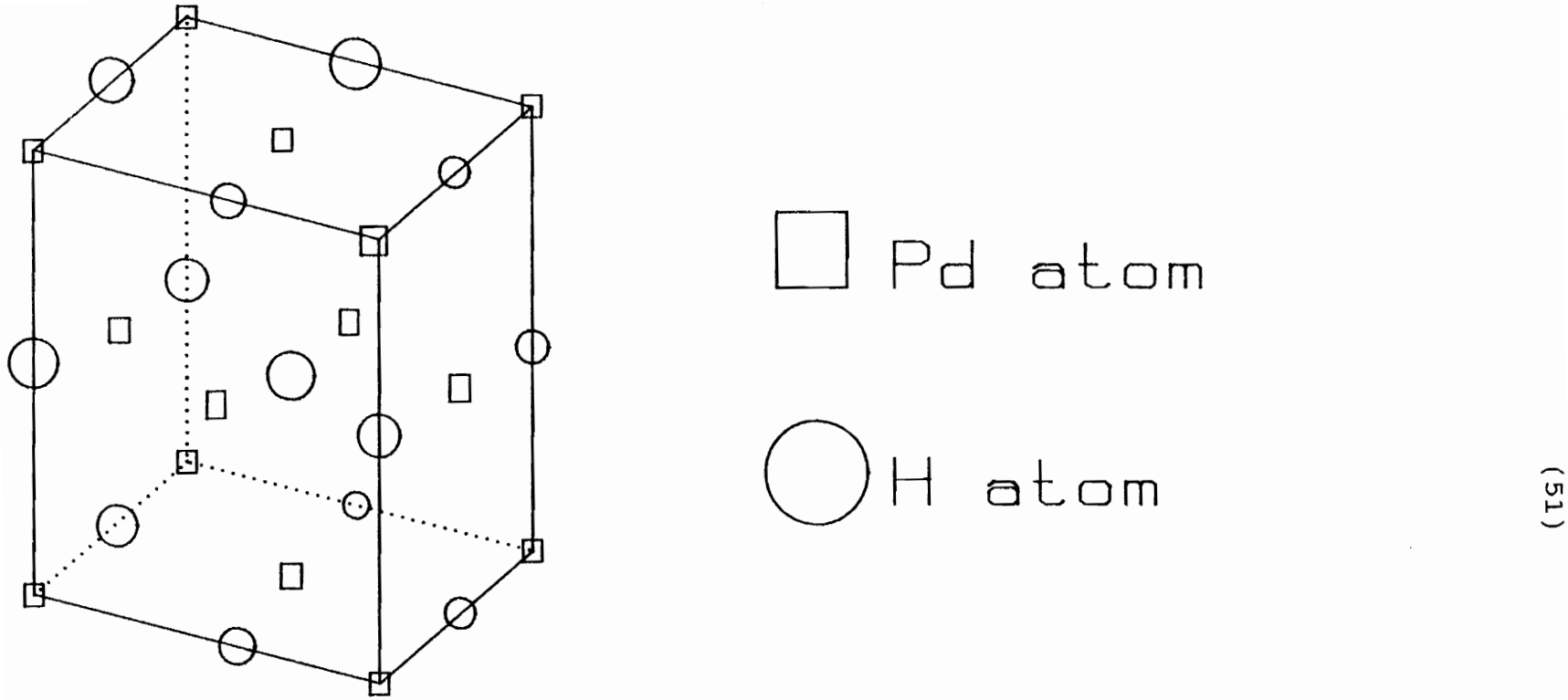

Figure 20. Palladium-Hydrogen lattice (face-centered cubic) dimensions 3.89-4.08 Å

ical processes would be operative. Without these processes the catalytic sensor no longer monitors events associated with hydrogen passing over the platinum/palladium sensing element.

V. OPTICS

Birefringent optical phenomena are the essence of the detector developed in this research. Birefringence describes the non-uniform refractive index profile of an optical quality glass structure. Normal glass (non-birefringent) has a refractive index profile which is nearly uniform throughout.

The birefringent "bow-tie" optical fiber (Newport) used in this research has a refractive index profile which is not uniform. In figure 4, an x and y axis has been placed over a transverse section of the bow-tie fiber. Along each axis, the refractive index is different.

A discussion of the interaction of light and matter is required to allow an understanding of polarization and refractive index phenomena. These optical processes can be manipulated to develop the signal required of the instrument in this research, a signal which is temperature sensitive and pressure insensitive.

A. Light and Matter

Light is energy which exists as two orthogonal coupled fields, one magnetic and one electric. An excellent review of the basic nature of light can be found in reference 33. Light travels through space and matter as a transverse electromagnetic wave. This wave, if it could be seen, is sinusoidal in shape. The electron cloud of a dielectric molecule through which such a beam is passing would appear

to oscillate up and down in a vertical plane perpendicular to the direction of light propagation (see figure 21). In matter, such as optical glass, visible light causes the electron cloud associated with the glass strucutre to oscillate at the same frequency and in the same plane as the propagating light. The electron cloud adsorbs light energy by vibrating. Upon relaxation, the molecule reradiates the light energy on to the next molecule. This process is repeated until light is transmitted out of the glass.

Natural light is composed of light vibrating in many different planes. If natural light is passed through an optical device known as a polarizer, only light vibrating in specific parallel planes will be transmitted (figure 22). Light traveling in other planes will not be transmitted. This is a measure of the polarizer's extinction coefficient. Polarization effects are a direct consequence of the birefringence associated with an optically transparent material. In one particular direction, the refractive index allows light vibrating in the correct plane to be transmitted. This plane is known as the "optical axis" of the polarizer. Light vibrating at 90^{o} to this axis is lost by absorption and scattering processes. All of the above optical phenomena are affected by the material's crystal geometry and elemental composition.

Plane polarized light is a vector quantity. As such, it is the sum of two orthogonal vectors (figure 23). In figure 24 a second polarizer (analyzer) has been placed in the

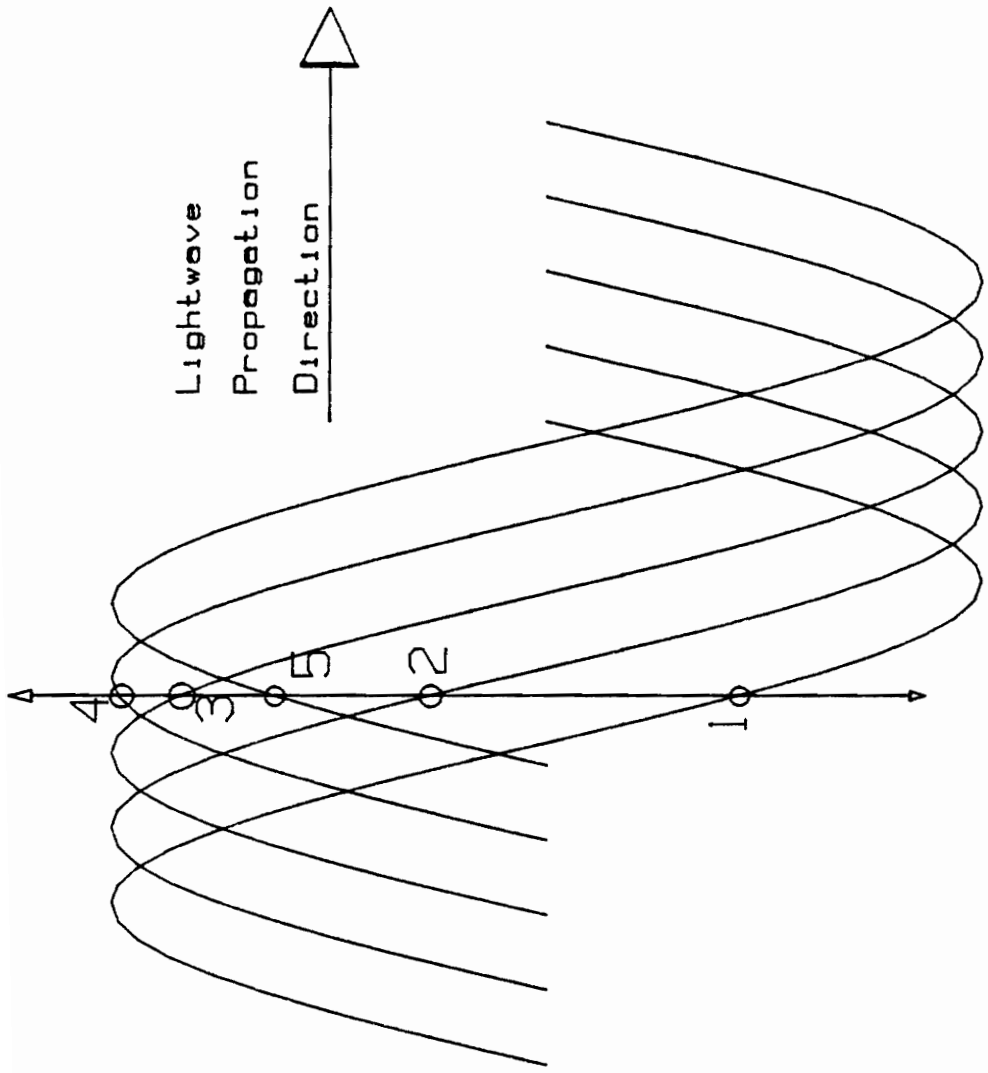

Figure 21. Transverse wave representation of light

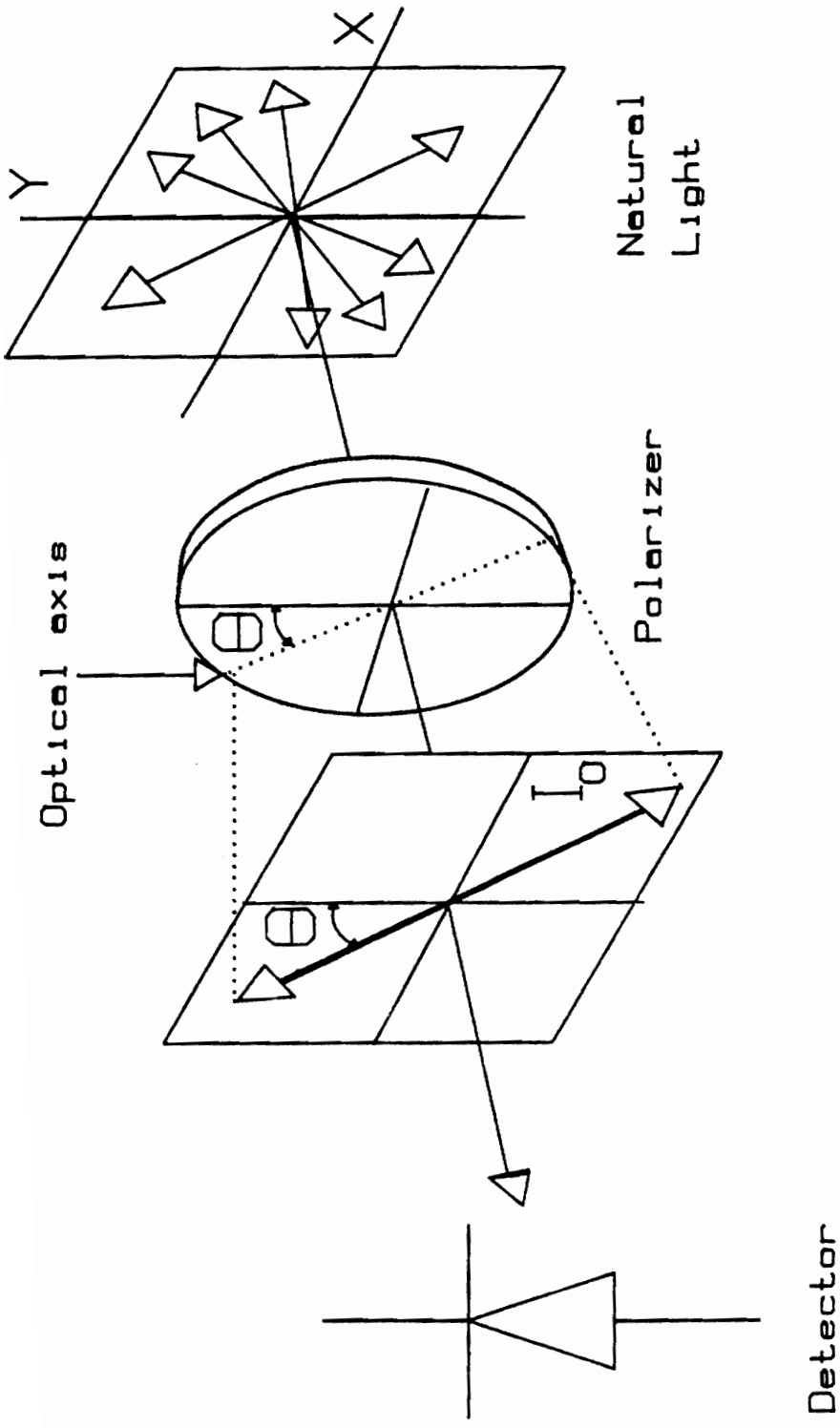

Figure 22. Generation of polarized light

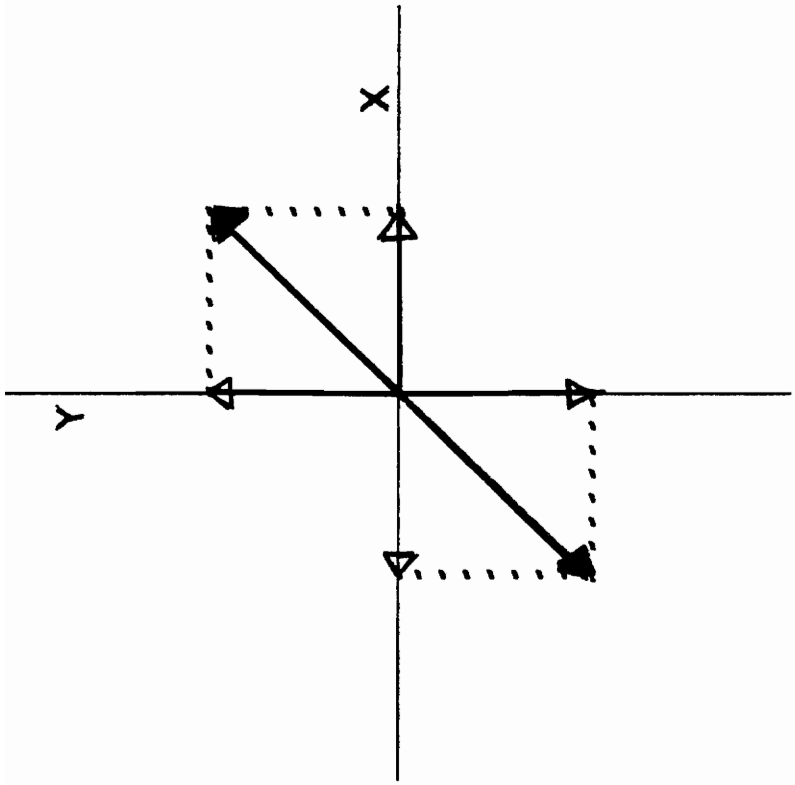

Figure 23. Polarization vector seperated into its X and Y components (z-axis is perpindicular to drawing plane)

polarized light path. When this analyzer is oriented with its optical axis parallel to the plane of incident polarized light, all of the polarized light is transmitted. If the analyzer is rotated 45 degrees to the plane of incident polarized light, only the vector of the incident polarized light oriented parallel to the analyzer's optical axis will be transmitted (figure 25).

Mathematically, the quantity which is measured by placing a photodetector at the output of the analyzer, is equal to:

1) $I_T = I_o \cos^2\theta$

I_o = initial power

θ = relative polarization angle

Because the frequency of visible light is between 10^{14} to 10^{15} hz it would be impractical for the detector to follow the magnitude of the oscillating electromagnetic wave. Instead, what is measured by the detector is an average quantity known as irradiance (equation 1). Irradiance is the amount of optical power passing a unit area per unit time (watts/meter^2 x second).

How well an optical material can perform as a polarizing medium is directly related to its refractive index profile. Refractive index is a measure of how effectively light can be transmitted in matter. It is the ratio of the speed of light in a vacuum to the speed of propagating

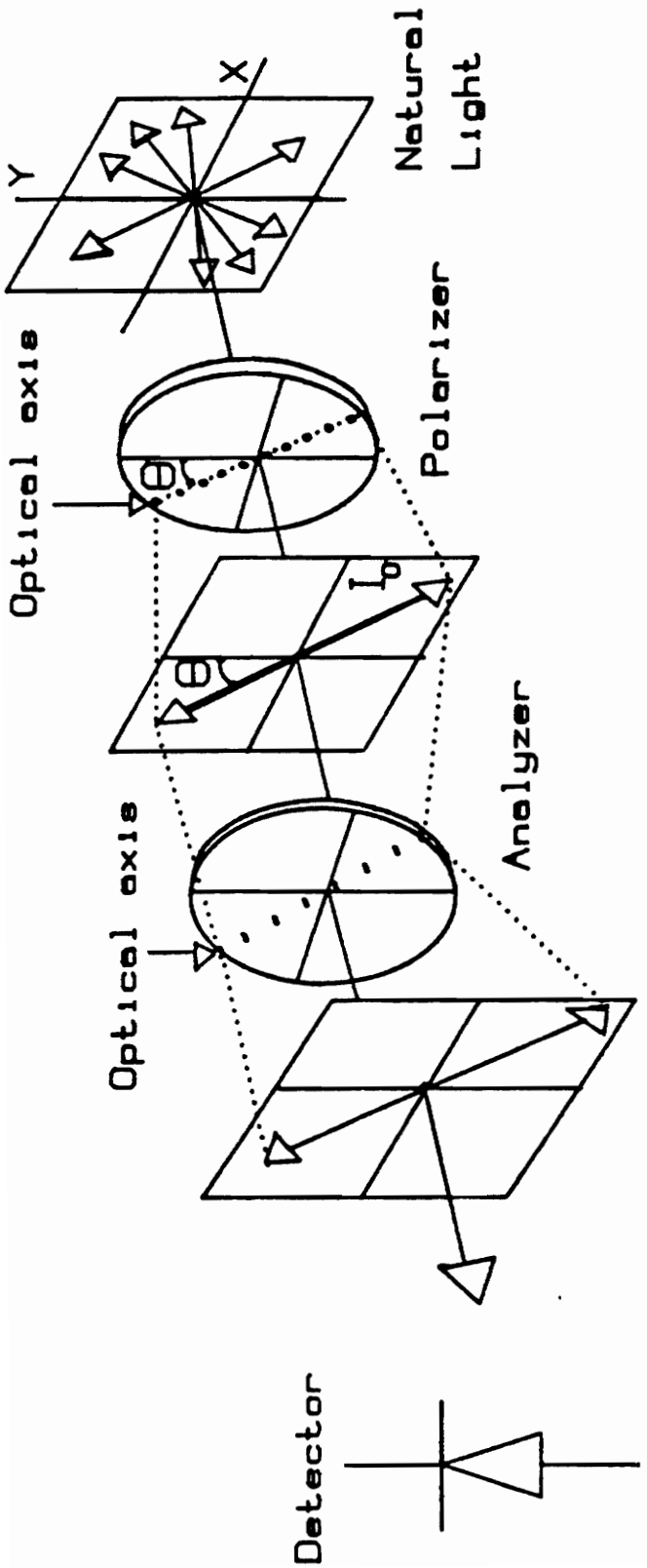

Figure 24. Analyzer aligned to pass I_o

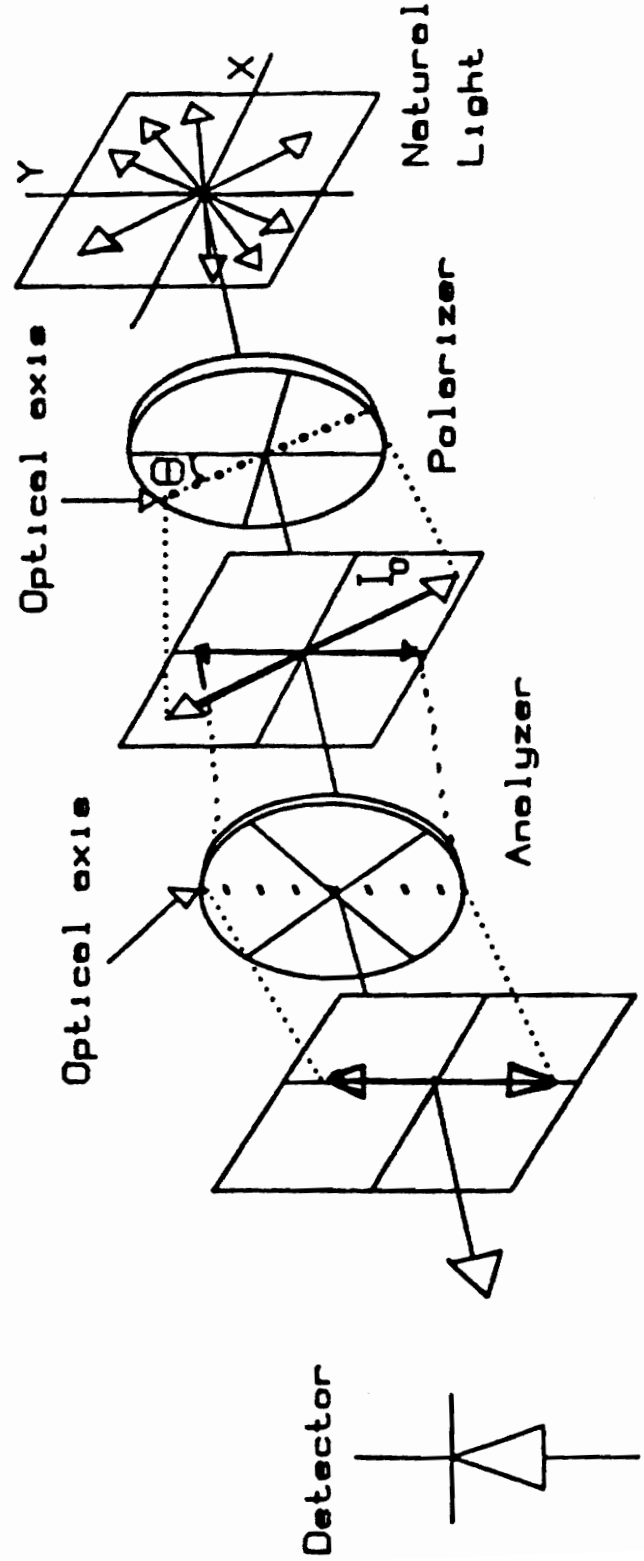

Figure 25. Analyzer aligned to pass polarization component along y-axis only.

light in the material of interest. Air has a refractive index very close to one. As optically transparent matter becomes denser, the refractive index increases. A denser material does not respond to the vibrating electric field of light as quickly as less dense material. This causes the velocity of the propagating light to decrease while traveling in the higher refractive index glass. Changes in velocity correspond to changes in the phase of light propagating in optical materials. Interferometry is a method which measures these changes in phase. In the development of the single-arm interferometer used in this research, the fiber, the optics, and the detection scheme were optimized to extract polarization information from the propagating light. Looking back at figure 6, the basic operation of the instrument is;

1) Linear polarized light is launched in a plane 45 degrees to the principle axis of the bow-tie fiber.

2) Catalytic reactions taking place on the surface of the fiber evolve heat, this heat effects the state of polarization of the light propagating in the bow-tie fiber.

3) A special optical device known as a Wollaston prism takes the single beam exiting from the bow-tie fiber and splits this beam into two beams carrying polarization and phase information.

4) Twin photodetectors and analog electronics extract signal from these two beams.

The special birefringent "bow-tie" fiber and the Wollaston prism interact with polarized light energy allowing development of this instrument. A closer analysis of how the bow-tie fiber and Wollaston prism affect polarized light follows.

B. Birefringent Bow-tie Optical Fiber

As described earlier the bow-tie fiber is birefringent because it has two distinct orthogonal axis which have different refractive indices (figure 4). Plane polarized light is launched into the fiber at 45 degrees to these orthogonal axis. At 45 degrees the plane polarized is split into its two equal orthogonal vector components. Because of the unequal refractive index values associated with the x and y directions, each vector component travels along the fiber with a different velocity.

This difference in light velocity can be described in terms of the phase of each vector component.

1) $\phi_y = k\ n_x\ L$

2) $\phi_y = k\ n_y\ L$

where k=2 pie/lambda

lambda=wavelength of propagating light

n=refractive index

L=length of fiber

ϕ=phase angle

The phase difference between light propagating in each

axis of the bow-tie fiber core is:

$$\phi_x - \phi_y = k\, n_x\, L - k\, n_y\, L = k\, L\, (n_x - n_y)$$

$$3)\ \Delta\phi = k\, L\, \Delta\, n_{x-y}$$

At room temperature and pressure the refractive index difference between the x and y planes of the bow-tie fiber core is small. Therefore the phase difference is also small. At the top left of figure 26 is depicted the sinusoidal phase relationship between light traveling in each plane. The vector diagram of this phase relationship is shown in the bottom left of figure 26. As long as ambient conditions are constant, the magnitude of the x and y components of the resultant are also constant. The angle made by the resultant vector with the y-axis of the bow-tie fiber is known as the "polarization angle". Under stable conditions this angle does not vary.

There are several processes which can take place in the bow-tie fiber which may change "delta n". Such a change can be monitored and related to the magnitude of a specific perturbation. Heat and pressure are two parameters which may vary when following a chemical reaction and can be used with the bow-tie fiber to sense a change in the reaction.

Heat is generated on the surface of the bow-tie fiber coated with palladium and platinum, when hydrogen gas is allowed to flow over the fiber. This can change the "delta

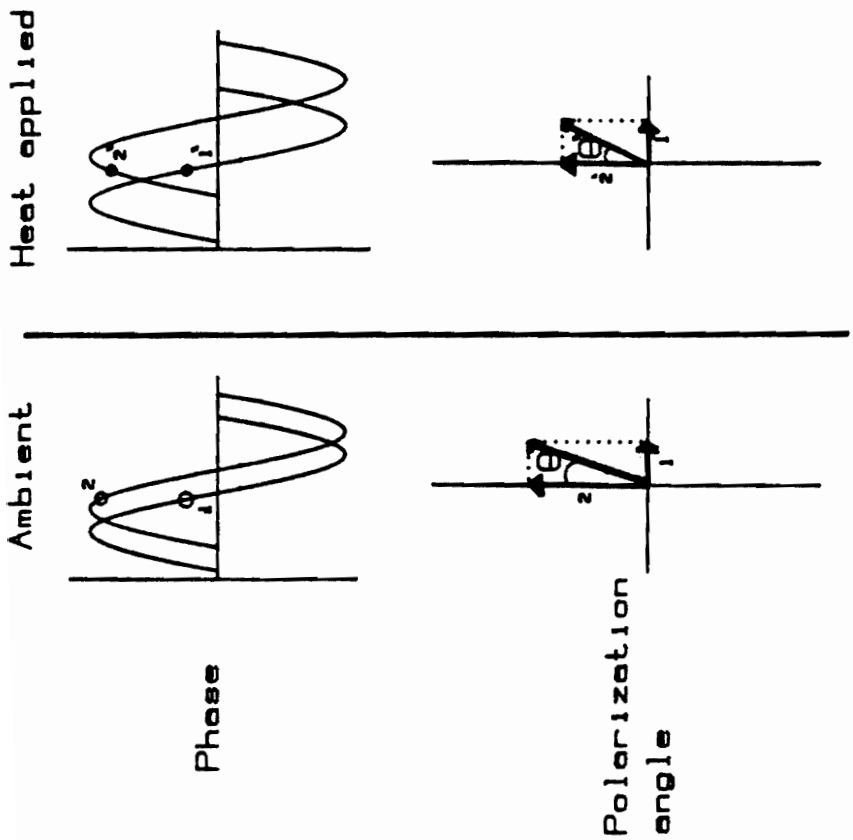

Figure 26. Phase and polarization relationship

n" of the bow-tie fiber in several different ways.

The x-axis of the bow-tie fiber in figure 4 is composed of silica glass heavily doped with B_2O_3. A larger thermal expansion coefficient is associated with this boron-doped silica compared to the fluorine-doped silica along the y-axis of the fiber. Upon exposure to heat, the x-axis responds differently than the y-axis. Expansion toward the center of the optical fiber compresses the fiber core along the x-axis. Compressing the core glass preferentially along the x-axis increases the density. This increases the refractive index. Light, therefore, travels along the x-plane at a lower velocity (slow axis) relative to light traveling in the y-plane (fast axis).

Because of the change in velocity there is an associated change in the phase relationship between light oscillating in the x and y directions along the fiber. At the top right of Figure 26 is a graph of the phases when heat is applied . The magnitude of the x and y vectors is depicted at the bottom right of figure 26. Heat causes the resultant vector (addition of the x and y vectors) to have a different polarization angle than that exhibited during ambient thermal conditions.

In the bow-tie fiber, the major process which change the phase difference (delta ϕ), can be represented mathematically as follows:

$$4)\ 1/L\ d(\Delta\ \phi)/d(T) = k\ [\Delta\ n(T)]/(T_A - T_S)$$

where

$n(T) = (n_x - n_y)$ as a function of T

T_A = Temperature at ambient

T_S = softening temperature of cladding

Examining the right hand side of equation 4, the T_S term in the denominator is the temperature at which the cladding becomes soft. T_S can be modified by changing the amount of fluoride in the doped silica of the cladding glass. It is important to note that since ambient temperature is approximately 25 ^oC and T_S > 700 ^oC, the overall sign of the quantity in equation 4 is negative. The softening temperature is important because it affects the stresses developed in the fiber when it is manufactured.

When the bow-tie fiber is produced, it begins as a relatively large silica tube. Modified chemical vapor deposition forms the different layers which eventually become the bow-tie, cladding and core structures (34). Finally the tube is heated and a vacuum is applied. It is then collapsed, and mechanically pulled into a fiber with a diameter of 125 microns.

From equation 4, if T_S is higher (more dense material) the magnitude of the change in "delta ϕ", after exposure to heat, will be smaller. A denser cladding diminishes the compression effect transmitted to the core by the expanding bow-tie structure. When the softening temperature of the cladding is lower (softer material), more of the compres-

sion effect will be transmitted to the core and the magnitude of the change in "delta O" will be greater.

There are several other processes affected by heat which can take place in the bow-tie fiber causing a change in "delta ϕ". A temperature increase affects the length of the optical fiber. In a two-arm Mach-Zehnder interferometer this would provide a significant contribution to the signal being developed. But in the single-arm interferometer, both light beams are being carried by the same fiber. When the length increases, it effects the path length of each beam equally. Therefore "delta ϕ" is minimally effected.

Associated with an increase in length is a decrease in fiber diameter (Poissson's ratio). Near uniform compression around the fiber caused by a decrease in diameter will have little effect on "delta ϕ". This is because both the x and y planes feel the same compressive forces and the refractive index along each plane changes by the same amount. The difference between the refractive index in the x and y directions does not change appreciably.

Finally, an increase in heat also effects the refractive index profile between the cladding and core. This effect causes a small change in the total power guided by the fiber (35).

Minute imperfections caused by the manufacturing of the bow-tie fiber account for some of the relatively insignificant signal changes produced by the alterations in length and overall refractive index discussed above. Equation 4

can be expanded to include these changes:

$$5)\ 1/L\ d(\Delta\phi)/dT = k/L\ [L\ (\Delta n/n)\ (dn/dT) + (\Delta n)\ (dL/dT) + L\ (\Delta n(T))/(T_A - T_S)]$$

A major portion of the signal developed from the single-arm interferometer is driven by processes shown in equation 4 (last expression on the right hand side of equation 5).

The portion of the signal derived from the first two terms on the right hand side of equation 5 (change in length and overall changes in refractive index profile) are relatively small. It should also be noted that the sign of these two expressions is positive (10). A signal produced by these effects would give a response opposite to that developed by changes in the differential stress profile of the bow-tie fiber caused by heat (equation 4).

Heat effects the bow-tie fiber much more than an isotropic pressure change. Eickhoff (10) has shown the theoretical pressure versus temperature sensitivity ratio to be approximately 1500 (bar/K) for the bow-tie configuration. Pressure changes affect the fiber in the same manner as a decrease in fiber diameter. Equal pressure around the fiber causes an equal change in refractive index along the x and y-planes of the bow-tie fiber. There is a small net effect on "delta n" and therefore little change in "delta ϕ".

Temperature <u>sensitivity</u> and pressure <u>insensitivity</u> are

requirements for the instrument developed in this research. An understanding of birefringent optical phenomena occurring in the bow-tie fiber has allowed insight into our development of just such an instrument.

Polarized light, which is modulated by heat, exits the bow-tie fiber. Next, it is focused onto an optical device known as a Wollaston prism.

C. Wollaston Prism

Figure 27 depicts a Wollaston prism. It is composed of 2 calcite prisms which have been glued together along their hypotenuse. Calcite is a crystal which is birefringent. Two optical axes (fast and slow) at 90^{o} to one another are found in each prism. In the Wollaston, the fast axis of each prism is arranged at 90^{o} to the fast axis of the other prism.

Light exiting the bow-tie fiber is polarized in a specific plane. This resultant plane of polarized light is composed of two vector components vibrating in planes which are at 90^{o} to each other. The Wollaston is positioned so that each plane of incident light will enter the first prism along a coincident optical axis of the Wollaston. In the first prism one of the vibrating components of the polarized light encounters the fast axis. At 90^{o} the other component travels along the slow axis. When both beams enter the second prism the situation is reversed (light traveling in the first prism's fast axis now travels in the second prism's slow axis, etc.). This configuration helps

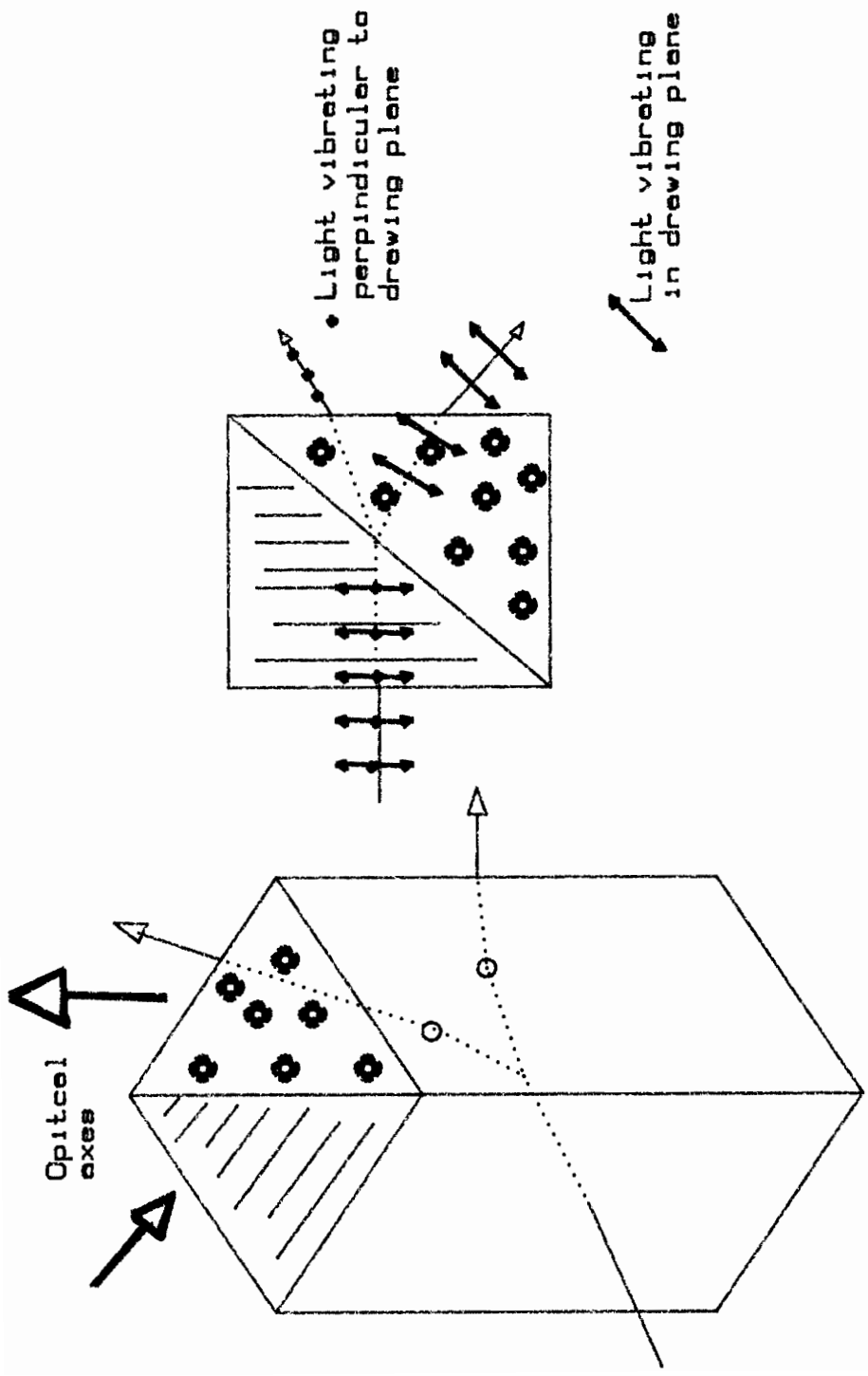

Figure 27. Wollaston Prism

to maintain the original phase relationship of the polarized light which exits the bow-tie fiber. When light enters the diagonal face of the second prism, the two beams deviate. Both of these beams exit the end face of the Wollaston in their own distinct path. The amount of deviation depends on the non-normal angle associated with the prisms.

Having two distinct beams is similar to the Mach-Zehnder double arm interferometer discussed in the introduction. However, in this instrument, the phase and polarization information is being carried by two beams propagating in a single optical fiber (single-arm interferometer). Both beams exiting the Wollaston are then transformed into data by signal processing electronics, discussed in the following section.

VI. Signal Processing

Each beam which exits the Wollaston prism is directed onto a separate silicon photodetector. Current developed in these detectors is sent to two channels in the circuit shown in figure 16. Devices 1 and 2 are Analog Device AD549 operational amplifiers. Both of these are configured as current to voltage converters. Gain is established using one megaohm wire-wound 1% precision resistors in the feed back loop of each amplifier. These operational amplifiers were chosen for their high performance specifications, having an input impedance of greater than 10^{13} ohms and an input bias current rated at 250 femtoamps maximum. A high input impedance prevents loading error (signal is developed across the amplifier rather than lost across the detector junction). Low bias current eliminates the need for external circuitry to establish zero potential across the amplifiers inputs. Test jacks are located at the output of each initial amplifier stage. This allows the monitoring of each channel independently.

Device 3 is an operational amplifier (OP07,Fairchild) configured as a summation circuit. Both signals from channel 1 and channel 2 are summed in this circuit. A test jack is connected to the output which allows the summation signal (Ix+Iy) to be monitored.

Device 4 is a difference circuit which uses an operational amplifier (OP07,Fairchild) to develop the difference

signal Ix-Iy. A test jack is also provided to monitor this signal.

An analog math processor (Analog Device's AD538) is used to divide the difference signal by the summation signal. Amplification factors between 2 and 10 can be established within the AD538 and applied to the difference/sum signal.

The signal produced by the sensor is basically a very low frequency signal. A low pass analog filter is the final stage of signal conditioning. This device passes the low frequency components associated with the output signal and rejects extraneous high frequency interference.

Dividing the difference signal by the summation signal performs the math operations shown in Appendix B. Initially, there is a 90^{o} phase difference between Ix and Iy. The optics and electronics are set up so that Ix = Iy:

where $Ix = Io \cos^2 \theta$

$Iy = Io \sin^2 \theta$

Io = initial power entering fiber

$\theta = \phi/2 = [d(\Delta\phi)/dT] (T-T_A)$

A major problem with intrinsic fiber optic sensing instruments are fluctuations in the power delivered to the core of the sensing fiber. Incorrect and unstable alignment and poor endface cleavage can contribute to signal instability. By following the mathematics in Appendix B, it can be seen that initially "Io" is present in the equations. Division of the difference by the sum eliminates "Io". The

final output is a cosine function dependent on temperature and free from source power fluctuations. Data collection, storage, and analysis are performed by a DEC LSI-11 computer.

Subtraction, summation, and division of "Ix" and "Iy" can be shown graphically. By placing a quarter wave retardation plate between the source and the fiber, an initial ambient phase difference of 90^{o} is introduced between "Ix" and "Iy". In figure 28 the final sensor response curve is shown along with the "Ix" and "Iy" signals. The Wollaston and laser polarization angles are adjusted so that the output is "0 volts". At this point on the graph the values of "Ix" and "Iy" are equal. The corresponding region of the output curve represents the greatest linear change in the output signal per linear change in polarization angle. Therefore, this is the portion of the output curve where the largest signal can be derived from the smallest perturbation.

A quarter wave plate is not used in the instrument configuration in this research. Small changes in the thermal environment may adversely modulate the light traveling through the quarter wave plate. Optics which are placed near the output of the laser must be specially coated to help eliminate reflection back into the laser cavity. Reflection can affect the polarization plane of the laser output, disrupting the final sensor output. For these reasons, and to keep the instrument design simple, the quarter

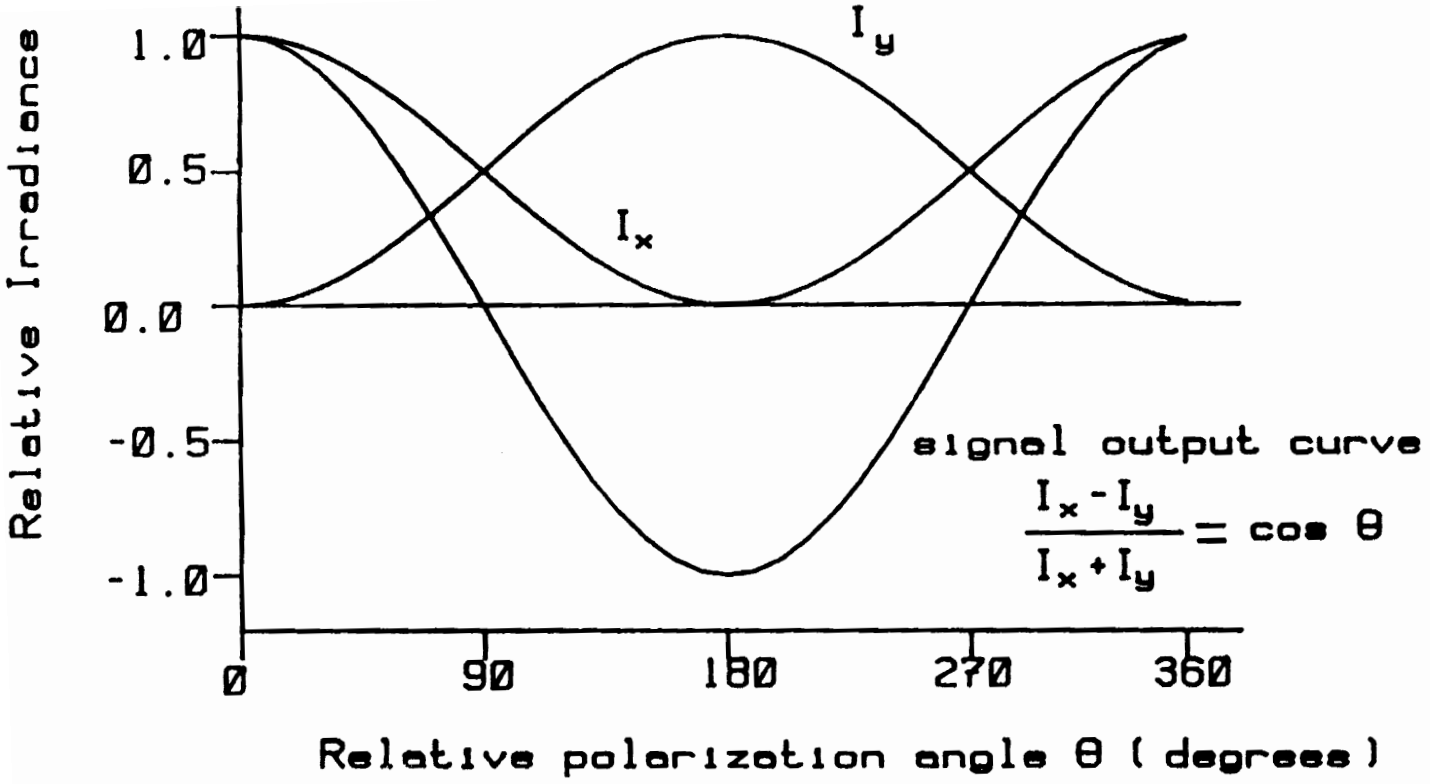

Figure 28. Output and irradiance curves for initial 90° phase difference

wave plate was not used.

Ambient phase differences between polarized light traveling in the x and y planes of the fiber allow sufficient signal to be developed with minimal noise and baseline drift. These initial phase differences are caused by the birefringence of the bow-tie fiber and imperfections in the manufacturing process. Figures 29 and 30 show "Ix" and "Iy" curves for 10^{o} and 40^{o} out-of-phase conditions. Output response curves for these do not follow the cosine function shown in figure 28 (90 degrees out-of-phase). However, portions of both the 10^{o} and 40^{o} curves can be used to develop a useful analytical signal.

Each response curve is unique and is dependent on the inherent phase difference associated with the bow-tie optical fiber. The operating region on the response curve can be chosen by adjusting the Wollaston and laser polarization angles to provide the desired signal. Discussion of this procedure is found in the following experimental section describing instrument initialization.

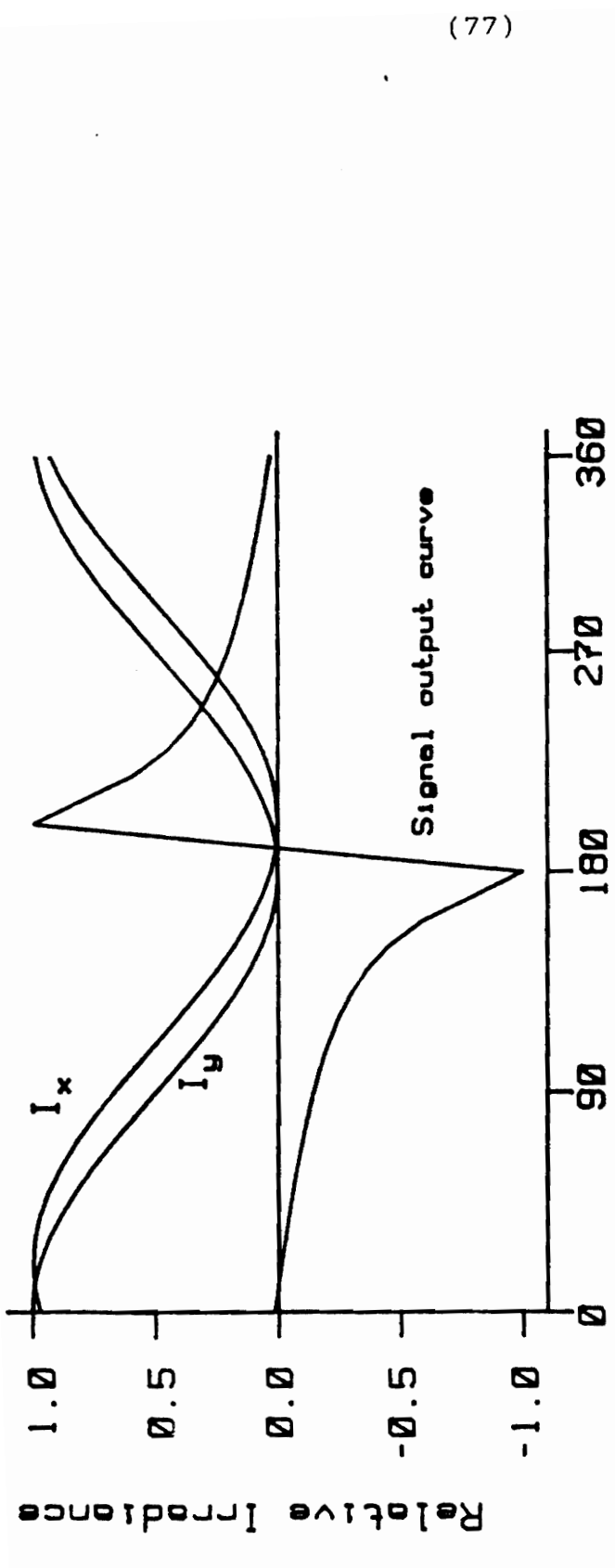

Figure 29. Output and irradiance curves for initial 10° phase difference

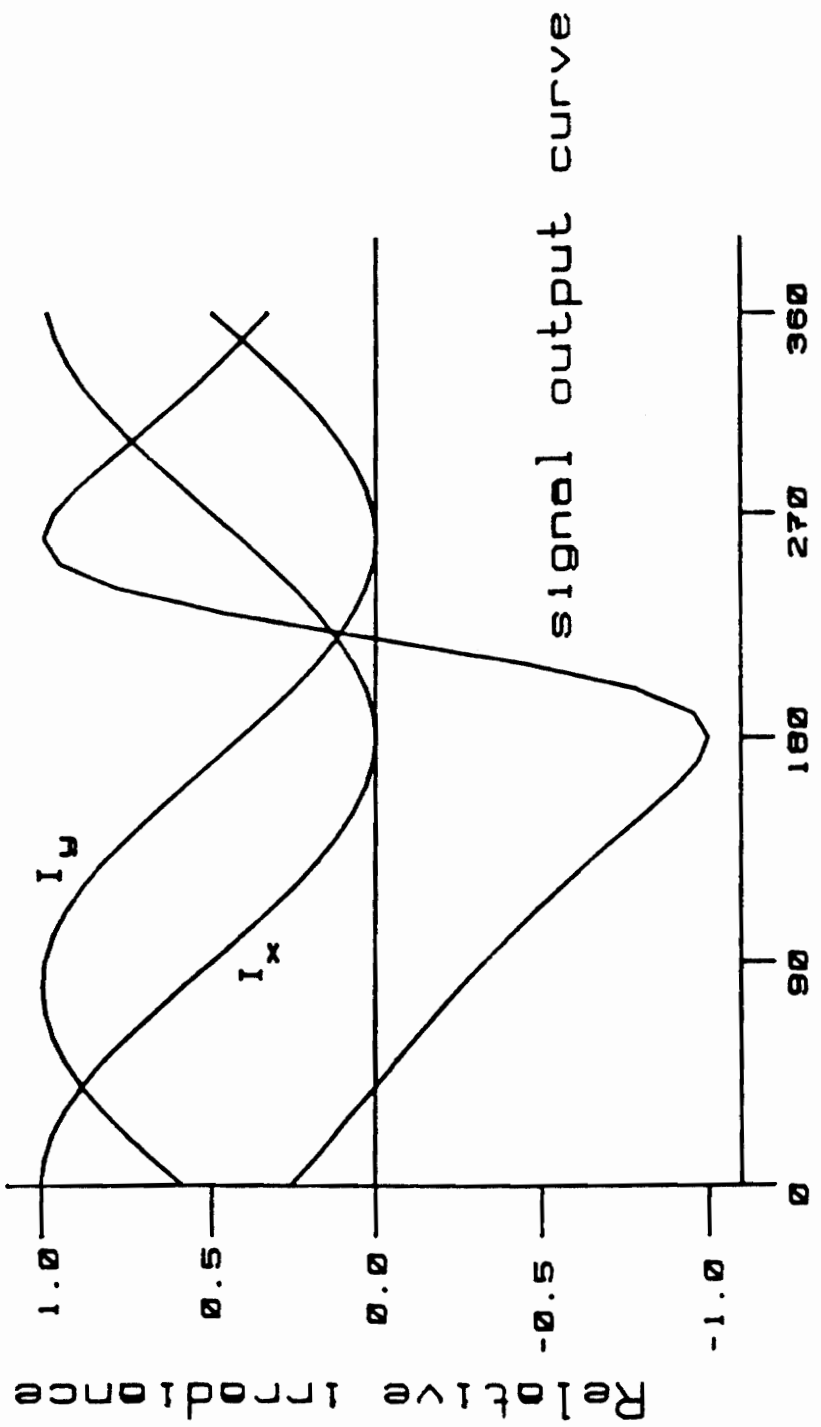

Figure 30. Output and irradiance curves for initial 40° phase difference

VII. Experimental

Each experiment in this research evolved from a need to further characterize and develop the birefringent sensor. Figure 31 depicts a general instrument setup. Where an experiment differs from this normal configuration, it is noted. A discussion of the background and results for each experiment, or group of experiments, is also given.

Experiment 1. Initialization

Examining figures 28, 29,and 30 it is easy to detect unique points along the curves representing "Ix" and "Iy" where the values of the two variables are equal. For this situation to occur, each axis of the bow-tie fiber must be equally excited by the incoming polarized light energy. Slightly different ambient phase angles associated with each bow-tie fiber require that the laser plane of polarization be varied to attain a "null point".

Alignment of the laser, Wollaston, and bow-tie fiber is performed by making sure that the plane of polarization of the laser and a diagonal of the Wollaston are coincident. Both the Wollaston diagonal and laser polarization plane are marked on the respective device. A circular 360^{o} scale is mounted around the laser tube. The Wollaston is mounted in a moving circular graduated support. By adjusting the laser and the Wollaston in unison and monitoring the "Ix" and "Iy" signals from the amplifier section, the crossover points can be located.

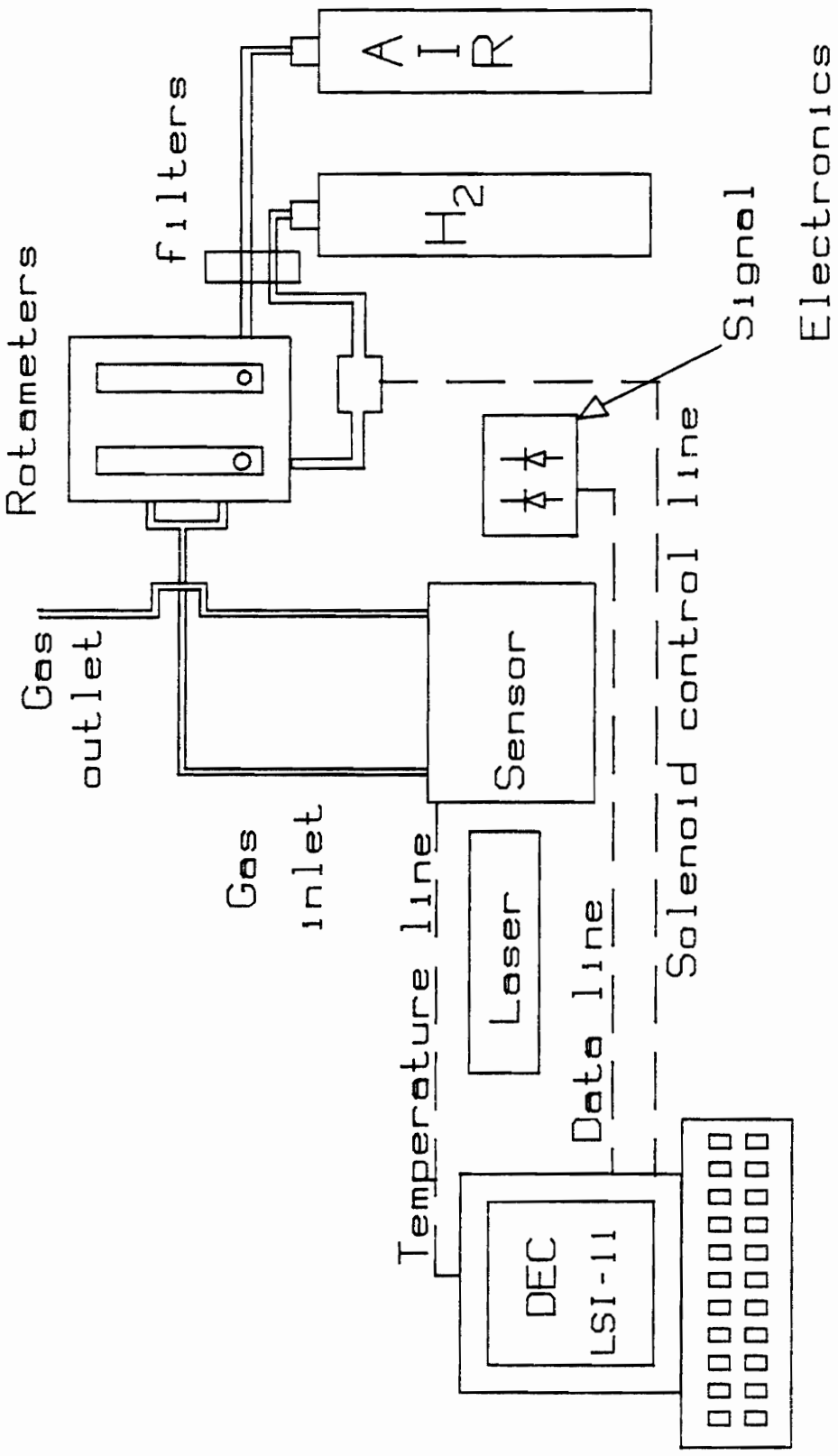

Figure 31. Typical experimental setup

Output curves for different phase relationships are shown in figures 28, 29, and 30. The most sensitive response is associated with the sharpest slope along the output curve.

During initialization, air is allowed to continuously flow over the fiber (1 liter per minute). Hydrogen gas is switched into the carrier gas stream by a computer controlled solenoid. Both flows are set by Matheson 603(air) and 602(hydrogen) rotameters. Calibration curves for each rotameter, to establish the percent hydrogen in air, were provided by Matheson. Mass spectrometry was performed on the different gas calibration mixtures to establish more accurate percentages.

Response of the sensor to hydrogen gas is monitored by the computer. Adjustment of both the Wollaston and laser are performed, depending on the desired output and the ambient phase difference in the bow-tie fiber.

Figure 32 shows the response of the sensor where the instrument was adjusted to provide a positive output signal. This signal shape was chosen to be used in all other experiments in this research. A negative going signal may be selected by rotating the Wollaston 90^{o}. "Ix" and "Iy" are interchanged by this procedure and the output curve is inverted.

In situations where there is a small ambient phase difference between the two axes, as shown in figure 30, it may be difficult to adjust for proper peak response. The linear

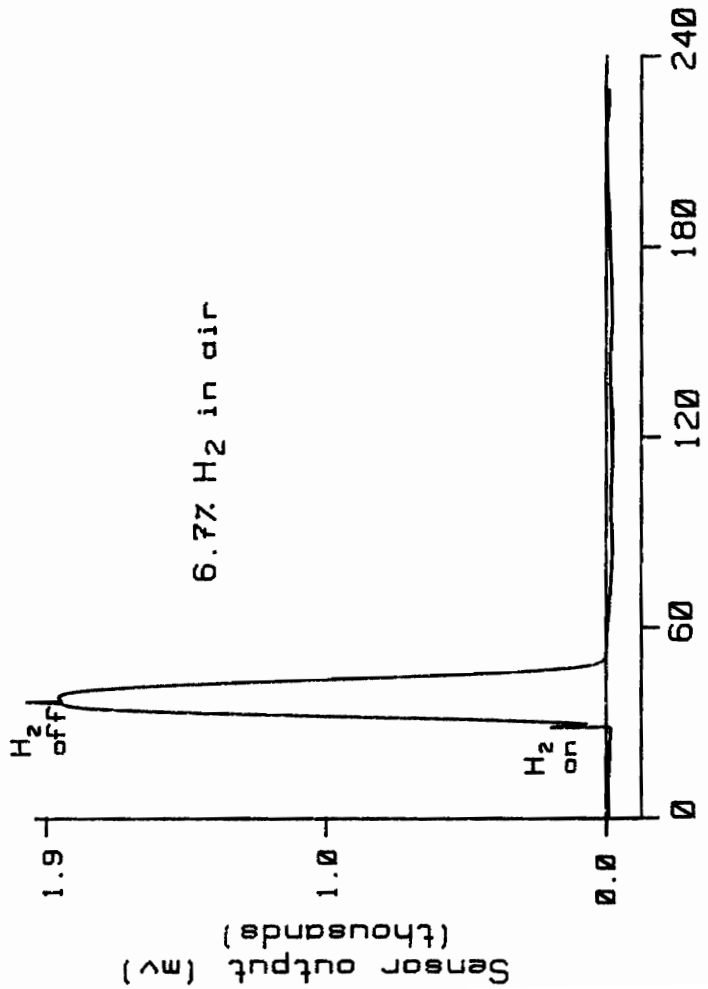

Figure 32. Typical sensor response

region is very sharp and may take several trial runs. When the instrument is not tuned correctly, the output signal will have an unusual shape (figure 33). This shape evolved because the adjustment of the Wollaston and the laser was slightly to the left of the center "null" point in figure 30.

As hydrogen passes over the fiber, heat causes the output signal to increase. The shape of output signal can be determined by following the output curve to the right. From the null point, the output signal will increase. If enough heat is applied the signal will be sinusoidal in shape. However, in this research the amount of heat evolved is small. The instrument is tuned so that it remains in the linear sloped region of the theoretical output curve. An almost symmetrical output curve would be expected, independent of the initial adjustment point along the curve. As the hydrogen is removed, the signal retraces the output curve back to ambient conditions. Differences in the slope of the leading and trailing edges of the output signal are due to the different dynamics between the processes evolving heat and those processes involving heat loss.

Experiment 2. Hydrogen Sensor Calibration

Hydrogen in air is explosive above concentrations of approximately 4% hydrogen. There are several hydrogen sensors which can measure either low or high concentrations of hydrogen in air (26). However, some of these require flame arresters to be installed to alleviate the explosion

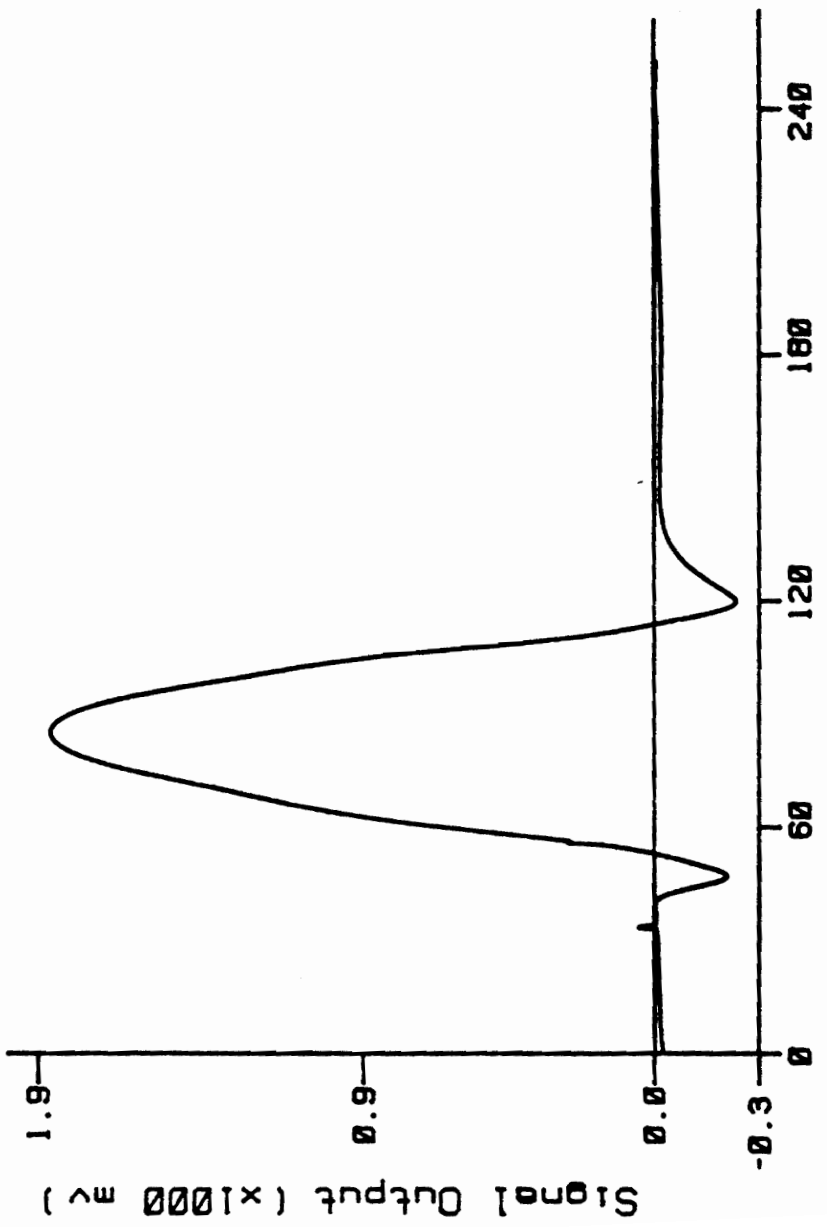

Figure 33. Atypical sensor response

hazard. The Mach-Zehnder interferometer discussed in the historical section detects hydrogen in nitrogen to an upper limit of 2% (7). Therefore there is interest in a sensor that could operate safely at higher concentrations.

Because light traveling in an optical fiber is not an ignition source, this instrument is ideally suited for detecting hydrogen within the explosive concentration ranges. Figures 34 and 35 show the statistics and response curves for the instrument developed in this research.

There are two ways to change the response of this instrument. First, adjusting the flow of the hydrogen rotameter to different levels will cause the ratio of hydrogen to carrier gas to vary. The second is to program the computer to allow the hydrogen solenoid to introduce gas for longer or shorter periods of time (see experiment 5).

It should be noted that the two lower concentrations were measured with the hydrogen solenoid set to allow the sample gas to flow for a longer time than the higher concentration. In an actual sensing procedure a calibration curve would need to be developed which would allow the instrument parameters to be the same for each calibration gas concentration.

Concentrations greater than 10% saturate the fiber chemistry and will quickly degrade the sensor response. Much lower concentrations can be detected, but problems with mixing the calibration gases and attaining repeatable

H_2% in air	Peak height
6.7	$\bar{X}_5$= 1.97 v SD= 0.16 v RSD= 7.9%
2.8	$\bar{X}_5$= 0.86 v SD= 0.05 v RSD= 6.2 %
1.4	$\bar{X}_5$= 0.62 v SD= 0.02 v RSD= 4.0 %

Figure 34. Sensor Statistics

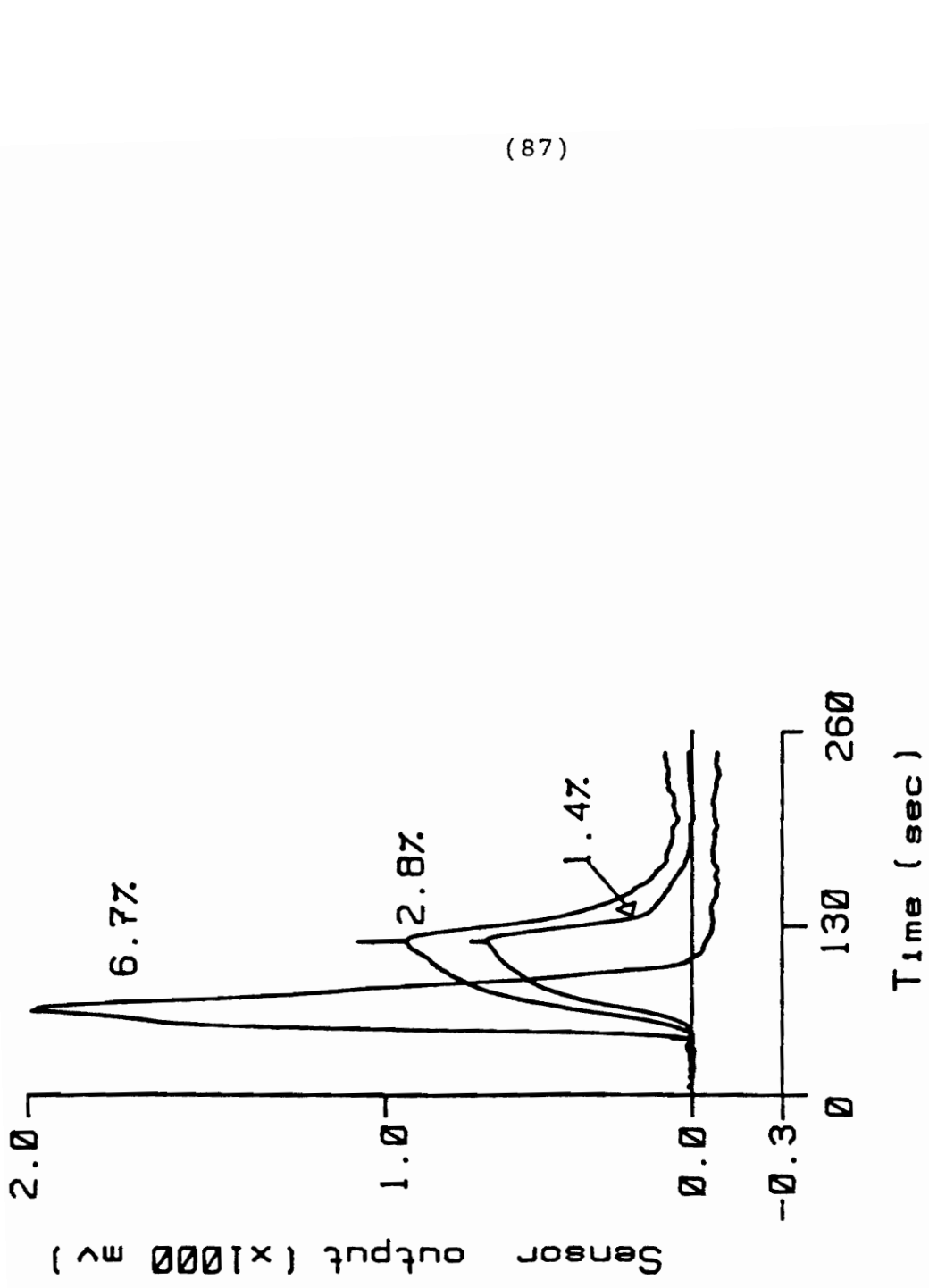

Figure 35. Average response curves ($\overline{X}_5$)

calibration mixtures were encountered.

Experiment 3. Characterizing Sensor Response

The source of the signal developed by the bow-tie fiber could be attributed to temperature and/or pressure. The following experiments were performed to determine the main process which creates the signal from this configuration of the bow-tie fiber.

In reference 7 which uses a double-arm Mach-Zehnder, the authors conclude that expansion of the palladium lattice produced the signal from their instrument. However, their sample fiber was coated with a thick film of palladium (10 microns), considerably thicker than the 6 nanometer palladium film used in this research. Expansion of the thick film palladium lattice upon uptake of hydrogen gas would stretch and squeeze the sample fiber, while the reference fiber remains unperturbed.

In contrast, the conclusion reached in this research is that the heat of formation of palladium hydride is responsible for signal development and that the bow-tie fiber effectively discriminates against pressure fluctuations.

In the earlier section describing catalytic chemistries, several reactions were shown which could evolve heat and affect a change in the birefringence. Figure 36 shows that the bow-tie fiber and its chemistry respond to hydrogen in air or nitrogen carrier gases. This would eliminate the combustion of water as a source of heat.

A change in temperature in the bow-tie fiber causes the

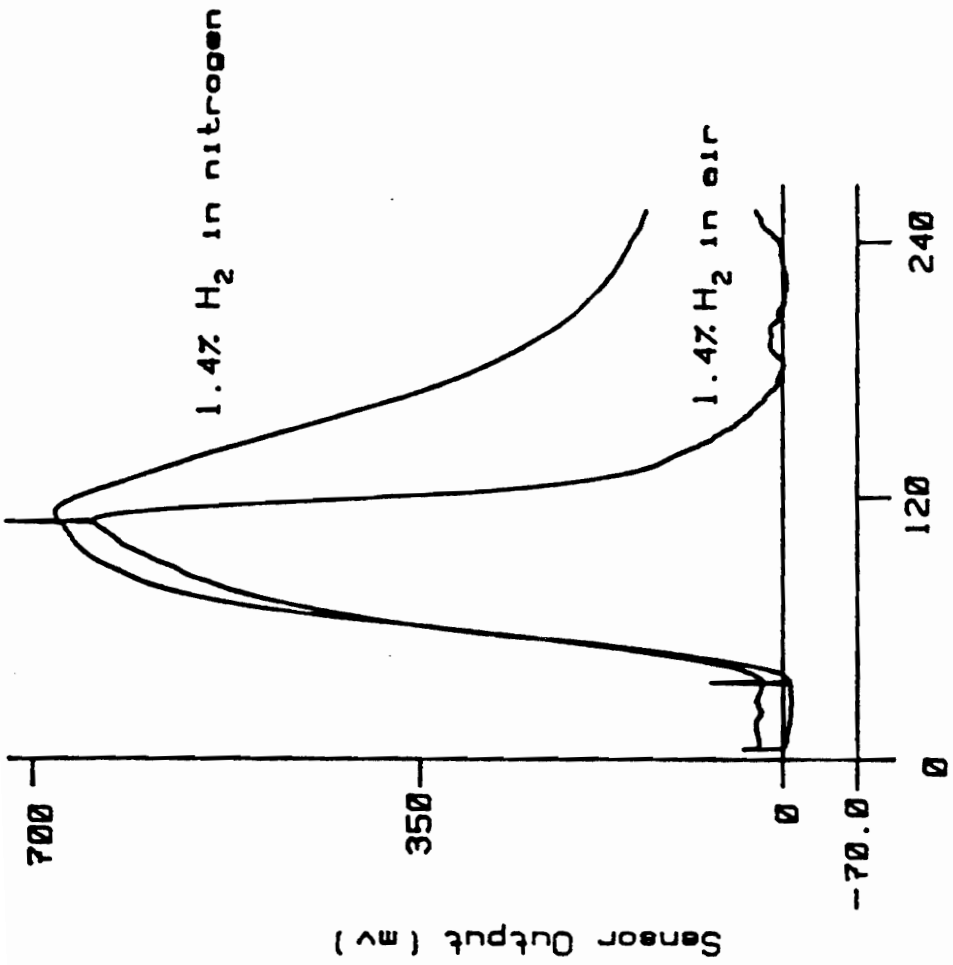

Figure 36. H_2 in air and nitrogen carrier gases

output signal excursion to be opposite to a signal that might be produced by other perturbations such as pressure. Figure 37 shows data for sensor output plotted against an artificially induced temperature change. A solid-state temperature transducer was imbedded in the sensor head. This was used as a classical reference measurement of the temperature rise produced by a flask of warm water placed near the sensor head. Sensor output and temperature were both recorded simultaneously during the experiment. At room temperature (23.9 ^{o}C), the initial response of the fiber to a rising temperature involves a positive deflection. Graphs of sensor response to hydrogen are also in the positive direction, indicating that it is indeed heat effecting the birefringence and creating the output signal. For the 6.7% H_2 signal shown in figure 35, the rise in fiber temperature is approximately 1 ^{o}C.

Experiment 4. Pressure Insensitivity

Any sensor using a carrier gas or liquid must be insensitive to pressure fluctuations caused by the introduction of sample into the carrier stream.

In an experiment to test for pressure sensitivity, gas is initially allowed to flow over the fiber as normal. At the exhaust, there is placed a plastic tee. One end of the tee is open, the other is connected to a 5 lb. psig pressure gauge. Figure 38 shows the sensor response when the open end of the tee is totally blocked allowing the pressure to rise between 1-2 lbs. The pressure is then released

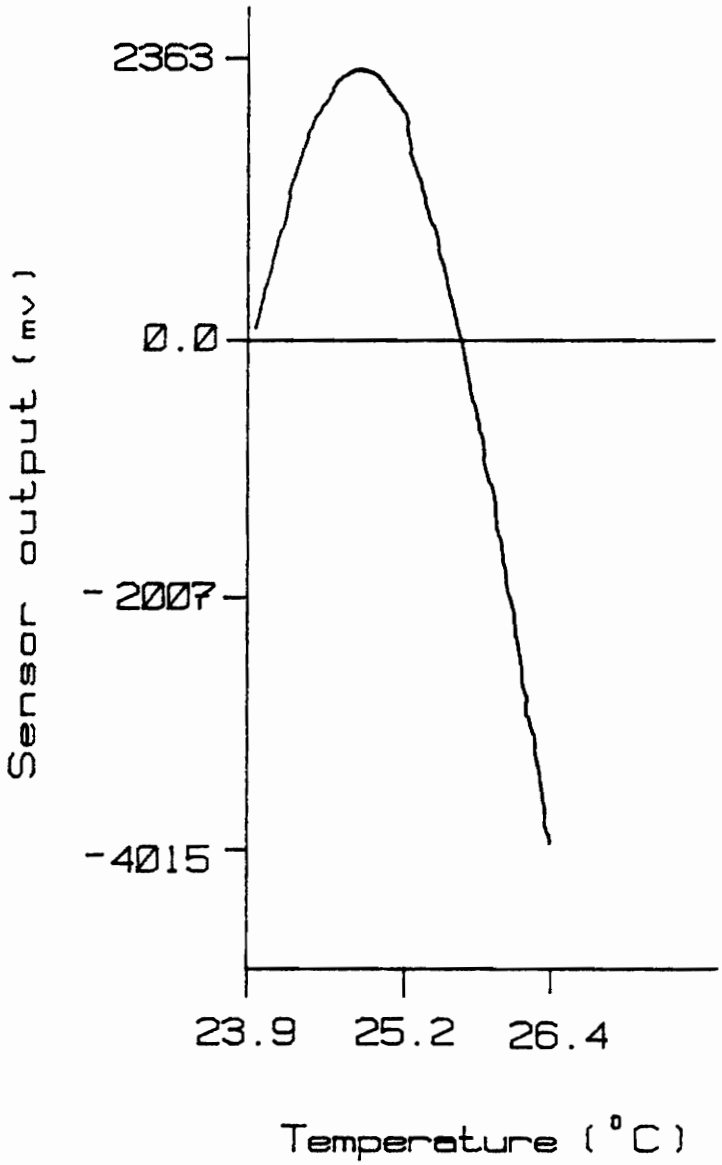

Figure 37. Signal vs. temperature direction

and the sequence repeated several times. It is important to note the direction of the output signal when pressure is applied. As expected from theory it is opposite to that caused by heat.

Figure 39 shows a typical sensor response to hydrogen in air with the output in figure 38 superimposed to scale. The response of the sensor to pressure is essentially baseline.

The signal produced by these relatively harsh pressure changes is approximately 20 mv which is about 1% of the normal response to 6.7% hydrogen in air (2 volts). The birefringent single arm interferometer is remarkably insensitive to isotropic pressure changes.

Experiment 5. Response Time of the Sensor

At a flow rate of approximately a liter per minute, the time required to completely flush the volume of the sensor head is in the millisecond range. In one experiment the computer has set the hydrogen solenoid to allow a pulse of 2.5 seconds of hydrogen into the carrier stream and in another experiment a 0.5 second pulse. Figure 40 shows that the sensor responds very quickly and with sufficient sensitivity to the presence of explosive concentrations of hydrogen gas.

Experiment 6. Hydrogen Vs. Deuterium

With the current renewed interest in hydrogen/palladium chemistry, an experiment comparing deuterium and hydrogen seemed necessary. Results showed no detectable difference

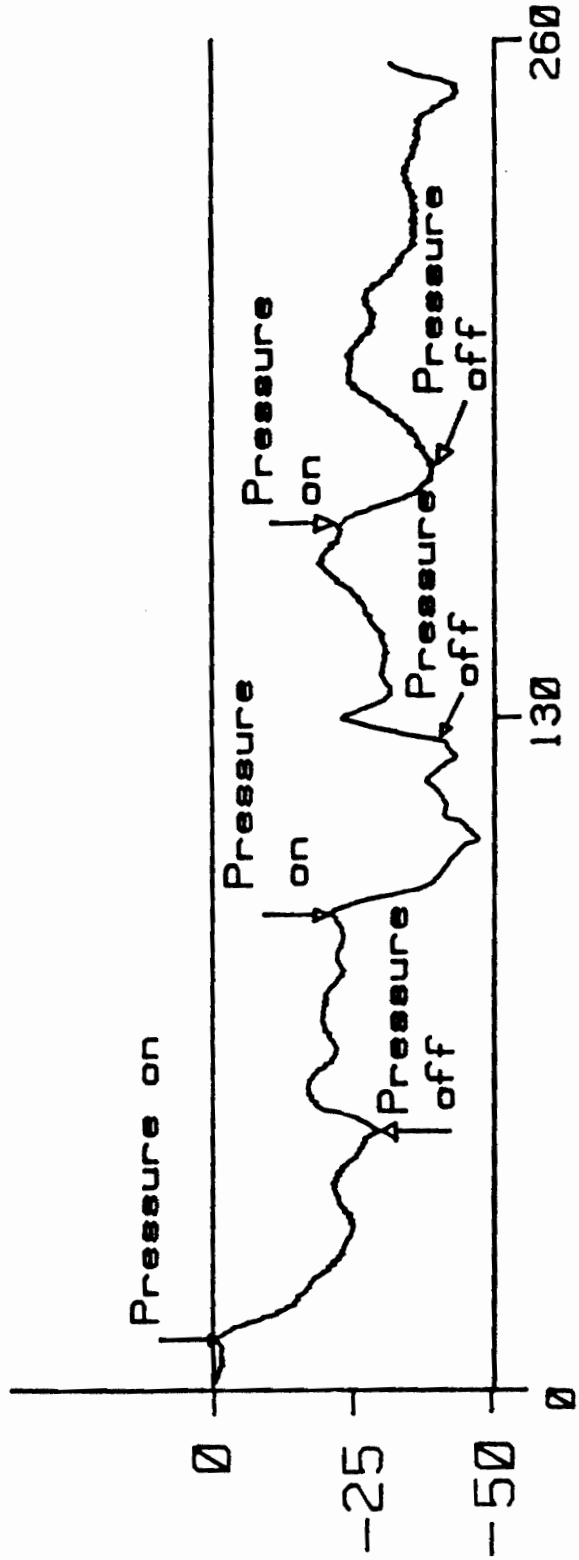

Figure 38. Sensor pressure response

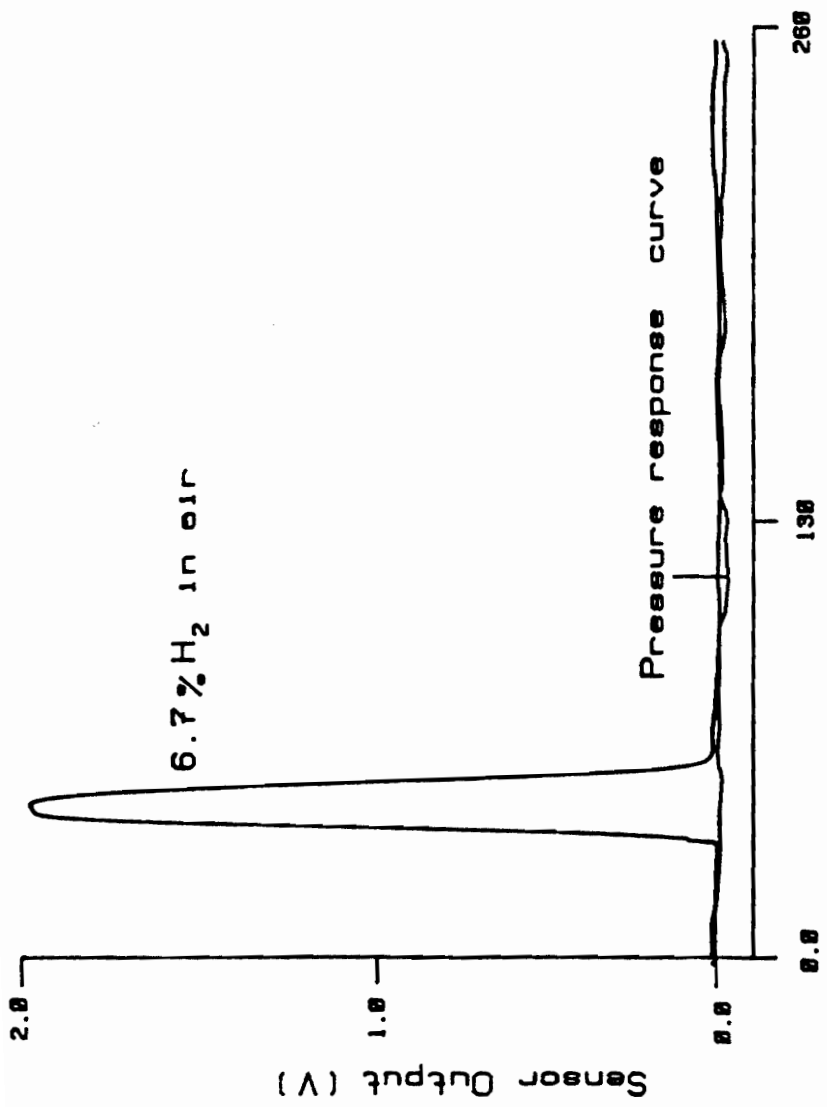

Figure 39. Sensor response to pressure and H_2

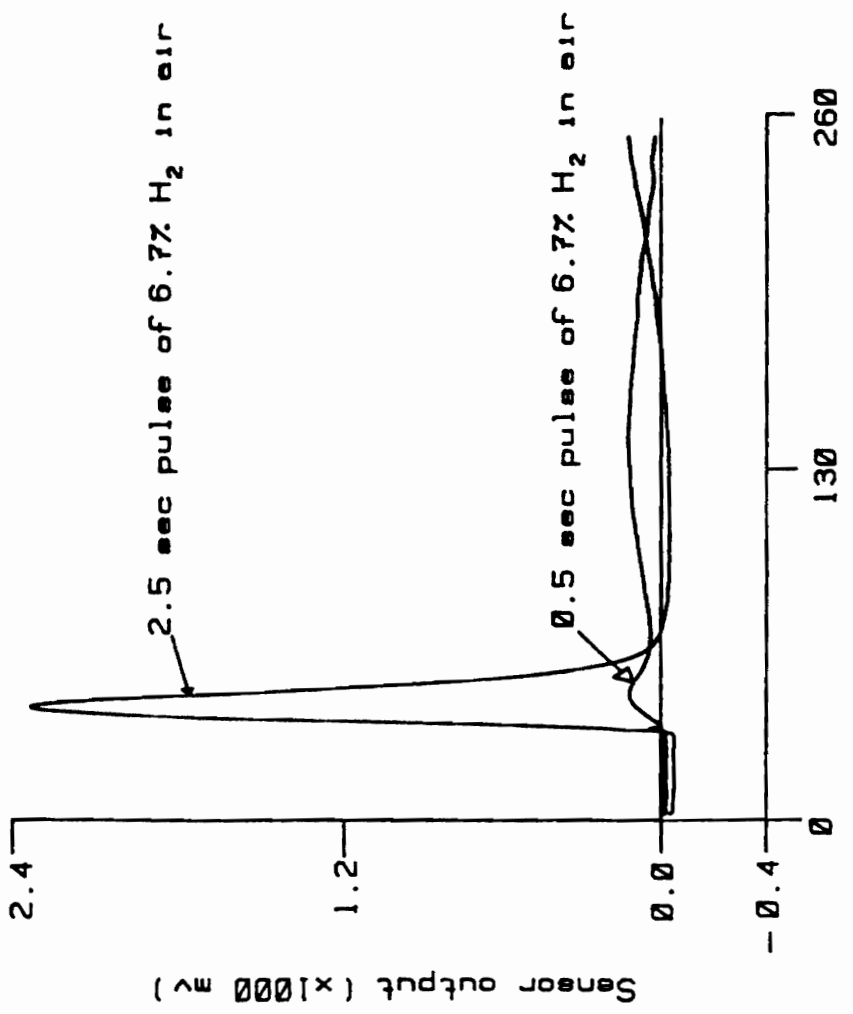

Figure 40. Sensor response time

between the two species (figure 41). This is not surprising. In order to generate appreciable heat, recent experiments have shown that the deuterium to palladium loading ratios must be as high as one (28).

In this research concentrations of hydrogen above 10% quickly destroyed the sensing capability of several of the bow-tie sensors. It appears that the 6 nanometer film of palladium can not support large quantities of hydrogen or deuterium. Therefore, the high loading ratios of hydrogen to palladium cannot be attained and no anomalous heat is generated.

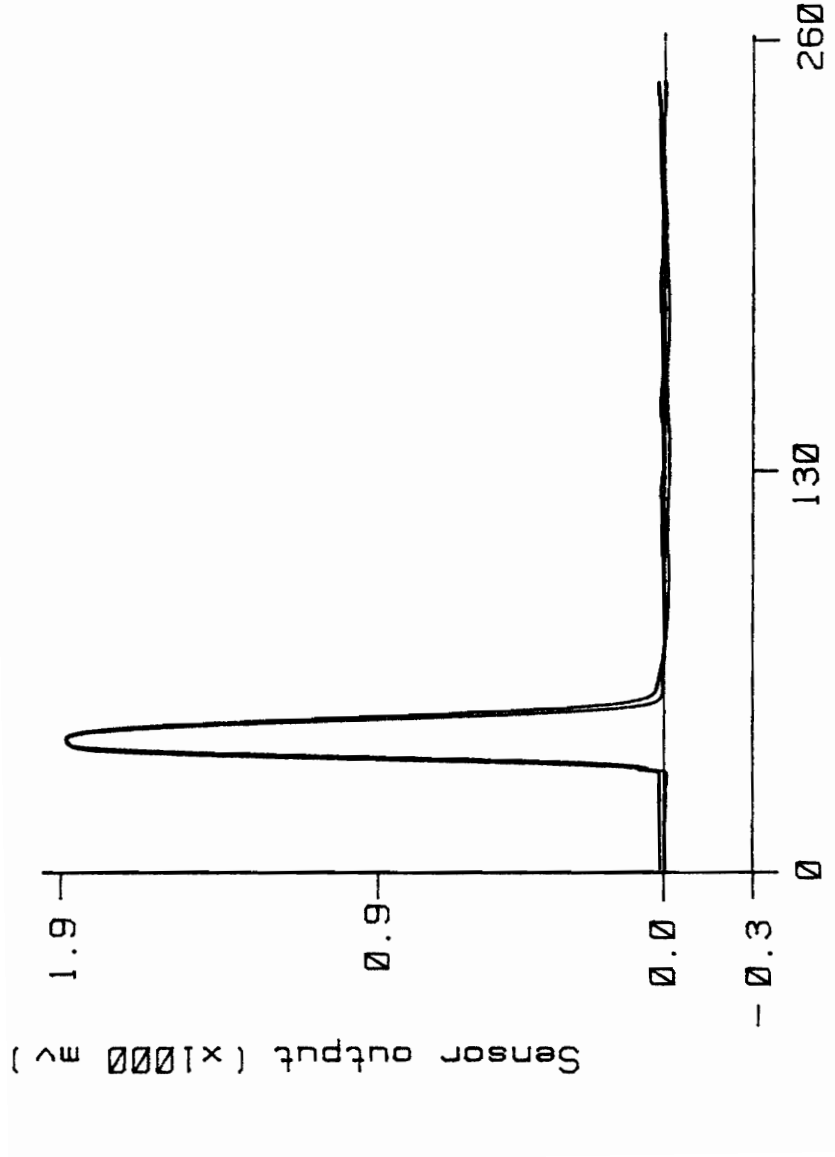

Figure 41. Sensor response to 6.7% H_2 and D_2 in air

VIII. Conclusions and Future Work

Heat phenomena are usually associated with chemical reactions regardless of whether the reaction is endo- or exothermic. A calorimetric probe that incorporates specificity, sensitivity, and a broad class of applicability would be the ultimate goal in an instrument development project.

In particular, analytical systems involving biosensor applications are currently receiving much attention. These systems depend on their biological component for specificity and sensitivity and make them unique and well suited for sensing a wide range of compounds (36).

A specific application requiring a rugged, small, and sensitive thermal detector would be detection of the eluting zones from isotachophoretic experiments (39).

Researchers have developed several instruments based on the heat evolved from enzyme biosensor reactions (5,37) . As with other calorimetric techniques they have encountered problems with sensitivity, pressure cross-sensitivity, and thermal isolation.

Although the thermal insulating techniques used in this research were not complicated, this device showed ample response and minimal baseline drift. Further development of thermal isolation techniques would help to lower signal to noise ratios. Ability to maintain stable ambient thermal conditions would allow longer sensing runs without substan-

tial drift in the baseline.

Adaptation of this instrument for a water jacket would allow for more effective temperature control. Water baths are currently the method of choice for thermally insulating precision calorimeters.

Designing the sensor head to allow liquid flow would make this instrument ideally suited for biosensor applications. The most crucial design problems would involve sealing against leaks, both from the flowing carrier stream and the surrounding water jacket. Also, preventing reactions between the carrier liquid and the sealing agent would be an important design criteria. This must be done without stressing the birefringent fiber. Work performed in other labs has shown that mounting stresses can cause inconsistent and unpredictable output signals (38).

With the advent of solid-state lasers and integrated optics, it may be possible to make this device into a small, rugged, package. Positive feedback from the integrated optics and digital control systems would allow for automatic initialization. The smaller size would make the thermal environment easier to control.

Cross-sensitivity to pressure and temperature plague most fiber optic sensing instruments. As discussed previously, and experimentally demonstrated in this work, the unique dynamics associated with the sensing mechanisms of the bow-tie fiber has all but eliminated pressure sensitivity. For flow injection analysis, such pressure insen-

sitivity is paramount.

Research performed early in the 80's reported the sensitivity of the bow-tie fiber to be around 0.9 radians per ^{o}C per meter of fiber (10). The instrument designed in this research has an experimental sensitivity 2 to 5 times higher (see appendix D). Theoretical output curves associated with instruments which have several different inherent phase relationships can be compared in figures 28, 29, and 30. Phase differences associated with the bow-tie fibers might well be dependent on how consistently the fibers are manufactured. Very small differences in the inherent birefringence of the fibers can change the sensitivity of the instrument. Of the seventeen fibers used in this research, all but one was able to perform with the same basic output response and sensitivity.

The electronics allows for ease of initialization, fewer optics, and simple, efficient data collection.

While this research did not focus in detail on the already well established chemistry of palladium, platinum, and hydrogen, the sensor is well suited for such in-depth experiments. Surface studies of the coated fiber may explain the decreased sensitivity of these sensors over several weeks time. Scanning electron micrographs were taken of the surface of used and pristine sensing fibers (appendix C). An obvious morphological change has taken place. Changes in the microstructure of the surface of palladium and platinum are thought to be a key to their cata-

lytic activity (32).

ESCA was performed on these same fibers and on pure platinum foil (Appendix E). Further studies would be needed to determine the significance of changes in the surface chemistry, in particular the decreased presence of platinum on the surface of the used, desensitized fiber.

Finally, although desirable, the modelling of the complex continuum mechanical processes taking place in the bow-tie fiber would be a considerable challenge. Numerous simplifying assumptions would need to be made to reduce the matrix and tensor mathematics to a tractable level.

This research, has tried to convey an understanding into the development of the single-arm interferometer as a thermal analytical probe. As with most research, the problems encountered, led to insight and continuous evolution of the design. Some engineering and theoretical work remains. However, as a chemical sensor, this instrument's potential has been established.

BIBLIOGRAPHY

1. L. S. Schuetz, J. H. Cole, J. Jarzynski, N. Lagakos, and J. A. Bucaro, Appl. Opt. 22, 478 (1983).
2. L. A. Bucaro, T. R. Hickman, Appl. Opt., 18, 938 (1979).
3. M. B. J. Diemeer, E. S. Trommel, Opt. Lett., 9, 260 (1984).
4. C. M. Davis, E. F. Carome, M. H. Weik, S. Ezekiel, R. E. Einzig, Fiberoptic Sensor Technology Handbook, (Optical Technologies, Inc., 1986).
5. L. W. Burgess, Ph.D. Dissertation, Virginia Polytechnical Institute and State University, Blacksburg, Virginia, 1984.
6. M.A. Butler, Appl. Phys. Lett., 45, 1007 (1984).
7. M. A. Butler, D. S. Ginley, J. Appl. Phys., 64, 3706 (1988).
8. B. Culshaw, Optical Fiber Sensing, (Peter Peregrinus Ltd., London, 1984), p. 96.
9. M. Gottlieb, G. B. Brandt, J. Butler, ISA Trans., 19, 55 (1980).
10. W. Eickhoff, Opt. Letts., 6, 204 (1981).
11. S. C. Rashleigh, Appl. Opt., 20, 1498 (1981).
12. F. A. Lewis, The Palladium Hydrogen System, (Academic Press, London, 1967), p. V.

13. S. E. Jones, J. B. Czir, d. L. Decker, G. L. Jensen, J. M. Thorne, S. F. Taylor, J. Rafelski, Nature 338, 737 (1989).

14. F. A. Lewis, The Palladium Hydrogen System, (Academic Press, London, 1967), p. 4.

15. W. M. Mueller, J. P. Blackledge, G. G. Libowitz, Metal Hydrides, (Academic Press, New York, 1968), p. 639.

16. N. N. Greenwood, A. Earnshaw, Chemistry of the Elements, (pergamon Press, New york, 1984), p. 1335.

17. D. N. Jewett, A. C. Makrides, Trans. Faraday Soc., 61, 932 (1965).

18. L. J. Gillespie, Henry A. Amborse, J. Phys. chem., 35, 3105 (1931).

19. D. M. Nace, J. G. Aston, J. Am. Chem. Soc., 79, 3619 (1957).

20. M. Flieschman, S. Pons, J. Electroanal. Chem., 261, 301 (1989).

21. J. H. Moore, C. C. Davis, M. A. Coplan, Building Scientific Apparatus, (Addison-Wesley Publishing Company, 1983), p. 41.

22. P. Horowtiz, W. Hill, The art of Electronics, (Cambridge University Press, London, 1980).

23. F. A. Lewis, The Palladium Hydrogen System, (Academic Press, London, 1967), p. 3.

24. J. F. Mcaleer, P. T. Moseley, P. Bourke, J. O. W. Norris, R. Stephan, Sensors and Actuators, 8, 251 (1985).

25. I. Lundstrom, S. Shivaraman, C. Svensson, L. Lundkvist, Appl. Phys. Lett., 26, 55 (1975).
26. B. Rosen, V. H. Dayan, R. L. Proffit, Hydrogen Leak and Fire Detection, (U. S. Government Printing Office, Washington, D. C., 1975), p. 19.
27. J. Harris, Surface Sci. Lett., 105, L288 (1981).
28. J. W. Shultze, V. Konig, A. Hochfeld, C. Van Calker, W. Kies, Electrochimica Acta, 34, 1289 (1989).
29. F. A. Lewis, The Palladium Hydrogen System, (Academic Press, London, 1967), p. 154.
30. L. G. Petersson, H. M. Dannetum, I. Lundstrom, Phys. Rev. Lett., 52, 1806 (1984).
31. B. K. Kasemo, E. Tornqvist, Phys. Rev. Lett., 44, 1555 (1980).
32. M. Nicholas, L. Dumoulin, J. P. Burger, J. Appl. Phys, 60, 3125 (1986).
33. E. Hecht, A. Zajac, Optics, (Addison-Wesley Publishing Company, 1975), p. 219.
34. R. D. Birch, D. N. Payne, M. P. Varnham, Electron. Lett., 18 , 1036 (1982).
35. M. Gottlieb, G. B. Brandt, Appl. Opt., 20, 3867 (1981).
36. L. D. Bowers, Anal. Chem., 58, 513a (1986).
37. L. Arney, Ph.D. Dissertation, Virginia Polytechnical Institute and State University, Blacksburg, Virginia, 1989.

38. K. Murphy, Fiber Optics Research Center, VPI and SU; private communication.

39. L. W. Jorgenson, Anal. Chem., 58, 743a (1986).

Appendix A

"Polyforth" by Forth, Inc. was the computer language used in the majority of the instrument control and data collection used in this research. Listed below are the four main routines used to control, collect, monitor, and analyze the output from the single-arm interferometer.

```
206 LIST
0 ( USE EXTERNAL CLOCK AND COLLECT DATA )
1 OCTAL
2 176770 CONSTANT ADCSR
3 CODE ATRIG ADCSR 32 # MOV BEGIN 176770 TST B 0< END NEXT
4 VARIABLE DAT 2000 ALLOT
5 : MEMAD 176772 @ 2000 0 DO ATRIG 176772 @ DAT I + ! 2
  +LOOP ;
6 : AXDUMP DAT 2000 DUMP ;
7 : AXIT MEMAD AXDUMP ;
8 VARIABLE WHERES
9 : RESTBLOCK# 317 WHERES ! ;
10 : SAVE1K DAT WHERES @ BLOCK 2000 MOVE UPDATE FLUSH ;
11 : NEXTBLOCK 1 WHERES + ! ;
12
13
14
15 DECIMAL


207 LIST
0 ( PULSE AND TICK MARK GENERATION )
1 OCTAL
2 16770 CONSTANT PCSR
3 CODE PULSE PCSR 0 # MOV PCSR 2 # MOV NEXT
4 : GO PULSE ;
5
6 : BASELINE 128 0 DO ATRIG 176772 @ DAT I + ! 2 +LOOP GO ;
7
8 : NPU 654 MOD 0= IF GO  THEN ;
9
10 : GATHER BASELINE 2000 75 DO ATRIG 176772 @ DAT I + ! 2
11 +LOOP ;
12 : BOT BASELINE 2000 75 DO ATRIG 176772 @ DAT I + ! I NPU
13 2 +LOOP ;
14
15 DECIMAL
```

```
248 LIST
0 (DIGITAL VOLTMETER )
1 : +1 ( -- SCALED "ONE") 16384 ;
2 : *. ( N N -- N ) +1 */ ;
3 : ##.## DUP ABS 0 <#  # # 46 HOLD # # ROT SIGN #> TYPE
  SPACE ;
4 : #.### DUP >R ABS 0 <# # # # 46 HOLD # R> MESS #> TYPE
  SPACE ;
5 : .T ##.## ;
6 : .F ( FRACTION -- ) #.### ;
7 OCTAL
8 : IATRIG 176772 @ DROP ATRIG 176772 @ DUP ;
9 : TATRIG 176772 @ DROP 1ATRIG 176772 @ DUP ;
10 : IDVM IATRIG 16077 *. SWAP 2 * + .F ;
11 : TDVM TATRIG 16077 *. SWAP 2 8 + .T ;
12 : DVM TDVM IDVM ;
13 : SCOPE 100000 0 DO DVM CR ESCAPE LOOP ;
14
15 DECIMAL

249 LIST
0 ( DATA COLLECTION 2 CHANNELS )
1 OCTAL
2 176770 CONSTANT ADCSR
3 CODE 1ATRIG ADCSR 432 # MOV BEGIN 176770 TST B 0< END NEXT
4 VARIABLE 1DAT 2000 ALLOT
5 : 1MEMAD 176772 @ 2000 0 DO 1ATRIG 176772 @ 1DAT I + !
6 2 +LOOP :
7 : 1AXDUMP 1DAT 2000 DUMP ;
8 : _ATRIG ATRIG 176772 @ DROP ATRIG 176772 @ DATT ;
9 : _1ATRIG 1ATRIG 176772 @ DROP 1ATRIG 176772 @ 1DAT :
10 : DMEMAD 176772 @ 2000 0 DO _ATRIG i + ! _1ATRIG I + !
11 2 + LOOP ;
12 VARIABLE 1WHERES
13 : 1SAVEK 1DAT 1WHERES @ BLOCK 2000 MOVE UPDATE FLUSH ;
14 : MESS ( N) 0< IF 55 HOLD THEN ;
15 DECIMAL
```

Appendix B

$$I_x = I_\emptyset \cos^2 \Theta/2$$

$$I_y = I_\emptyset \sin^2 \Theta/2$$

$$= \frac{\left(1+\cos\Theta - 1-\cos\Theta\right)}{\left(1+\cos\Theta + 1-\cos\Theta\right)}$$

1) $$\frac{I_x - I_y}{I_x + I_y} = \frac{I_\emptyset\left(\cos^2\Theta/2 - \sin^2\Theta/2\right)}{I_\emptyset\left(\cos^2\Theta/2 - \sin^2\Theta/2\right)}$$

$$= \frac{\left(1+\cos\Theta - 1-\cos\Theta\right)}{\left(1+\cos\Theta + 1-\cos\Theta\right)}$$

Given: $$\sin^2\Theta/2 = \frac{1-\cos\Theta}{2}$$

$$\cos^2\Theta/2 = \frac{1+\cos\Theta}{2}$$

$$= \frac{1+\cos\Theta - 1 + \cos\Theta}{1+\cos\Theta + 1-\cos\Theta}$$

1) $$\frac{I_x - I_y}{I_x + I_y} = \frac{I_\emptyset\left(\frac{1+\cos\Theta}{2} - \frac{1-\cos\Theta}{2}\right)}{I_\emptyset\left(\frac{1+\cos\Theta}{2} + \frac{1-\cos\Theta}{2}\right)}$$

$$= \frac{2\cos\Theta}{2} = \cos\Theta$$

APPENDIX C

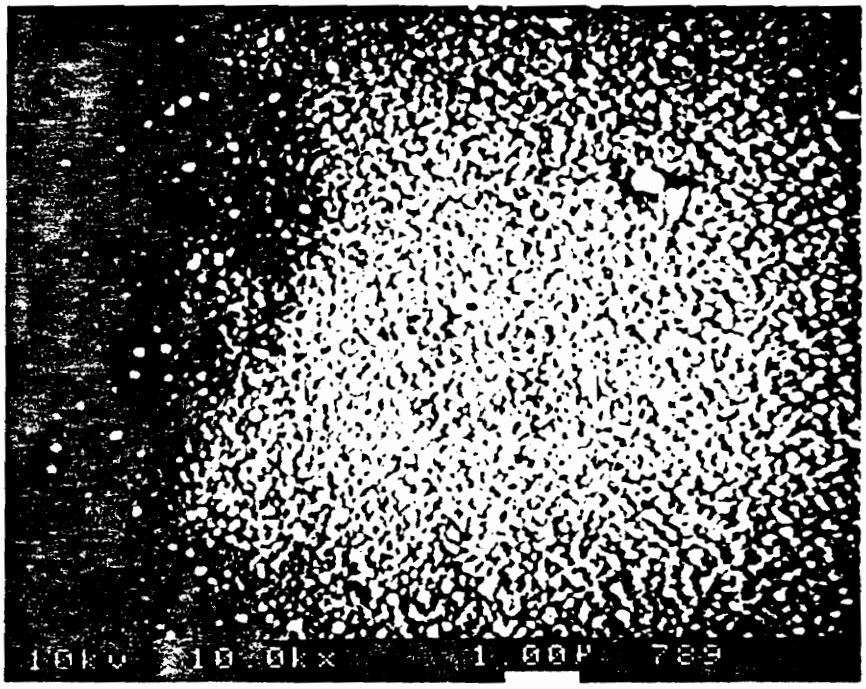

SEM of unexposed fiber surface

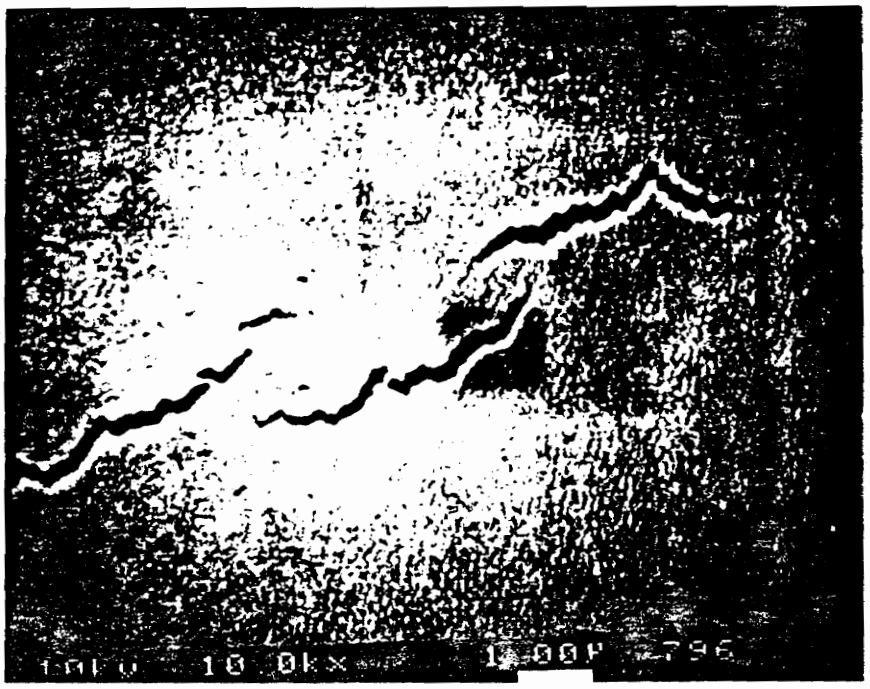

SEM of exposed, desensitized fiber

Appendix D

In order to calculate the sensitivity of the bow-tie fiber, an artificially induced temperature increase was monitored (see experimental). Data were obtained for both temperature in ^{o}C and sensor output in millivolts. Plots were made of sensor output vs. temperature change. An assumption is made that the output approximates the cosine function associated with the theoretical output curve for this device. From the linear portion of the cosine output two points were extracted. These voltages were scaled to allow the inverse cosine of the sensor output to be calculated. Taking the difference between these two angular values and dividing by the difference in temperature at these two points gives us the overall sensitivity of the fiber. The sensitivity is then normalized by dividng by the active sensing length of the bow-tie fiber in meters, e.g.

Sensor output (mv)	Scaled	$\cos^{-1}$	Temp^{o}C)	Sensitivity
-831	-0.0831	1.66 rad	22.3	2.63
-308	-0.0308	1.60 rad	22.6	rad/^{o}C meter

Appendix E

Electron Spectroscopy for Chemical Analysis was performed on pristine platinum foil, an unexposed sensing fiber, and on an exposed sensing fiber which has lost its sensitivity to hydrogen over several days.

	Element	Concentration (%)
Platinum Foil	Oxygen 1s	13.4
	Platinum 4f	23.6
	Palladium 3d	0.00
Unexposed sensing fiber	Oxygen 1s	27.3
	Platinum 4f	7.53
	Palladium 3d	0.00
Exposed Sensing Fiber	Oxygen 1s	15.2
	Platinum 4f	5.16
	Palladium 3d	0.07

Appendix F

The following sets of raw data are from designated experiments. All data was sampled at 0.5 second intervals. A 9-point unweighted moving window software filter and a multiplication factor of 2.441 (analog-to-digital converter step height) were applied to the data points before analysis and graphing were performed.

Raw data for statistics shown in figure 34; 6.7% H_2; 1 of 5 data sets:

15 16 14 15 14 15 14 15 14 13 15 15 14 16 15 16 15 16 16 16
15 17 16 17 16 16 15 16 17 17 15 15 15 17 15 17 15 15 16 17
17 16 15 16 17 15 16 15 14 13 14 12 13 9 9 7 7 7 6 7 4 3 3
2 6 4 2 1 2 4 7 9 11 13 18 29 40 65 83 125 173 217 261 319
383 425 464 497 529 557 592 609 625 643 658 670 680 688 694
704 706 710 714 716 721 726 727 731 739 740 748 754 753 753
752 746 741 729 719 711 691 677 658 640 623 605 591 573 558
544 527 511 487 464 441 417 394 375 359 349 337 326 313 301
287 272 253 236 214 198 176 158 142 130 118 107 97 91 85 80
72 66 60 54 45 39 33 28 22 15 12 8 6 2 0 -4 -5 -8 -9 -12
-12 -12 -13 -11 -9 -10 -10 -12 -11 -12 -11 -11 -12 -11 -11
-10 -9 -7 -5 -4 -2 -1 1 0 0 1 0 2 1 3 2 2 2 2 3 2 4 4 4 3 3
5 4 3 2 2 2 2 2 0 1 3 1 3 1 2 2 1 3 2 3 3 3 2 0 2 0 2 3 2 3
1 4 2 3 4 2 4 3 2 4 3 3 2 3 1 2 2 1 2 2 2 1 0 2 1 2 2 0 2 0
1 1 1 1 1 2 1 0 2 0 0 0 1 1 1 1 2 1 3 2 3 2 2 1 0 1 1 -2 0
-1 -3 -2 -5 -4 -6 -6 -6 -6 -5 -3 -5 -3 -2 -2 0 -1 -2 0 0 -1
-3 -2 -2 -3 -3 -1 -3 0 -1 -2 -1 -2 -1 0 -1 0 -1 0 1 -1 0 0
0 0 0 0 1 0 0 1 1 2 2 1 2 1 0 1 -1 1 1 -1 0 0 0 0 0 0 1 1 1
0 1 0 1 1 1 0 -2 0 -1 -3 -3 -5 -5 -4 -6 -7 -7 -8 -9 -9 -9
-11 -10 -11 -12 -13 -15 -13 -14 -15 -14 -14 -17 -14 -14 -16
-16 -16 -15 -17 -17 -17 -16 -17 -18 -18 -17 -19 -18 -17 -18
-16 -17 -16 -19 -16 -18 -17 -17 -19 -17 -17 -17 -16 -16 -17
-16 -15 -15 -13 -14 -15 -15 -14 -12 -14 -13 -12 -12 -11 -11
-12 -11 -8 -9 -10 -8 -8 -8 -6 -6 -5 -7 -5 -7 -6 -5 -5 -6 -4
-4 -5 -4 -3 -4 -4 -4 -4 -5 -4 -5 -6 -6 -7 -7 -5 -5 -6 -6 -5
-6 -8 -6 -6 -8 -6 -8 -9 -8

2 of 5:

-9 -6 -6 -6 -6 -6 -4 -5 -6 -8 -7 -7 -7 -9 -7 -8 -8
-9 -9 -8 -9 -9 -11 -9 -9 -11 -11 -9 -10 -11 -11 -10 -11 -11
-12 -12 -11 -12 -11 -10 -11 -11 -12 -11 -12 -13 -14 -15 -15
-15 -18 -18 -19 -18 -20 -20 -19 -19 -19 -18 -17 -14 -15 -16
-12 -12 -11 -11 -9 -2 4 18 37 51 72 100 134 176 225 272 317
382 438 485 518 540 559 575 590 604 614 623 629 635 637 645
651 657 662 667 671 684 691 698 708 713 723 728 733 736 743
751 749 748 751 748 742 735 722 712 696 677 660 641 624 604
584 564 547 531 514 500 492 481 470 456 439 420 400 383 372
362 351 344 340 329 318 311 298 290 274 256 238 221 205 190
173 161 148 139 133 122 116 111 104 97 91 84 78 69 61 51 46
39 32 28 21 15 7 2 0 -3 -5 -6 -8 -9 -10 -13 -12 -14 -14 -17
-19 -20 -20 -21 -24 -22 -24 -23 -25 -24 -24 -25 -25 -26 -24
-25 -26 -24 -24 -25 -25 -25 -25 -26 -26 -26 -25 -28 -26 -27
-26 -25 -24 -25 -24 -24 -22 -23 -22 -23 -22 -22 -22 -22 -24
-25 -26 -25 -25 -26 -26 -25 -25 -24 -25 -25 -26 -27 -26 -25
-25 -26 -27 -27 -26 -24 -26 -25 -24 -25 -21 -22 -22 -21 -21
-20 -20 -17 -19 -18 -19 -21 -18 -20 -18 -18 -21 -20 -21 -20
-20 -20 -20 -21 -20 -19 -20 -19 -20 -20 -21 -20 -19 -19 -20
-20 -22 -21 -21 -21 -21 -21 -23 -22 -22 -23 -24 -22 -22 -21
-22 -21 -20 -22 -21 -21 -21 -21 -21 -19 -19 -20 -20 -19 -17
-18 -18 -19 -18 -20 -20 -19 -19 -22 -20 -21 -21 -21 -19 -20
-21 -21 -21 -23 -22 -21 -22 -23 -23 -24 -25 -25 -24 -26 -26
-27 -27 -29 -27 -28 -28 -29 -30 -30 -32 -31 -31 -31 -33 -34
-35 -35 -36 -37 -38 -37 -37 -40 -40 -39 -40 -41 -41 -42 -42
-45 -45 -44 -45 -45 -46 -46 -48 -48 -47 -49 -51 -50 -46 -47
-48 -48 -47 -47 -47 -46 -46 -47 -47 -46 -47 -47 -47 -45 -44
-43 -43 -41 -41 -40 -41 -41 -39 -39 -38 -38 -37 -38 -38 -36
-36 -35 -35 -35 -34 -35 -34 -33 -33 -32 -33 -32 -32 -33 -33
-35 -36 -35 -37 -35 -36 -36 -36 -34 -36 -35 -36 -38 -38 -39
-40 -40 -40 -40 -38 -37 -37 -38 -37 -38 -38 -39 -40 -42 -41
-42 -43 -46 -46 -46 -45 -44 -42 -41 -41 -38 -39 -38 -40 -41
-41 -41 -42 -43 -44 -45 -45 -46 -44 -45 -44 -43 -42 -40 -38
-36 -36 -36 -36 -37

3 of 5:

-37 2 3 2 0 0 3 0 -1 -2 -1 -4 -5 -4 -3 -5 -3 -4 -4 -5 -3 -3
-4 -2 -4 -2 -3 -1 -1 -4 -5 -2 -3 -5 -4 -5 -4 -4 -4 -4 -4 -3
-4 -6 -2 -3 -2 -4 -3 0 -2 -3 -2 -2 -2 -5 -3 -5 -4 -3 -4 -4
-3 -2 -3 -2 -4 0 0 6 11 26 44 61 81 111 130 165 211 251 303
354 404 450 497 555 590 616 635 645 656 664 669 672 677 681
686 693 699 708 715 724 731 741 751 758 768 780 791 808 813
823 829 832 831 828 822 814 802 789 773 757 737 715 690 667
646 629 612 594 578 563 549 537 525 512 498 486 471 457 449
444 436 425 415 401 398 383 373 359 342 319 304 280 266 245
231 218 203 188 173 166 158 152 144 137 128 121 113 102 91
81 72 62 55 44 36 30 24 17 12 10 6 6 5 4 2 4 1 0 0 -3 -5 -6
-8 -11 -12 -12 -15 -15 -17 -17 -16 -17 -16 -17 -15 -17 -16
-18 -18 -19 -18 -18 -20 -18 -21 -20 -22 -22 -22 -25 -23 -22
-24 -25 -26 -26 -25 -24 -26 -27 -26 -30 -28 -30 -29 -25 -28
-27 -28 -29 -29 -28 -28 -28 -29 -30 -30 -28 -31 -28 -28 -29
-29 -27 -25 -28 -30 -29 -26 -27 -27 -24 -27 -27 -29 -25 -27
-27 -26 -25 -27 -29 -28 -30 -29 -31 -30 -30 -31 -30 -30 -32
-33 -35 -35 -33 -34 -32 -35 -34 -33 -32 -30 -33 -33 -33 -34
-34 -34 -33 -35 -37 -34 -36 -37 -37 -34 -37 -35 -34 -30 -32
-32 -34 -31 -32 -29 -31 -32 -33 -35 -34 -36 -34 -34 -36 -36
-36 -36 -35 -35 -35 -32 -30 -26 -28 -31 -29 -30 -29 -27 -30
-29 -30 -26 -29 -30 -32 -28 -31 -29 -27 -27 -29 -28 -26 -29
-29 -29 -28 -28 -29 -30 -29 -30 -31 -30 -31 -31 -31 -31 -29
-31 -34 -30 -33 -32 -32 -32 -31 -32 -28 -29 -31 -29 -30 -31
-31 -33 -32 -36 -36 -35 -36 -35 -32 -32 -32 -35 -34 -31 -32
-33 -31 -33 -32 -32 -30 -30 -30 -28 -33 -31 -31 -29 -31 -31
-31 -31 -32 -31 -31 -32 -31 -30 -29 -28 -28 -29 -28 -29 -28
-28 -27 -30 -30 -32 -31 -31 -30 -29 -31 -31 -34 -31 -32 -32
-32 -31 -33 -30 -34 -34 -35 -34 -31 -33 -33 -34 -35 -34 -32
-33 -32 -35 -35 -35 -34 -35 -37 -38 -36 -38 -37 -39 -38 -38
-36 -38 -35 -38 -36 -32 -33 -34 -32 -35 -33 -32 -34 -30 -35
-31 -32 -35 -34 -33 -35 -34 -34 -34 -34 -34 -34 -35 -36 -37
-35 -35 -33

4 of 5:

-36 -11 -11 -9 -12 -11 -15 -11 -13 -13 -15 -15 -17 -20 -17
-22 -23 -22 -25 -25 -27 -29 -28 -29 -27 -27 -27 -27 -30 -28
-28 -33 -33 -33 -32 -32 -34 -32 -31 -33 -33 -33 -37 -34 -36
-36 -35 -36 -37 -35 -37 -37 -35 -38 -38 -36 -37 -34 -36 -32
-28 -32 -29 -27 -25 -24 -22 -23 -19 -12 0 19 46 72 108 150
200 258 319 307 346 402 448 483 516 540 567 593 608 617 624
632 640 647 654 666 672 677 682 688 692 701 713 725 741 755
770 787 800 812 830 838 843 849 851 846 840 831 821 803 789
765 743 717 696 676 655 632 612 591 571 553 535 521 511 506
500 494 485 477 475 471 461 451 443 430 425 410 401 389 379
362 355 335 316 306 279 272 262 241 230 209 195 183 173 161
155 146 139 130 123 118 105 96 90 79 70 61 53 44 37 31 24
20 16 12 10 10 8 9 7 9 10 7 7 5 3 3 -1 -3 -4 -8 -10 -15 -13
-17 -20 -23 -26 -27 -29 -31 -30 -30 -34 -36 -35 -36 -37 -39
-37 -40 -42 -42 -42 -44 -42 -45 -44 -45 -47 -46 -48 -44 -51
-50 -49 -49 -49 -49 -49 -48 -48 -51 -49 -48 -49 -45 -49 -48
-47 -47 -47 -42 -42 -44 -43 -41 -40 -40 -42 -42 -43 -44 -44
-45 -47 -45 -45 -47 -45 -45 -49 -48 -48 -49 -50 -51 -50 -52
-51 -51 -50 -51 -51 -52 -52 -50 -50 -51 -50 -50 -50 -48 -50
-49 -48 -48 -47 -45 -44 -44 -44 -44 -43 -44 -44 -44 -42 -44
-42 -42 -42 -41 -42 -45 -43 -45 -42 -42 -44 -45 -43 -42 -45
-44 -44 -47 -46 -44 -43 -45 -44 -44 -45 -44 -43 -43 -44 -42
-45 -44 -45 -44 -42 -44 -45 -44 -42 -45 -43 -44 -44 -45 -44
-46 -43 -43 -43 -44 -45 -44 -43 -43 -42 -42 -43 -44 -40 -41
-39 -41 -42 -40 -41 -41 -40 -39 -40 -40 -39 -40 -39 -42 -42
-41 -40 -42 -39 -40 -41 -41 -42 -42 -45 -44 -45 -46 -44 -45
-45 -46 -44 -42 -46 -43 -44 -45 -47 -44 -43 -45 -43 -44 -46
-45 -45 -44 -43 -45 -45 -43 -45 -45 -44 -46 -48 -46 -47 -47
-44 -46 -48 -47 -48 -49 -47 -47 -47 -46 -48 -46 -45 -48 -46
-47 -47 -48 -45 -46 -47 -48 -46 -48 -47 -46 -49 -47 -46 -47
-45 -47 -48 -48 -45 -45 -43 -39 -42 -41 -43 -41 -39 -42 -41
-41 -40 -41 -39 -39 -41 -40 -42 -40 -42 -42 -42 -42 -42 -43
-42 -42 -42 -40 -43 -43 -41 -40 -43 -41 -41 -41 -39 -43 -44
-42 -42 -40 -42 -41 -41 -42

5 of 5:

-41 -6 -7 -9 -8 -7 -10 -8 -8 -11 -12 -14 -11 -11 -13 -12
-12 -13 -12 -12 -13 -12 -13 -9 -12 -9 -12 -10 -10 -9 -11 -8
-9 -8 -9 -9 -9 -10 -11 -7 -8 -8 -7 -10 -10 -9 -10 -9 -9 -9
-10 -11 -9 -11 -9 -9 -10 -8 -11 -9 -10 -8 -7 -10 -8 -7 -8
-4 -7 -2 3 22 38 63 98 138 191 248 310 355 408 429 466 508
538 560 578 593 606 616 628 639 650 663 669 678 691 701 711
719 733 743 754 769 777 789 801 818 841 859 878 888 900 904
904 905 894 887 876 856 835 812 799 783 759 736 709 685 661
634 614 594 580 567 555 543 535 533 529 524 523 513 506 498
486 481 466 450 443 432 423 399 399 380 354 326 301 274 250
231 205 194 173 159 148 137 130 123 121 121 112 107 102 96
92 83 76 71 67 61 54 49 44 40 37 35 33 31 30 31 29 29 29 30
27 28 26 24 24 22 19 18 16 11 10 9 9 7 3 2 -1 0 -2 -7 -8
-10 -10 -12 -13 -14 -17 -13 -16 -18 -17 -16 -17 -16 -18 -17
-20 -20 -20 -19 -21 -21 -22 -23 -24 -23 -20 -22 -24 -22 -24
-24 -25 -23 -27 -25 -23 -25 -26 -25 -24 -25 -27 -27 -29 -28
-29 -28 -28 -29 -30 -29 -30 -32 -28 -30 -30 -30 -29 -28 -28
-29 -29 -29 -27 -26 -28 -29 -26 -27 -26 -28 -26 -29 -23 -26
-27 -26 -26 -28 -29 -26 -27 -28 -27 -29 -29 -29 -29 -29 -28
-31 -28 -30 -30 -30 -29 -30 -31 -30 -29 -28 -28 -27 -27 -28
-28 -28 -27 -26 -30 -30 -28 -28 -27 -29 -27 -28 -26 -27 -27
-25 -28 -26 -26 -26 -27 -26 -26 -24 -24 -26 -24 -25 -24 -25
-24 -23 -23 -27 -23 -25 -25 -22 -26 -26 -26 -26 -28 -27 -26
-27 -28 -27 -26 -25 -29 -28 -29 -30 -28 -28 -29 -29 -29 -30
-28 -27 -27 -28 -26 -27 -28 -26 -26 -26 -27 -24 -27 -24 -26
-26 -25 -26 -27 -27 -26 -25 -27 -27 -28 -27 -28 -29 -27 -28
-27 -25 -24 -24 -24 -25 -26 -25 -25 -25 -26 -23 -24 -23 -26
-21 -25 -23 -23 -22 -21 -21 -20 -22 -21 -21 -21 -21 -21 -21
-19 -23 -21 -22 -23 -24 -23 -24 -23 -23 -24 -25 -24 -22 -25
-26 -25 -25 -26 -25 -27 -25 -26 -27 -26 -25 -25 -25 -29 -27
-27 -26 -25 -25 -26 -25 -25 -24 -25 -22 -25 -24 -23 -24 -23
-25 -24 -24 -23 -26 -26 -27 -25 -22 -25 -24 -24 -23 -24 -24
-24 -25 -24 -25 -24 -23 -23 -24 -23 -25 -23 -24

Raw data for statistics shown in figure 34; 1.4% H_2; 1 of 5 data sets:

-3 13 11 15 13 10 10 9 9 12 11 10 11 10 9 9 12
11 9 11 8 10 7 13 6 7 10 7 10 9 12 9 8 8 7 6 7 3 3 8 2 5 8
3 4 4 6 3 4 2 0 -1 1 -2 0 0 -1 -3 -4 -4 -2 -6 -5 -6 -5 -6
-8 -4 -3 -6 -5 -7 -6 -9 -6 -8 -7 -8 -7 -5 -7 -5 -3 -4 -2 -2
-5 -4 -2 -5 -1 0 0 1 3 4 7 7 9 11 13 12 13 16 19 19 22 25
27 29 34 38 36 43 43 47 51 54 56 62 63 69 70 81 76 83 91 88
90 93 94 98 104 107 111 112 114 119 118 122 124 128 129 131
132 136 139 141 144 147 145 153 150 152 152 154 157 158 159
161 164 164 167 167 170 175 174 174 176 179 179 180 179 181
183 184 184 188 189 189 189 190 193 192 199 196 194 197 197
196 201 200 200 204 208 205 205 210 208 206 208 210 209 212
212 212 212 219 216 218 221 220 221 224 224 226 228 229 230
231 233 229 229 226 222 220 215 210 204 199 193 188 184 175
167 157 151 146 140 129 125 117 111 108 101 95 93 88 83 77
75 72 71 70 69 66 70 64 62 62 58 55 55 52 54 49 52 51 54 48
47 45 45 41 42 40 39 39 36 38 35 33 38 32 32 30 29 28 27 27
26 27 27 26 25 24 24 22 25 24 20 22 20 20 22 20 19 15 15 15
15 14 17 17 15 16 17 17 20 16 19 22 17 15 17 19 15 15 17 20
15 15 15 14 11 14 14 10 13 11 11 10 11 9 13 7 8 8 7 6 9 7 5
6 6 5 6 6 1 2 2 5 1 1 2 1 -1 0 -1 -4 -3 -4 -5 -3 2 -1 -2 0
1 -4 -3 -1 1 0 2 -1 0 0 0 -3 -1 1 -3 -2 -4 -1 -3 -1 0 3 5 7
5 6 6 7 7 5 4 6 8 7 9 9 4 4 6 4 3 2 4 4 3 2 2 2 7 5 5 5 4 4
3 10 7 8 8 7 8 7 9 8 7 11 7 6 10 6 8 7 9 9 9 8 7 8 8 7 6 8
10 8 7 8 8 9 9 10 8 11 8 9 7 11 10 8 9 9 11 7 6 7 2 6 4 5 6
5 5 2 2 5 5 2 3 3 5 5 7 5 3 6 8 6 3 5 4 6 6 5 6 7

2 of 5:

10 10 10 10 8 8 7 8 7 10 10 10 9 8 6 8 11 8 10 10 10 10 9 9
10 8 11 10 9 10 12 8 9 9 9 7 8 5 8 7 9 9 6 7 10 11 11 7 9 9
9 10 11 8 10 7 8 8 6 9 6 9 8 9 7 8 6 6 3 7 8 6 10 11 10 14
11 14 12 16 20 20 23 23 24 29 33 36 36 40 41 44 47 47 56 55
63 61 64 68 72 71 79 82 84 91 92 98 100 105 109 112 117 121
121 128 135 133 135 140 142 145 151 152 152 157 159 159 163
165 170 170 174 176 177 181 184 183 186 188 190 191 194 194
198 201 201 203 205 204 208 206 211 211 212 218 217 215 219
217 218 221 221 223 224 228 231 229 231 229 229 230 231 230
232 235 238 236 238 240 237 242 241 242 243 245 245 244 247
246 247 251 249 251 251 252 256 253 254 256 255 252 256 255
257 258 259 261 260 259 260 260 262 262 265 265 264 264 266
265 261 260 260 257 252 249 243 237 231 225 218 211 203 195
189 182 174 165 158 149 143 135 129 124 115 112 106 101 97
95 91 86 83 80 75 74 71 67 69 65 63 60 58 55 54 52 51 51 50
49 47 46 45 45 46 42 42 42 42 39 40 39 36 35 35 32 34 34 31
29 28 28 32 24 23 24 23 27 28 25 24 22 17 18 21 18 18 18 19
16 14 17 17 13 12 15 14 11 12 13 9 10 10 13 9 9 10 6 8 7 6
6 5 4 6 11 4 5 4 3 2 1 1 2 1 3 2 1 -1 0 2 2 2 0 -1 -1 -1 -1
-1 2 -1 0 -3 -3 -2 -2 -1 0 0 3 0 -1 1 4 1 5 4 6 4 5 3 4 4 5
3 7 4 4 3 3 3 4 4 3 5 5 6 6 2 4 4 4 2 1 2 0 0 1 -1 0 0 1 6
2 1 0 0 -3 -4 -1 -2 0 0 -1 -4 -1 -1 -2 -1 -2 -4 0 -1 -1 -4
-3 -3 -5 -3 -2 -1 -1 -3 -1 -3 -4 -2 -3 -2 -2 -1 -1 -1 1 -3
-3 1 -1 -1 -2 -1 0 2 -1 0 0 -1 0 1 -2 2 -3 1 1 -2 0 1 0 0 2
3 0 1 3 2 5 7 4 4 5 5 6 9 10 8 9 8 8 7 7 8 7 9 8 11 14 10
11 9 8 10

3 of 5:

9 -20 -21 -22 -18 -20 -21 -20 -23 -22 -23 -21 -20 -19 -20
-19 -22 -21 -18 -21 -20 -17 -20 -20 -21 -21 -19 -17 -21 -19
-19 -21 -18 -21 -20 -19 -18 -20 -19 -17 -17 -20 -21 -19 -21
-20 -19 -21 -20 -21 -22 -21 -21 -16 -22 -22 -19 -20 -21 -20
-20 -17 -18 -16 -17 -16 -16 -17 -14 -14 -15 -12 -14 -12 -12
-9 -11 -11 -9 -12 -9 -9 -9 -6 -2 -1 0 0 0 3 3 6 5 9 13 13
15 15 19 18 21 25 28 33 34 39 41 44 45 52 56 58 60 69 73 70
73 79 85 85 90 93 95 103 104 105 112 117 118 119 125 126
130 133 136 139 143 144 148 149 154 155 159 158 161 161 164
168 171 172 175 174 178 178 178 182 185 184 188 187 189 192
191 193 194 198 197 197 198 200 201 202 202 203 204 205 205
207 206 206 209 208 210 216 214 212 218 216 216 218 220 220
224 224 224 224 224 224 226 226 228 226 229 232 230 228 231
233 232 233 235 235 238 238 238 239 237 238 241 242 240 240
236 235 233 228 222 218 212 206 199 193 187 180 173 163 161
150 142 135 126 124 117 107 103 99 90 84 80 76 73 69 67 60
61 55 55 54 51 50 49 47 46 45 42 43 44 42 44 40 39 40 37 36
37 37 35 34 32 30 28 29 34 29 25 27 24 24 21 23 21 19 19 19
21 19 20 19 19 19 22 24 21 21 20 18 17 16 17 17 19 21 17 17
15 15 13 12 13 13 13 12 9 10 12 11 11 12 13 10 10 7 5 6 7 8
8 7 5 5 6 5 5 7 6 6 5 5 3 4 3 2 4 6 4 7 4 4 1 6 2 3 1 4 1 1
2 3 -2 -3 2 -1 -1 0 -4 -5 -4 -6 -8 -4 -3 -6 -7 -7 -6 -2 -7
-6 -5 0 -7 -7 -7 -9 -8 -9 -6 -6 -8 -10 -9 -7 -8 -9 -9 -8 -8
-7 -7 -7 -7 -9 -9 -10 -7 -10 -10 -8 -7 -10 -6 -11 -9 -11 -9
-11 -9 -9 -11 -11 -9 -8 -12 -9 -6 -6 -9 -6 -5 -6 -6 -4 -5
-5 -6 -4 -4 -2 -4 -5 -5 -4 -1 -5 -3 -3 -6 -6 -5 -5 -4 -4 -2
-4 -3 -6 -2 -3 2 -3 -2 -3 -3 -3 -3 -1 -4 -3 -4 -4 -6 -6 -6
-2 -6 -4 -3 -1 -2 -1 0 0 -1 -3 -2 -3 -1 -3 0 -3 -2 -1 -1 -1
1 1 0 -3 -1 0 -1 1

4 of 5:

-1 -3 -1 -4 -3 -3 -1 -2 -2 0 -3 -5 -4 -1 -3 -1 1 3 0 -3 -1
-2 3 -3 -2 -2 -6 -5 -3 -3 -4 -5 -7 -6 -6 -2 -5 -5 -5 -6 -3
-5 -7 -4 -6 -5 -3 -7 -5 -7 -8 -5 -3 -4 -3 -4 -3 -3 -4 -3 -2
-1 -5 -4 -6 -3 -6 -4 -5 -3 -7 -5 -4 -6 -6 -3 -1 -5 -4 -5 -4
0 0 0 1 3 2 4 5 5 7 8 9 12 14 15 22 20 24 25 29 31 36 38 42
45 48 54 55 63 63 68 74 76 78 85 91 95 97 103 113 113 116
121 127 127 132 134 136 140 143 151 149 152 155 156 159 161
166 169 171 172 175 176 178 182 184 186 187 191 190 194 194
196 198 198 200 203 201 204 206 207 208 209 208 211 215 211
216 219 218 216 217 218 221 222 229 226 225 228 229 231 231
232 233 231 234 235 238 237 238 240 240 239 242 241 241 243
242 244 245 246 244 244 246 248 250 249 249 250 249 250 250
253 254 255 255 256 255 257 258 255 255 248 247 243 240 234
227 221 217 207 201 195 187 179 169 162 152 145 139 130 124
116 109 103 101 91 87 79 75 72 68 65 62 60 56 55 53 56 51
52 48 49 48 46 47 46 45 46 42 42 42 42 43 40 38 39 39 40 36
34 36 34 33 33 34 34 32 33 31 31 28 30 30 27 28 26 25 26 28
25 24 23 25 26 20 24 23 21 21 19 18 21 19 20 16 19 15 14 17
15 15 13 13 12 11 11 10 11 8 8 8 8 6 8 7 4 4 6 5 7 7 5 2 4
3 4 3 1 3 8 1 0 3 0 3 0 -1 0 0 0 0 2 0 -4 1 1 -1 -2 -1 -2
-1 -3 -1 0 -1 -3 -1 -3 0 -1 0 -1 -1 0 -1 -2 -2 1 -1 -3 -1 2
2 0 2 -1 0 0 -2 -3 -2 -4 -7 -5 -2 -5 -5 -5 -6 -6 -6 -1 -1
-6 -4 -5 -3 -4 -3 -2 -2 -4 -3 -4 -2 -4 -2 -4 -4 -4 -4 -3 -2
-4 -4 -3 -4 -4 -3 -3 0 -3 -4 -1 -2 -1 -2 0 -2 -3 1 -1 -1 0
-1 0 0 3 0 1 -1 -2 0 0 1 0 1 0 1 0 1 3 2 -2 0 0 1 1 3 1 0
-1 0 3 1 1 1 3 3 2 2 2 2 0 0 1 2 3 -1 3 2 3 2 0 1 1 1 2 0 0

5 Of 5:

1 1 4 1 0 4 1 1 2 1 1 1 2 2 1 2 0 4 3 2 0 0 -1 1 1 3 1 -1 0
-2 -1 0 0 -1 0 -1 2 0 -1 -1 -4 -1 0 -1 0 -2 2 -3 -4 0 -1 -1
0 0 0 -1 2 0 3 1 -1 -1 -1 1 2 4 2 1 0 3 4 2 6 1 0 4 3 9 6 7
13 9 15 14 19 19 21 24 29 29 33 35 41 47 44 48 53 56 62 63
69 68 73 76 82 83 88 89 95 99 103 109 113 117 116 119 126
129 129 135 136 140 144 147 149 153 154 158 161 164 166 168
170 171 176 178 185 182 183 185 187 189 192 193 194 197 197
198 205 203 202 206 209 207 209 212 214 211 215 215 217 217
218 221 221 220 224 223 224 226 224 226 225 229 230 231 230
229 234 234 234 235 236 237 236 236 241 242 242 239 241 240
243 242 245 247 246 245 248 249 250 248 250 250 254 254 251
253 254 255 254 256 257 256 256 259 259 259 260 261 263 260
257 257 255 250 245 240 236 228 223 219 208 202 193 189 179
171 163 154 147 141 130 122 115 110 100 97 91 87 82 75 73
68 66 64 60 56 56 54 53 54 51 48 48 50 48 47 45 44 45 45 45
47 45 41 43 43 44 42 41 41 38 36 38 36 33 34 31 33 33 36 31
31 28 29 29 29 28 23 25 26 26 24 22 21 22 20 22 23 20 18 18
18 17 22 16 16 13 14 15 16 14 16 12 11 13 14 14 13 13 11 15
14 14 13 15 12 12 11 12 12 9 9 9 7 11 8 7 7 9 7 9 9 5 5 5 3
6 4 3 4 2 1 2 2 1 0 -1 -2 0 -1 -1 1 -3 -3 -3 0 -3 -3 0 -4
-4 -4 -2 -3 -3 0 -4 -4 -1 -1 -4 -5 -4 -3 -2 2 -2 -1 -6 -2
-3 -3 -3 -2 -4 -4 -6 -4 0 -5 -5 -3 -3 0 -3 -4 -5 -5 -2 -2
-1 -2 -4 -5 -5 -2 -2 -5 -2 -2 -1 -2 -3 -2 -7 -5 -4 -1 -4 -1
-5 -3 -3 -4 -4 -3 -3 -5 -5 -4 -2 -2 3 -2 0 0 1 1 0 0 -1 -1
-1 0 -1 -2 -1 -2 0 2 -1 -1 -2 -2 -2 0 -2 0 0 0 4 8 1 0 1 1
6 6 4 3 5 3 3 6 5 2 4 5 4 8 3 6 6 4 6 3 1 5 4 4

Raw data for statistics shown in figure 34; 2.8% H_2; 1 of 5 data sets:

23 27 20 21 17 20 20 24 23 24 15 15 18 19 21 17 20 17 20 23
19 18 15 16 17 25 19 20 19 26 24 16 15 22 17 23 19 20 15 15
15 14 17 22 26 28 15 19 19 22 14 17 18 16 15 21 23 26 24 17
15 19 18 19 21 18 25 21 18 17 21 20 19 24 21 17 20 21 19 17
17 22 17 21 19 23 23 22 19 25 22 16 16 24 27 20 20 23 21 17
17 18 20 20 22 22 19 28 32 25 31 32 28 50 46 45 51 50 61 57
64 66 69 78 81 91 87 96 103 111 107 111 121 124 137 137 135
147 150 157 156 162 169 171 174 175 177 203 185 188 197 195
204 202 207 221 216 222 228 231 227 229 236 235 245 243 246
249 247 253 258 257 259 268 269 268 269 269 272 273 285 285
288 282 285 288 289 294 296 299 305 309 306 311 309 317 315
324 324 318 324 327 329 333 330 331 333 337 339 339 339 343
339 343 343 348 346 344 346 348 347 347 348 342 345 337 333
335 329 319 310 307 294 289 278 283 267 263 251 245 234 235
225 215 210 207 199 194 191 185 183 177 173 165 164 157 156
152 149 146 142 139 134 138 133 128 131 126 127 120 120 115
120 118 113 112 110 108 104 109 100 98 95 97 88 90 97 87 98
85 81 87 80 82 77 79 76 74 72 73 74 74 74 76 75 73 73 70 69
72 67 68 70 68 68 73 67 68 63 62 67 65 74 60 63 58 61 60 56
57 58 54 58 57 58 57 53 56 61 57 53 52 52 55 60 58 56 57 52
54 56 54 56 55 54 48 51 47 53 57 53 56 58 51 55 49 55 47 50
51 49 51 48 53 51 46 51 48 52 49 49 51 48 48 53 47 44 49 45
45 43 47 44 43 44 44 42 46 43 45 40 45 47 51 49 47 48 56 49
52 51 52 47 57 51 52 51 52 54 49 51 54 47 45 45 50 57 51 57
58 57 50 52 54 55 52 50 54 52 51 66 53 56 57 54 55 59 57 51
60 68 57 51 54 54 53 54 56 58 53 55 52 64 69 57 55 53 50 60
51 57 58 56 57 58 55 55 56 55 55 55 52 60 65 58 54 62 55 58
61 61 56 57 54 61 55 54 56 55 55 55 55 52 53 55 55 49 61 56
52 54

2 of 5:

52 46 38 38 41 40 41 44 49 38 41 42 43 45 40 44 45 44 40 35
39 42 39 35 39 41 43 45 40 41 44 44 42 47 45 44 50 47 45 47
43 44 41 39 43 54 42 51 47 45 43 49 53 50 49 51 45 46 51 48
47 45 45 39 39 41 39 46 40 43 44 46 42 41 40 40 48 49 50 51
54 60 54 58 58 61 72 70 73 76 78 81 94 89 95 103 100 108
114 119 134 129 133 139 146 155 154 159 169 171 186 193 191
193 199 200 209 206 213 220 225 232 235 237 247 242 255 252
261 258 266 270 277 275 281 276 280 284 289 299 300 301 304
305 304 308 307 312 319 315 320 321 323 321 326 326 331 332
329 333 335 336 340 345 346 345 343 350 346 350 348 352 351
354 353 356 364 363 357 359 365 359 371 362 369 372 376 370
369 369 368 372 373 373 376 376 380 385 383 383 383 382 385
390 394 394 393 395 396 391 406 395 400 397 397 398 401 400
398 401 397 398 401 402 398 394 390 387 381 375 377 359 355
354 341 332 324 319 310 300 294 284 275 275 259 255 253 245
244 233 229 222 215 212 207 202 202 197 199 189 182 183 182
177 172 171 169 166 167 162 160 157 154 148 147 149 143 142
139 140 135 135 135 127 132 126 128 121 122 127 124 116 116
114 116 114 111 114 120 119 109 104 105 110 98 102 100 98
99 96 96 94 93 96 95 94 91 89 87 89 89 87 93 85 88 86 82 92
84 81 81 81 77 78 82 77 78 73 75 78 72 74 71 73 75 74 74 81
74 79 74 71 74 72 73 73 71 74 69 77 73 68 68 74 69 72 67 69
67 69 65 70 66 68 68 78 65 62 64 71 64 63 66 69 75 62 66 68
66 64 71 74 65 71 65 65 62 63 60 64 62 68 63 57 57 57 58 57
66 62 59 61 66 61 60 66 65 62 67 67 63 64 59 68 72 64 65 63
75 66 66 63 62 62 63 64 68 65 66 70 64 64 63 69 63 66 66 74
71 64 77 71 73 77 75 71 71 71 70 71 72 70 70 78 72 80 75 72
75 76 71 69 76 71 73 69 76 76 74 73 72 70 72 68 70 74 75 76
79 77 74 74 76 75 71 73 74 78 77 76 76 85 76 75 78 75 73 74
77 78 80 78

3 of 5:

-4 -5 -3 -4 -5 0 0 0 1 -2 -1 3 5 2 5 3 3 6 6 4 6 8 4 5 9 3
7 8 11 9 16 12 10 15 17 14 10 12 9 21 15 7 27 13 18 15 9 7
12 9 8 5 7 9 4 6 3 8 13 7 12 12 8 11 17 10 9 6 5 6 3 7 1 4
16 5 1 0 0 -3 0 -1 2 4 7 26 15 19 24 28 31 39 42 43 47 51
55 64 62 71 72 82 85 85 95 97 98 100 108 109 114 122 122
129 134 137 143 154 158 160 165 176 171 177 184 186 195 192
199 203 205 208 215 219 218 225 229 230 232 238 237 241 248
248 249 257 252 260 258 258 262 264 267 269 272 275 277 277
281 284 279 282 283 285 285 290 288 290 296 294 293 296 297
300 302 300 308 310 304 307 305 305 309 306 311 310 313 310
311 311 315 316 319 320 321 320 319 320 319 321 322 323 327
325 325 330 327 330 333 331 337 335 336 335 336 335 337 340
337 336 336 334 334 326 320 320 312 309 303 297 289 284 274
266 262 251 244 234 219 213 204 192 187 179 174 165 161 154
150 146 149 138 134 133 126 121 120 125 114 109 112 104 102
99 96 96 94 90 86 85 88 83 78 78 77 76 72 75 69 71 67 67 63
63 59 64 61 59 57 53 48 47 45 41 41 44 40 38 36 37 40 35 35
39 35 48 27 27 29 28 28 24 23 23 24 16 19 15 20 14 19 15 21
17 13 14 13 14 18 11 12 13 12 10 9 4 8 10 8 6 7 13 5 2 1 1
3 0 0 7 9 0 2 5 5 1 1 1 0 3 5 6 3 -1 1 5 2 4 1 2 -2 3 5 0 6
5 -2 0 -1 -1 0 -1 -1 -3 -1 -2 9 -2 0 -3 -4 2 1 0 5 0 0 9 -1
1 4 2 5 4 2 10 5 7 7 12 6 9 8 8 4 1 4 3 2 4 4 1 1 -2 0 2 4
0 7 2 5 14 0 1 4 2 0 8 0 3 0 5 2 1 5 4 5 7 6 4 2 5 4 3 4 11
6 3 10 4 4 2 11 7 8 6 9 8 6 9 9 8 9 11 11 12 9 10 11 15 11
13 11 11 14 13 11 12 16 11 7 15 6 10 9 10 14 10 16 11 9 9 6
10 5 8 5 10 6 7 6

4 of 5:

6 4 5 5 5 3 5 1 4 5 2 2 0 0 -1 4 1 4 1 -1 6 5 5 4 4 3 5 0 3
4 10 1 8 3 7 7 6 7 3 3 3 7 12 11 1 2 6 8 12 6 5 8 9 7 12 10
12 8 12 11 11 9 12 15 14 15 16 18 18 25 16 19 13 17 15 15
17 20 21 24 21 33 34 37 42 40 53 53 56 55 60 63 72 75 80 87
98 105 110 113 122 137 131 136 145 151 159 168 168 173 177
180 188 201 197 209 210 213 217 220 225 230 235 243 243 246
249 261 257 260 265 267 269 272 274 275 278 280 284 286 286
289 290 291 295 298 303 300 304 303 307 308 307 309 312 313
318 318 320 325 321 322 326 331 327 329 330 335 336 335 335
340 339 337 341 344 345 344 344 349 350 350 349 351 351 354
354 358 355 356 357 354 362 357 357 357 360 361 364 364 360
366 363 366 366 366 365 367 368 367 368 369 372 370 373 373
374 375 376 375 375 376 373 371 368 367 360 355 363 348 341
334 324 318 310 300 294 285 272 266 255 243 236 230 218 211
201 197 188 185 174 173 165 166 163 159 158 152 146 142 142
137 141 132 132 130 127 127 125 126 121 120 118 117 117 115
113 118 111 111 107 104 103 101 100 97 99 96 92 96 93 89 86
89 80 81 82 82 88 79 77 73 77 73 71 69 71 71 69 65 65 64 63
67 61 61 61 60 67 60 54 57 56 57 52 57 52 51 50 48 52 47 46
48 45 45 41 47 45 44 47 39 40 40 40 47 41 44 48 41 42 43 42
39 41 40 37 43 36 48 37 39 36 35 36 35 39 36 32 35 41 37 37
42 33 35 35 34 35 38 36 35 38 33 32 31 32 34 36 35 36 40 36
39 37 35 36 33 35 33 42 36 33 34 39 33 31 36 31 35 36 33 33
31 34 35 33 36 41 31 40 28 33 33 35 35 34 36 37 39 33 34 36
38 36 35 42 37 37 35 33 32 34 36 38 37 36 37 33 37 36 32 36
31 34 35 35 32 30 35 38 37 37 34 33 34 34 35 34 34 34 38 36
38 35 34 34 36 34 36 40 40 36 35 38 36 38 39 36 35 37 40 34
42 36 38 37 36 36 41 38 36 39 45 37 39 36 43 37 37 34 43

5 Of 5:

-4 -6 -5 0 -4 -2 -2 2 -5 -3 2 -2 -3 -3 -4 0 1 2 -3 0 -1 1 4
-2 0 -1 0 0 0 0 -3 -2 -1 -3 -2 -1 -3 -2 -1 -2 -1 0 -1 0 -2
-1 7 -2 -1 -1 0 -1 3 4 -1 -1 0 9 -1 1 0 2 0 3 12 3 1 0 2 6
3 1 9 10 2 2 1 6 8 8 6 7 12 16 17 16 25 23 28 34 35 38 44
48 53 53 61 69 70 83 84 89 97 99 108 113 115 120 128 135
140 148 152 158 165 166 171 178 179 182 191 191 197 200 208
209 215 226 223 222 229 231 234 237 241 245 242 247 252 253
258 262 259 266 270 271 273 271 275 283 279 279 284 282 287
288 288 290 294 295 295 295 296 297 298 301 300 305 308 306
308 314 312 311 314 316 313 319 318 317 324 321 320 321 323
323 324 324 325 326 324 328 327 329 328 330 333 331 331 329
327 332 330 326 329 330 327 332 330 333 332 332 333 338 336
335 338 341 341 339 338 339 339 335 329 327 321 315 316 306
298 289 284 277 266 258 251 240 230 221 210 199 190 185 176
166 159 155 147 139 133 129 126 122 121 117 110 109 107 104
103 97 93 91 92 88 88 83 83 82 82 73 74 74 76 72 65 66 66
62 60 60 60 56 56 57 53 50 51 47 46 43 44 42 40 40 41 37 36
36 36 37 34 40 33 35 28 27 29 26 25 23 22 21 21 21 19 18 19
21 15 17 15 16 17 12 13 15 15 12 14 10 12 13 10 12 10 7 10
6 9 7 7 8 3 3 2 5 1 5 -1 0 0 -2 1 0 -3 -3 -2 -4 -4 -4 -1 -3
-3 -4 1 -6 -4 -8 -7 -7 -6 -8 -5 -7 -6 -7 -5 -3 -5 -4 -3 -2
-4 -3 -7 -7 -1 -2 -1 -5 -7 -8 -7 -5 -6 -4 -2 -3 -7 -4 -5 -5
-6 -7 -7 -4 -6 -5 -7 -7 -5 1 -5 -4 -6 -9 -6 -7 -7 -7 -2 -5
-5 -2 -7 -5 -4 -9 -7 0 -8 -10 -11 -8 -6 -10 -8 -11 0 -12
-10 -6 -12 -9 -13 -11 -14 -7 -12 -8 -12 -11 -10 -7 -5 -8 -3
-4 -3 -8 -6 -8 -6 -8 0 -3 -5 -5 -7 -4 -4 -7 -8 -3 -6 -8 -8
-7 -3 2 -1 3 1 -3 -4 -1 -2 -1 0 0 3 -1 1 0 3 -1 0 3 1 4 -3
-1 3 0 1 -2 0 -3 -2

Raw data for temperature shown in figure 37:

979 981 981 982 982 983 983 984 984 984 984 985 985 984 986
988 986 987 989 988 990 987 989 988 989 990 990 992 992 991
992 992 997 993 993 993 993 993 994 994 995 994 996 996 996
997 998 996 997 998 998 999 999 1000 999 999 1002 1000 1001
1001 999 1001 1003 1003 1004 1003 1003 1004 1004 1004 1007
1007 1006 1005 1008 1011 1007 1007 1008 1008 1008 1010 1009
1009 1008 1011 1011 1009 1011 1011 1011 1012 1015 1012 1012
1013 1016 1014 1014 1015 1015 1016 1015 1016 1016 1016 1017
1017 1023 1018 1017 1018 1019 1019 1020 1018 1020 1020 1022
1020 1021 1022 1022 1021 1023 1024 1024 1024 1023 1025 1024
1024 1024 1025 1025 1027 1027 1026 1026 1026 1027 1026 1027
1028 1029 1028 1029 1029 1029 1030 1030 1030 1030 1032 1031
1036 1032 1032 1032 1033 1033 1038 1034 1034 1033 1034 1034
1037 1035 1035 1035 1036 1036 1036 1036 1036 1040 1038 1037
1038 1038 1039 1040 1039 1038 1039 1040 1040 1041 1040 1040
1040 1041 1041 1041 1042 1042 1043 1042 1044 1043 1048 1043
1044 1044 1044 1044 1043 1045 1045 1045 1046 1046 1046 1049
1046 1046 1047 1047 1047 1047 1048 1048 1048 1049 1048 1049
1048 1049 1051 1049 1051 1049 1051 1050 1050 1051 1051 1052
1051 1053 1052 1052 1053 1053 1053 1053 1052 1055 1053 1054
1054 1054 1054 1055 1055 1054 1055 1055 1055 1055 1056 1056
1055 1056 1056 1057 1056 1057 1060 1059 1057 1057 1058 1057
1058 1059 1059 1060 1058 1059 1063 1059 1060 1059 1060 1060
1059 1060 1060 1060 1060 1060 1061 1062 1061 1061 1062 1062
1062 1062 1063 1067 1064 1063 1063 1063 1063 1063 1064 1066
1064 1064 1063 1064 1064 1064 1064 1065 1064 1066 1066 1065
1065 1066 1068 1066 1066 1065 1066 1065 1067 1067 1067 1067
1067 1067 1067 1068 1068 1068 1067 1067 1068 1068 1067 1068
1068 1069 1069 1069 1069 1070 1070 1070 1069 1070 1070 1072
1070 1070 1071 1071 1069 1070 1071 1071 1071 1071 1071 1071
1071 1071 1072 1072 1072 1072 1072 1072 1072 1072 1072 1074
1073 1072 1073 1073 1073 1072 1073 1073 1073 1073 1072 1074
1072 1073 1074 1074 1074 1075 1074 1074 1075 1075 1075 1075
1075 1075 1068 1075 1075 1075 1075 1075 1076 1074 1076 1076
1076 1076 1076 1076 1076 1077 1077 1077 1078 1077 1080 1077
1076 1077 1077 1077 1078 1077 1078 1077 1077 1078 1078 1078
1078 1078 1079 1078 1078 1078 1079 1079 1079 1079 1079 1079
1080 1079 1079 1079 1079 1079 1080 1080 1080 1080 1079 1080
1080 1080 1080 1080 1080 1080 1080 1081 1080 1081 1081 1081
1081 1080 1081 1081 1080 1081 1080 1080 1082 1079 1081 1080
1081 1081 1081 1081 1080 1083 1082 1081 1081 1082 1082 1083
1082 1083 1082 1082 1083 1082 1082 1082 1082

Raw data for sensor output shown in figure 37:

43 54 69 80 95 108 123 138 149 167 181 196 212 228 243 256
270 284 298 310 323 336 350 363 376 392 406 418 434 445 460
474 486 499 511 525 538 549 561 572 584 595 605 617 626 637
648 658 669 680 690 700 709 719 729 736 746 753 762 772 779
785 794 800 808 816 823 832 838 843 852 857 862 869 874 879
884 888 894 900 903 908 914 918 921 926 929 932 936 939 941
945 945 949 952 954 955 958 960 961 962 964 964 966 968 968
968 968 968 968 968 968 968 967 964 964 964 963 964 962 960
957 957 955 952 949 947 945 942 940 937 933 931 929 925 921
916 914 911 906 902 899 896 890 885 882 878 871 868 864 858
853 849 842 839 835 827 823 819 812 805 752 720 713 706 697
690 683 676 669 659 652 645 636 628 621 612 606 597 588 580
571 564 556 546 538 529 523 513 505 496 487 480 470 464 453
445 435 429 420 412 401 393 385 378 368 359 348 341 331 323
313 305 296 287 279 268 261 251 243 233 224 216 207 200 190
181 174 163 155 145 137 127 119 110 99 91 83 74 65 55 48 38
29 20 11 3 -6 -15 -24 -33 -42 -52 -59 -69 -79 -86 -96 -104
-112 -121 -130 -138 -145 -156 -163 -174 -182 -189 -198 -205
-214 -225 -233 -242 -251 -257 -266 -275 -283 -293 -299 -310
-316 -325 -333 -340 -351 -358 -367 -376 -382 -389 -397 -405
-412 -421 -429 -438 -448 -454 -462 -470 -478 -485 -496 -503
-511 -519 -527 -533 -541 -548 -556 -563 -572 -581 -588 -596
-603 -611 -616 -622 -632 -638 -646 -653 -663 -671 -678 -685
-694 -702 -709 -715 -720 -729 -735 -743 -750 -756 -764 -772
-779 -786 -792 -799 -807 -815 -823 -829 -835 -840 -847 -855
-861 -869 -875 -881 -888 -894 -902 -910 -916 -923 -927 -935
-942 -948 -955 -961 -968 -975 -981 -987 -993 -999 -1006
-1013 -1019 -1025 -1032 -1037 -1043 -1049 -1055 -1061 -1067
-1074 -1080 -1086 -1091 -1099 -1105 -1111 -1116 -1122 -1127
-1133 -1139 -1145 -1151 -1156 -1161 -1167 -1174 -1179 -1184
-1190 -1194 -1200 -1205 -1212 -1217 -1223 -1227 -1231 -1236
-1241 -1250 -1256 -1263 -1267 -1272 -1276 -1279 -1285 -1290
-1296 -1302 -1307 -1312 -1317 -1322 -1327 -1331 -1337 -1341
-1346 -1353 -1357 -1361 -1363 -1368 -1374 -1380 -1385 -1389
-1393 -1398 -1402 -1408 -1414 -1419 -1423 -1427 -1431 -1434
-1440 -1446 -1450 -1455 -1461 -1466 -1470 -1474 -1477 -1482
-1488 -1490 -1494 -1498 -1505 -1510 -1513 -1519 -1523 -1528
-1531 -1536 -1542 -1545 -1550 -1555 -1562 -1565 -1570 -1574
-1576 -1579 -1584 -1588 -1591 -1597 -1599 -1601 -1605 -1607
-1609 -1613 -1616 -1619 -1623 -1629 -1632 -1638 -1642 -1646
-1648 -1654 -1654 -1658

Raw data for sensor output during random pressure changes shown in figure 38:

2 0 3 0 3 0 2 0 2 0 1 0 2 0 1 -1 2 0 2 0 1 1 0 3 0 4 -4 -1
-4 -1 -6 -3 -6 -2 -6 -4 -7 -5 -7 -5 -6 -5 -6 -8 -5 -9 -5 -9
-6 -10 -7 -10 -7 -10 -7 -10 -8 -10 -8 -9 -10 -8 -11 -8 -12
-8 -11 -8 -10 -7 -10 -8 -10 -7 -9 -8 -7 -9 -7 -10 -6 -10 -6
-10 -6 -10 -8 -10 -8 -10 -9 -10 -11 -9 -13 -8 -12 -8 -12 -9
-12 -10 -13 -16 -11 -8 -6 -9 -5 -9 -4 -8 -5 -8 -5 -7 -5 -6
-6 -5 -7 -5 -9 -5 -9 -6 -8 -7 -10 -7 -10 -8 -7 -10 -6 -9 -6
-9 -6 -8 -7 -8 -6 -7 -8 -5 -9 -6 -9 -6 -9 -6 -9 -6 -7 -8 -6
-11 -7 -11 -8 -10 -7 -10 -7 -8 -9 -6 -10 -7 -10 -7 -10 -8
-10 -8 -8 -10 -7 -10 -6 -10 -7 -9 -6 -8 -8 -5 -13 -11 -15
-13 -16 -14 -17 -15 -15 -18 -15 -18 -14 -18 -16 -18 -16 -17
-19 -16 -20 -16 -20 -17 -20 -18 -20 -20 -15 -17 -15 -17 -16
-18 -16 -16 -18 -15 -18 -15 -18 -15 -16 -16 -14 -17 -13 -16
-12 -16 -16 -18 -19 -16 -19 -16 -18 -16 -18 -16 -15 -18 -14
-19 -15 -10 -5 -7 -10 -6 -10 -8 -12 -9 -12 -12 -10 -15 -11
-14 -12 -13 -12 -11 -13 -10 -12 -10 -13 -11 -12 -14 -10 -14
-10 -13 -10 -12 -14 -10 -14 -10 -12 -10 -12 -12 -9 -12 -9
-12 -9 -11 -11 -8 -12 -9 -11 -8 -9 -10 -7 -10 -7 -9 -6 -7
-9 -5 -9 -4 -9 -5 -7 -9 -6 -10 -7 -10 -8 -7 -11 -6 -10 -7
-10 -8 1 -7 -11 -9 -12 -11 -12 -15 -12 -14 -13 -16 -15 -14
-17 -13 -17 -14 -16 -17 -14 -17 -14 -17 -14 -14 -16 -13 -16
-13 -15 -15 -12 -16 -13 -15 -12 -12 -15 -11 -13 -11 -12 -13
-10 -12 -9 -12 -10 -8 -11 -8 -9 -9 -8 -11 -7 -11 -8 -10 -10
-8 -10 -8 -10 -9 -7 -12 -9 -12 -11 -9 -12 -9 -12 -11 -10
-13 -10 -12 -10 -10 -12 -8 -12 -8 -11 -12 -9 -12 -10 -12
-13 -11 -14 -12 -13 -14 -11 -13 -12 -15 -14 -12 -15 -13 -16
-14 -13 -16 -12 -15 -14 -12 -16 -13 -16 -14 -12 -16 -13 -14
-15 -12 -16 -13 -14 -15 -12 -15 -11 -14 -14 -12 -15 -12 -14
-15 -12 -15 -13 -14 -16 -13 -15 -14 -13 -16 -13 -16 -14 -13
-16 -13 -16 -14 -13 -17 -15 -18 -18 -16 -19 -16 -18 -18 -16
-18 -17 -16 -18 -13 -12 -9 -7 -13 -11 -13 -14

Raw data for 6.7% H_2 shown in figure 39:

-3 -5 -4 -4 -2 -3 -2 -5 -3 -3 -3 -2 -3 -2 -4 -4 -4 -2 -3 -2
-3 -3 -3 -4 -2 -2 -1 -3 -3 -3 -3 -2 -3 -3 -5 -3 -3 -3 -3 -4
-4 -4 -5 -5 -3 -3 -3 -5 -5 -4 -4 -4 -3 -4 -6 -5 -6 -4 -4 -5
-6 -7 -7 -7 -5 -5 -5 -7 -5 1 26 84 176 289 413 538 643 720
760 772 768 761 757 756 761 766 774 778 781 779 773 759 739
711 674 632 578 522 457 392 325 261 200 147 105 70 46 26 16
10 8 4 2 1 0 0 0 0 0 0 0 0 0 0 2 1 2 0 0 0 0 0 0 0 -2 -2 -3
-1 -2 -2 -1 -4 -3 -4 -2 -3 -3 -3 -4 -4 -5 -3 -4 -4 -4 -5 -5
-6 -4 -5 -5 -7 -6 -6 -7 -5 -6 -5 -7 -7 -7 -7 -6 -7 -6 -8 -7
-8 -7 -7 -7 -7 -9 -8 -8 -8 -7 -8 -7 -9 -8 -9 -8 -8 -8 -7 -9
-8 -8 -7 -7 -7 -7 -8 -8 -7 -6 -6 -5 -5 -7 -6 -6 -5 -5 -5 -5
-7 -7 -7 -6 -6 -6 -6 -8 -7 -7 -5 -6 -5 -5 -7 -6 -7 -6 -6 -6
-6 -8 -7 -8 -7 -6 -7 -6 -8 -8 -8 -8 -7 -8 -7 -9 -8 -9 -8 -7
-8 -7 -9 -8 -9 -9 -7 -8 -7 -9 -9 -9 -8 -7 -8 -7 -9 -8 -9 -9
-7 -8 -8 -9 -9 -9 -9 -6 -6 -7 -8 -7 -7 -7 -5 -6 -5 -6 -7 -6
-7 -5 -4 -5 -5 -6 -5 -6 -4 -5 -4 -4 -7 -6 -6 -4 -5 -5 -4 -6
-5 -6 -5 -4 -5 -3 -6 -5 -6 -6 -4 -5 -5 -7 -7 -6 -8 -6 -6 -6
-7 -9 -7 -8 -7 -7 -7 -7 -9 -8 -8 -8 -7 -8 -6 -9 -8 -8 -8 -7
-7 -7 -8 -9 -8 -8 -7 -7 -7 -7 -9 -8 -8 -7 -7 -7 -7 -8 -7 -7
-7 -6 -6 -6 -7 -7 -7 -7 -4 -6 -6 -5 -7 -6 -6 -4 -4 -4 -4 -6
-5 -5 -5 -4 -5 -4 -5 -5 -4 -5 -3 -3 -4 -3 -5 -4 -5 -3 -4 -4
-4 -6 -5 -5 -4 -4 -4 -2 -5 -4 -5 -4 -2 -3 -2 -3 -3 -2 -2 0
-1 0 0 -2 -1 0 0 1 0 1 0 0 0 0 2 1 1 0 0 1 0 2 1 1 1 0 0 -1
1 1 1 1 -1 0 0 1 1 1 1 0 0 0 0 0 1 0 1 -1 -1 -2 -2 0 -2 -2 -3
-4 -3 -4 -1 -3 -3 -3 -5 -4 -4 -3 -3 -3 -3 -5 -3 -4 -3 -2 -2
-2

Appendix G

```
0 ( TU58 data transfer to pc)
1 OCTAL
2 177546 CONSTANT TB
3 CODE ?DONE BEGIN 177544 TST B 0< END NEXT
4
5 : CONV ( CONVERT FOR SCREEN ) DUP ABS 0 <# 40 HOLD #S
6 SIGN #>0 DO DUP i + C@ TB C! ?DONE ESCAPE LOOP DROP ;
7 : SBS ( SEND TO SCREEN ) BLOCK 2000 OVER + SWAP DO I
8 @ CONV ESCAPE 2 +LOOP ;
9
10 ( PROPER DATA FORMAT FOR PC FILES )
11 : SEND DUP ABS 0 <# 12 HOLD 15 HOLD #S SIGN #> 0 DO
   DUP I
12 + C@ TB C! ?DONE ESCAPE LOOP DROP ;
13 : SBP BLOCK 2000 OVER + SWAP DO I @ SEND ESCAPE 2
   +LOOP ;
14
15 DECIMAL --> OK
```

```
0 ( TU58 TRANSFER TO PC CONTINUED )
1 OCTAL
2
3
4 :HUND 144 * ;
5 : SWIT ROT HUND ROT 12 * + + 400 + ;
6 : ?DONE BEGIN 177540 C@ 0 > END ;
7 : RECEIVE 3 0 DO ?DONE 177542 C@ LOOP SWIT ;
8 : SHIP 10 0 DO RECEIVE SBP LOOP ;
9
10
11
12
13
14
15 DECIMAL OK
```

```
0 ( TU58 DATA TRANSFER TO AED )
1 OCTAL
2 177546 CONSTANT TB
3
4 CODE ?DONE BEGIN 177544 TST B 0< END NEXT
5
6 177542 CONSTANT BL
7
8 CODE ?BLST BEGIN 177540 TST B 0< END NEXT
9
10 : QWE BL @ . ;
11
12 : PLUG BLOCK 2000 OVER + SWAP DO QWE I C@ DUP TB C!
```

```
13 ?DONE ?BLST LOOP ;
14
15 DECIMAL


0 ( AED DATA TRANSFER FROM TU58 )
1 OCTAL
2 176576 CONSTANT TB
3 : BLAST 100 TB ! ;
4 : PU 1 176570 ! ;
5 17672 CONSTANT BC
6
7 CODE ?FIN BEGIN 176570 TST 0< END NEXT
8 : FU 0 176570 ! ;
9 VARIABLE STUF 2000 SLLOT
10 : BORG 0 BC ! ;
11 : SOME BC @ . BC @ . ;
12 : TUD PU 20000 0 DO ?FIN BC C@ STUF I + C! FU BLAST
   LOOP
13 BLAST;
14
15 DECIMAL --> OK
```

Apenndix H

Linear regression was applied to the data from figure 35. This gave the following equation:

$y = 283x + 91$ where

y = sensor output (mv)

x = % H_2 in air

Regression yielded a correlation coefficient of 0.987, indicating that the calibration curve is only approximately linear. Four concentrations were used including zero percent. The standard error of the slope was 23 (mv/%). A standard error in the baseline or blank was calculated by using the data collected before the injection of hydrogen gas into the carrier stream, this standard deviation was equal to 6.4 (mv). From the above information, a minimum detectable concentration was calculated:

$c_L = k\ s_b\ /\ [m + (t_{0.005})\ (s_m)]$ where

k = 3 (confidence level)

s_b = standard deviation of the blank

m = slope (mv/%)

$t_{0.005}$ = statistical value for a t distribution at 99.5% confidence for 3 degrees of freedom

s_m = standard error in the slope

$c_L = 3\ (6.4)\ /\ (0.283 + 5.841 \times 0.023)$

$= 0.05$ % H_2 in air

Appendix I

The following computer programs were written in Basic to allow; (1) data transfer between a personel computer and a DEC TU58, (2) application of a software filter to collected data.

9-POINT UNWEIGHTED MOVING WINDOW :

```
10 DIM (9600)
20 DIM A(600)
30 INPUT "FILE NUMBER";N$
40 FILE$="B:" + N$ + "D.PRN"
50 OPEN FILE$ FOR INPUT AS #1
60 FOR I=1 TO 512
70 INPUT#1 ,A(I)
80 NEXT I
90 CLOSE #1
100 FOR B=5 TO 508
110 I=B-4
120 S=A(I)+A(I+1)+A(I+2)+A(I+3)+A(I+4)+A(I+5)+A(I+5)+A(I+6)
      +A(I+7)+A(I+8)
130 Q(I)=S/9 * 2.4414
140 NEXT B
150 Q(64) = Q(64) + 50
160 Q(107) = Q(107) + 50
170 FILE$="B:" +N$ + "F.PRN"
180 OPEN FILE$ FOR OUTPUT AS #2
190 FOR I=1 TO 504
200 PRINT#2,Q(I)
210 NEXT I
220 CLOSE #2
230 END
```

PC TRANSFER FROM TU58:

```
10 CLEAR
20 OPEN "COM1:9600,N,8,1,CS,DS" AS #1
30 CLS
40 FOR I=1 TO 5
50 PRINT " "
60 NEXT I
70 PRINT "LOAD BLOCK 210; TYPE SHIP ON FORTH TERMINAL"
80 FOR I=1 TO 5
90 PRINT " "
100 NEXT I
110 INPUT "BLOCK # TO BE TRANSFERRED";A$
120 FOR I=1 TO 5
130 PRINT " "
140 NEXT I
150 INPUT "DATE DATA WAS TAKEN";T$
160 FILE$="B:" + A$ + T$ + "D.PRN"
170 OPEN FILE$ FOR OUTPUT AS #3
180 A= VAL(A$)
190 B= A/100
200 C= INT(B)
210 D= C*10
220 E= A-D
230 F= E/10
240 G= INT(F)
250 H= G*10
260 I= H+D
270 J= A-I
280 PRINT #1, CHR$(C);
290 PRINT #1, CHR$(G);
300 PRINT #1, CHR$(J);
310 PRINT C
320 PRINT G
330 PRINT J
340 IF LOC(1)=0 THEN 340
350 FOR I=1 TO 15000
360 NEXT I
370 A$=INPUT$(LOC(1),#1)
380 PRINT A$;
390 PRINT #3, A$;
400 IF LOC(1)>0 THEN 370
410 CLOSE #3
420 CLS
430 FOR I=1 TO 3
440 PRINT " "
450 NEST I
460 INPUT "DO YOU WISH TO TRANSFER ANOTHER BLOCK
(Y OR N)";A$
470 IF A$="Y" THEN 80
480 IF A$="y" THEN 80
490 CLEAR
500 OPEN "COM1:9600,N,8,1,CS,DS" AS #1
510 PRINT #1, CHR$(1);
520 PRINT #1, CHR$(0);
530 PRINT #1, CHR$(0);
540 END
```

Appendix J.

Under normal conditions bulk platinum is not permeable to hydrogen. Discussions with Russ Messier from Penn State, who has researched thin film deposition, implicates "void networks" or "density deficits" as the mechanism for hydrogen movement through the thin film of platinum used in our research.

These networks or voids arise from processes which are occurring during the deposition of the thin film. The platinum, deposits in small droplets, which coalesce to form larger droplets. As different size droplets join, they leave voids in the platinum layer. A thick film, put down in several layers, could eventually inhibit the passage of hydrogen through the metal by an overlapping effect. These deposition processes would be an interesting area for future investigation.

Vita

Eric was born in Spokane, Washington on April 15, 1951. One of seven children. His father was a mining engineer, his mother is a registered nurse.

He attended James Madison University as an undergraduate and graduated in 1981 with a B.S. in Chemistry. Went to work upon graduation for approximately 4 years and returned to graduate school in 1985 at Va. Tech.

Currently, he is employed in the pharmaceutical industry for Merck and Company. He has a wife, Sharon, two children, Lauren and Ben, and a dog named Libby.

Being home and running are his favorite pastimes.

Eric William Richmond